NATIONAL AERONAUTICS AND SPACE ADMINISTRATION

Space Programs Summary 37-63, Vol. I

Flight Projects

For the Period March 1 to April 30, 1970

JET PROPULSION LABORATORY
CALIFORNIA INSTITUTE OF TECHNOLOGY
PASADENA, CALIFORNIA

May 31, 1970

NATIONAL AERONAUTICS AND SPACE ADMINISTRATION

Space Programs Summary 37-63, Vol. I

Flight Projects

For the Period March 1 to April 30, 1970

JET PROPULSION LABORATORY
CALIFORNIA INSTITUTE OF TECHNOLOGY
PASADENA, CALIFORNIA

May 31, 1970

JPL SPACE PROGRAMS SUMMARY 37-63, VOL. I

Prepared Under Contract No. NAS 7-100
National Aeronautics and Space Administration

Preface

The Space Programs Summary is a multivolume, bimonthly publication that presents a review of technical information resulting from current engineering and scientific work performed, or managed, by the Jet Propulsion Laboratory for the National Aeronautics and Space Administration. The Space Programs Summary is currently composed of four volumes:

Vol. I. *Flight Projects* (Unclassified)

Vol. II. *The Deep Space Network* (Unclassified)

Vol. III. *Supporting Research and Advanced Development* (Unclassified)

Vol. IV. *Flight Projects and Supporting Research and Advanced Development* (Confidential)

Contents

Contents (contd)

I. *Mariner* Mars 1971 Project

A. Project Description and Status

1. Description

The primary objective of the *Mariner* Mars 1971 Project is to place two spacecraft in orbit around Mars that will be used to perform scientific experiments directed toward achieving a better understanding of the physical characteristics of that planet. Principal among these experiments are measurements of atmospheric and surface parameters at various times and locations to determine the dynamic characteristics of the planet. Approximately 70% of the Martian surface will be observed during a minimum of 90 days of orbital operations.

During Mission A, it is planned to map the topography of a large portion of the Martian surface at a resolution significantly higher than that achievable with earth-based methods or by the *Mariner* Mars 1969 spacecraft. In addition, measurements will be made of the composition, density, pressure, and thermal properties of the planet's atmosphere. Other measurements will be directed toward an understanding of Mars' surface temperatures, composition, and thermal properties (particularly at the polar caps); its apparent lack of internal activity; its mass distribution; and its shape.

During Mission B, data will be sought on time-variable features of the Martian surface associated with the wave of darkening wherein both seasonal and secular changes occur. Also, information on atmospheric structure and gross dynamics will be obtained, as well as information directed toward an understanding of Mars' mass distribution, its shape, and its apparent lack of internal activity.

A capability will exist to redirect goals for either mission to the alternate mission if desired. The two launches are anticipated for May 1971, with arrival at the planet during the following November.

An engineering objective of the project is to demonstrate the ability of the spacecraft to perform orbital operations in an adaptive mode wherein information from one orbital pass is used to develop the operations plan for subsequent orbital passes. Studies indicate a high probability that at least one of the spacecraft will survive the sun occultation period which occurs shortly after the 90-day mission is

completed. This makes it possible to conduct an Extended Mission for about a year after orbit insertion. The Extended Mission will probably consist of one or two data taking sequences per week with the capability of recording and playing back about a half-recorder of data (16 TV frames and 11 min of spectrometer data).

One of the *Mariner* Mars 1971 flight spacecraft will be new, and the other will be the spare flight spacecraft of the *Mariner* Mars 1969 Project modified to meet the requirements of the 1971 missions and to enhance mission reliability. The proof test model spacecraft of the *Mariner* Mars 1969 Project will be modified to become the proof test model for the *Mariner* Mars 1971 Project, to be used for preliminary testing and as a simulator in support of flight operations. A major modification for the *Mariner* Mars 1971 mission will be the addition of a rocket motor required to decelerate the spacecraft and place it in orbit around Mars.

Separate scientific instrument subsystems will be required to accomplish the television, infrared radiometer, ultraviolet spectrometer, and infrared spectrometer interferometer experiments given in Table 1. The S-band occultation and celestial mechanics experiments will require no additional equipment on the spacecraft.

Management responsibilities for the overall project, the Spacecraft System, the Mission Operations System, and the Tracking and Data System have been assigned to JPL.

Table 1. *Mariner* Mars 1971 scientific experiments and principal investigators

Television	
H. Masursky	Team leader
H. Masursky	PI/U.S. Geological Survey
R. Batson	CI/U.S. Geological Survey
W. Borgeson	
M. Carr	
J. F. McCauley	
D. Milton	
R. Wildey	
D. Wilhelms	
J. Lederberg	PI/Stanford University
E. Levinthal	CI/Stanford University
J. B. Pollack	CI/Cornell University
C. Sagan	CI/Cornell University
G. de Vaucouleurs	PI/University of Texas
W. B. Thompson	PI/Bellcomm
G. A. Briggs	CI/Bellcomm
P. L. Chandeysson	CI/Bellcomm
E. N. Shipley	CI/Bellcomm
B. Smith	PI/New Mexico State University
M. E. Davies	CI/Rand Corp.
W. K. Hartmann	CI/Arizona State University
N. H. Horowitz	CI/Caltech
R. B. Leighton	CI/Caltech
C. B. Leovy	CI/University of Washington
T. B. McCord	CI/MIT
B. C. Murray	CI/Caltech
R. P. Sharp	CI/Caltech

Ultraviolet spectrometer	
C. Barth	PI/University of Colorado
C. W. Hord	CI/University of Colorado
J. B. Pearce	CI/University of Colorado

Infrared interferometer spectrometer	
R. A. Hanel	PI/Goddard Space Flight Center
B. J. Conrath	CI/Goddard Space Flight Center
W. A. Hovis	CI/Goddard Space Flight Center
V. Kunde	CI/Goddard Space Flight Center
G. V. Levin	CI/Biospherics
P. D. Lowman	CI/Goddard Space Flight Center
C. Prabhakara	CI/Goddard Space Flight Center
B. Schlachman	CI/Goddard Space Flight Center

Infrared radiometer	
G. Neugebauer	PI/Caltech
S. C. Chase	CI/Santa Barbara Research Center
H. Kieffer	CI/UCLA
E. D. Miner	CI/JPL
G. Munch	CI/Caltech

Celestial mechanics	
J. Lorell	Team leader
J. Lorell	PI/JPL
J. D. Anderson	CI/JPL
W. L. Martin	CI/JPL
W. L. Sjogren	CI/JPL
I. Shapiro	PI/MIT
M. Ash	CI/MIT
W. Smith	CI/MIT

S-band occultation	
A. Kliore	PI/JPL
D. L. Cain	CI/JPL
G. Fjeldbo	CI/JPL
B. L. Seidel	CI/JPL

PI = Principal investigator, who is the proposer for each experiment.

CI = Co-investigator, who assists the proposer on each experiment.

Team leader heads a particular group of PIs and CIs on an experiment where there is more than one PI.

Lewis Research Center has been assigned management responsibility for the Launch Vehicle System. The launch vehicle will be an *Atlas/Centaur* developed by General Dynamics/Convair.

The *Mariner* Mars 1971 missions will be supported by the Air Force Eastern Test Range launch facilities at Cape Kennedy, the tracking and data acquisition facilities of the Deep Space Network, and other NASA facilities.

2. Status

Mission Operations System major software requirements were delivered, and the Division Engineering Planning Documents, which give detailed design of the programs, were prepared. The Air Force Eastern Test Range Program Support Plan and the Deep Space Network Systems Description were completed for the Tracking and Data System. The Mission and Analysis and Engineering Planetary Quarantine Plan, the preliminary Interplanetary Trajectory Characteristics Document, and the Mission Specification and Plan, Part II, were published.

The Orbit Trim Design Program was completed and is now operational. The Orbit Insertion Design and Analysis Program and the Statistical Linking Program were delivered, completing the maneuver design and analysis software. A preliminary study determined that a minimum periapsis altitude of 1250 km will allow camera-A frontlap for Mission A.

Spacecraft power, telemetry, and pyro subsystems were assembled into the proof test model in the Spacecraft Assembly Facility. Initial subsystem checkout and payload integration testing with the science support equipment, the UV spectrometer, the IR radiometer, and the data automation subsystem breadboard are nearly complete and no major difficulties have occurred.

Temperature control model tests were completed in the space simulator and the data are being evaluated. The propulsion engineering test model was assembled, tested, and will be shipped to Edwards Test Station for vibration and firing tests.

Figure 1 shows the television team matrix, which was revised to include the Mission Operations Group.

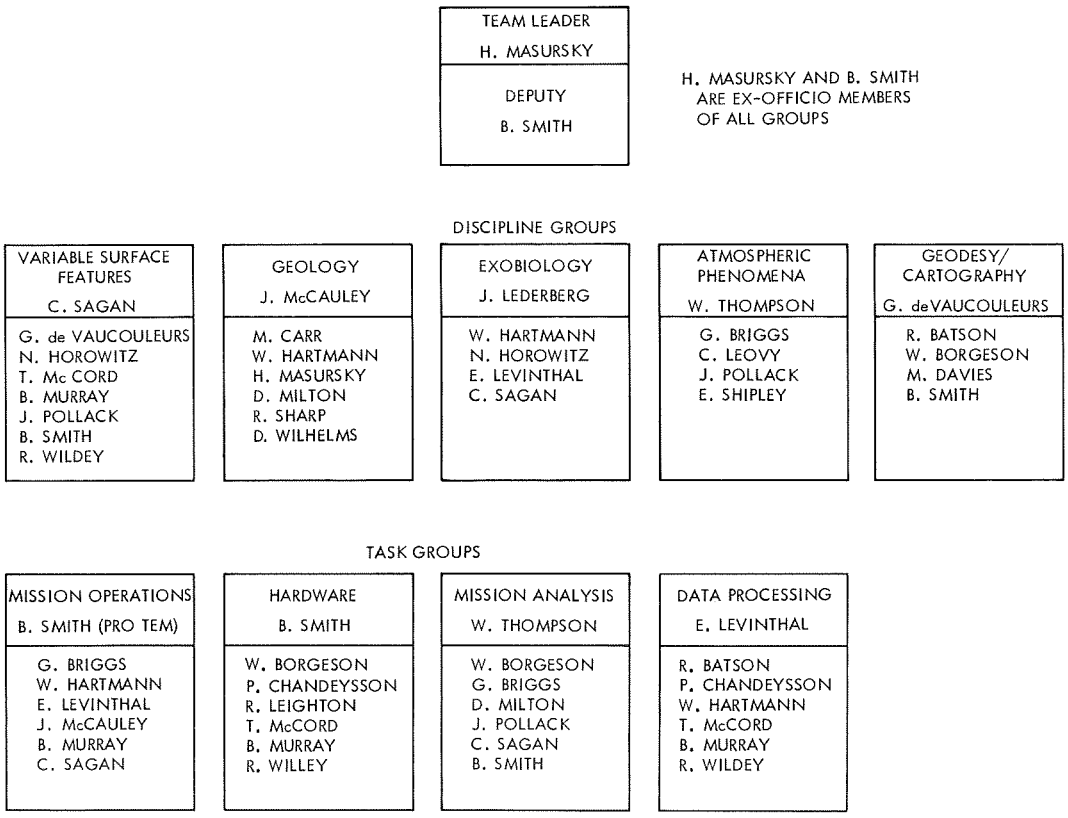

Fig. 1. Television team matrix

B. Data Systems

1. Mission and Test Computer System[1]

This article reports development of the mission and test computer (MTC) system, which is a product of the *Mariner* Mars 1969 and *Surveyor* Univac 1219 data processing systems. The principal *Mariner* Mars 1969 applications consisted of processing TV calibration data, supplementing CDC 3300 system test complex data system (STCDS) functions during spacecraft system tests, providing the total data processing support for proof test model testing after shipment of the STCDS to the Air Force Eastern Test Range and the subsequent return of the computer system to the vendor, and performing real-time video data processing, including TV data distribution, to network television during encounter operations.

The higher data rates required for *Mariner* Mars 1971, and the need to handle and process as much as possible of the data in real time to increase testing efficiency and avoid saturating the system with nonreal-time processing requests, required additional computing capability to supplement that of the existing two Univac 1219 systems. The combined worst-case input data rate for two *Mariner* Mars 1971 spacecraft undergoing test simultaneously was estimated to reach 500 kbits/s. Because of these requirements, a dual high-rate data preprocessor, consisting of a Univac 1230 computer and peripheral equipment, was leased to receive, deblock code as necessary, decommutate, and perform all input processing functions on all high-rate data streams. This system will verify the format of and, insofar as possible, the content of the high-rate data in real time. A block diagram of the system test complex data streams, showing the alternative sources of data available to the MTC system, appears in Fig. 2.

The data system capability for supporting spacecraft test is being developed in three phases, with the first phase to provide single Univac 1219 support of proof test model testing, which began on March 18, 1970 with initial turn-on of the spacecraft power subsystem. This capability consists of logging all data acquired, including low-rate orbital-science-format data, decommutation of engineering telemetry, acquisition of events and status-change signals, commands, and central computer and sequencer memory dump functions, and the display of an appropriate extract of this data on a line printer on the system test complex. The first 30-character/s printers (Univac DCT-500) for obtaining hardcopy printout of data associated with each spacecraft subsystem were delivered and made operational in late April.

Hardware and software capabilities will continue to be added in modular fashion to the system as they are developed, which is intended to provide a dual Univac 1219 configuration in May 1970. This system will provide the additional capability to record the 132-kbits/s science data automation system hardline data, block decode the 86.4-kbits/s high-rate data to provide a real-time estimate of block coder performance, or decommutate and process at the maximum rates of 16.2 and 8.1 kbits/s the science telemetry data which is received from various sources in any of the three formats: spectral science (S486, 8.1 kbits/s), selected video (V972), or recorded science (R7938). This system will, however, be limited in processing capability to a total input data rate of 100 kbits/s.

Online real-time processing of all high-rate data, and UV spectrometer/IR interferometer spectrometer frame decommutation (U4800, U5400, and I4725 formats), will be provided by the full Univac 1230/dual Univac 1219 configuration scheduled to become operational in August 1970. This configuration, shown in abbreviated form in Fig. 3, will accommodate the simultaneous testing of two flight spacecraft. Each of the two spacecraft test complexes will be provided with the following equipment (Fig. 3), listed by subsystem.

Control subsystem:

(1) Keyboard and printer; for controlling the recording and processing of data streams, changing data channel assignments on the output displays, and changing parameters such as alarm limits, plot scale size, etc.

(2) Display device thumbwheel control stations (8); for selecting the data mode and format for each display device.

(3) Control console; for selecting serial data sources, and inhibiting the flow of serial data or information from data acquisition registers to the computer to allow control of the input data rate to the system.

(4) Card reader; for quickly changing tolerances and alarm limits applied in testing of each data sample.

(5) Step number box; for entering test-step numbers specified in the system test procedures into the computer.

[1]The mission operations system software is described in the following article (*Subsection 2*).

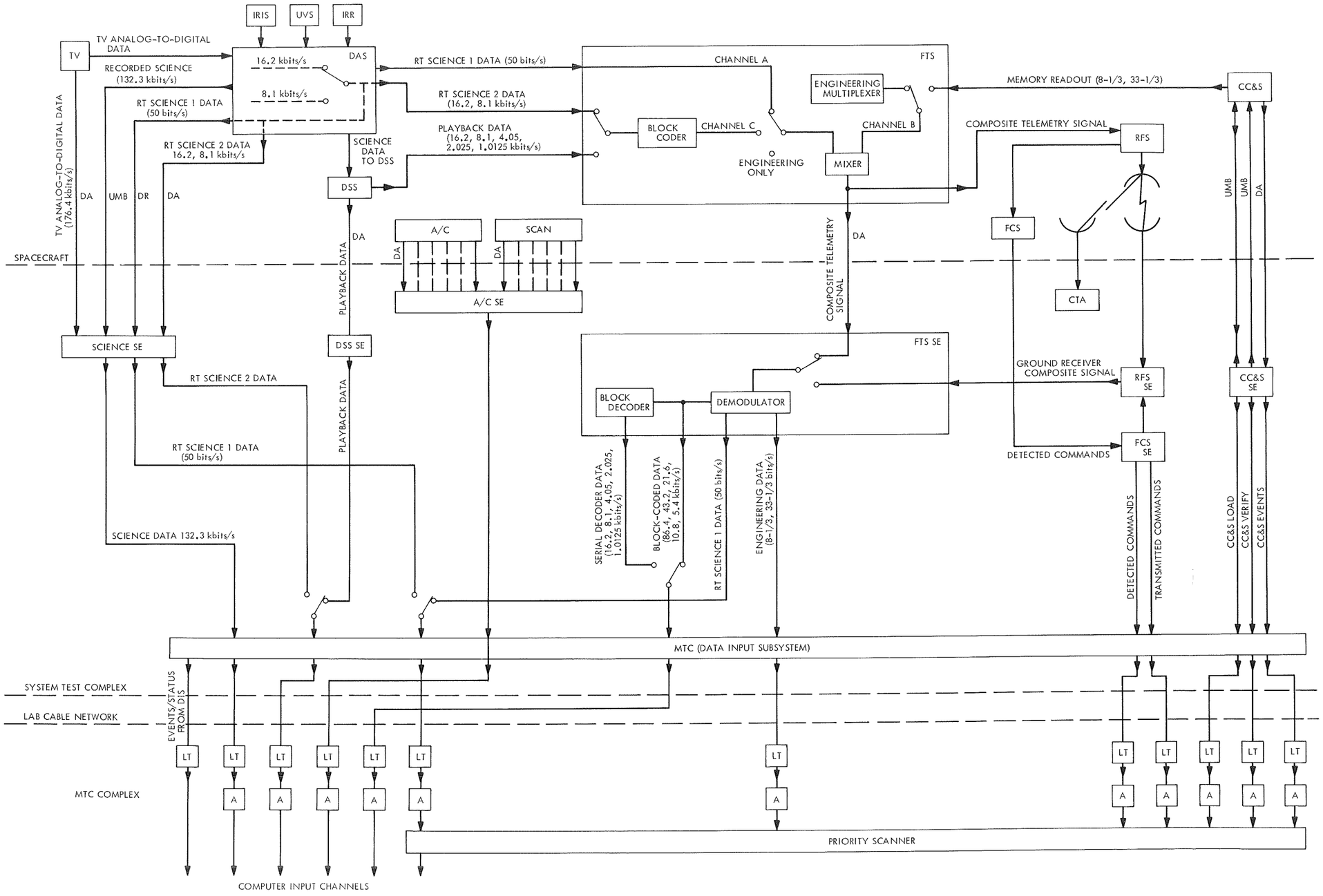

A	ASSEMBLER (SERIAL-TO-PARALLEL CONVERTER)
A/C	ATTITUDE CONTROL
CC&S	CENTRAL COMPUTER AND SEQUENCER
CTA	COMPATIBILITY TEST AREA AT JPL
DA	DIRECT ACCESS
DAS	DATA AUTOMATION SUBSYSTEM
DIS	DATA INPUT SUBSYSTEM
DSS	DEEP SPACE STATION
FCS	FLIGHT COMMAND SUBSYSTEM
FTS	FLIGHT TELEMETRY SUBSYSTEM
IRIS	IR INTERFEROMETER SPECTROMETER
IRR	IR RADIOMETER
LT	LINE TERMINATOR
MTC	MISSION TEST COMPUTER
RFS	RADIO FREQUENCY SUBSYSTEM
RT	REAL TIME
SE	SUPPORT EQUIPMENT
UMB	UMBILICAL
UVS	UV SPECTROMETER

Fig. 2. System test complex data streams available to the MTC system

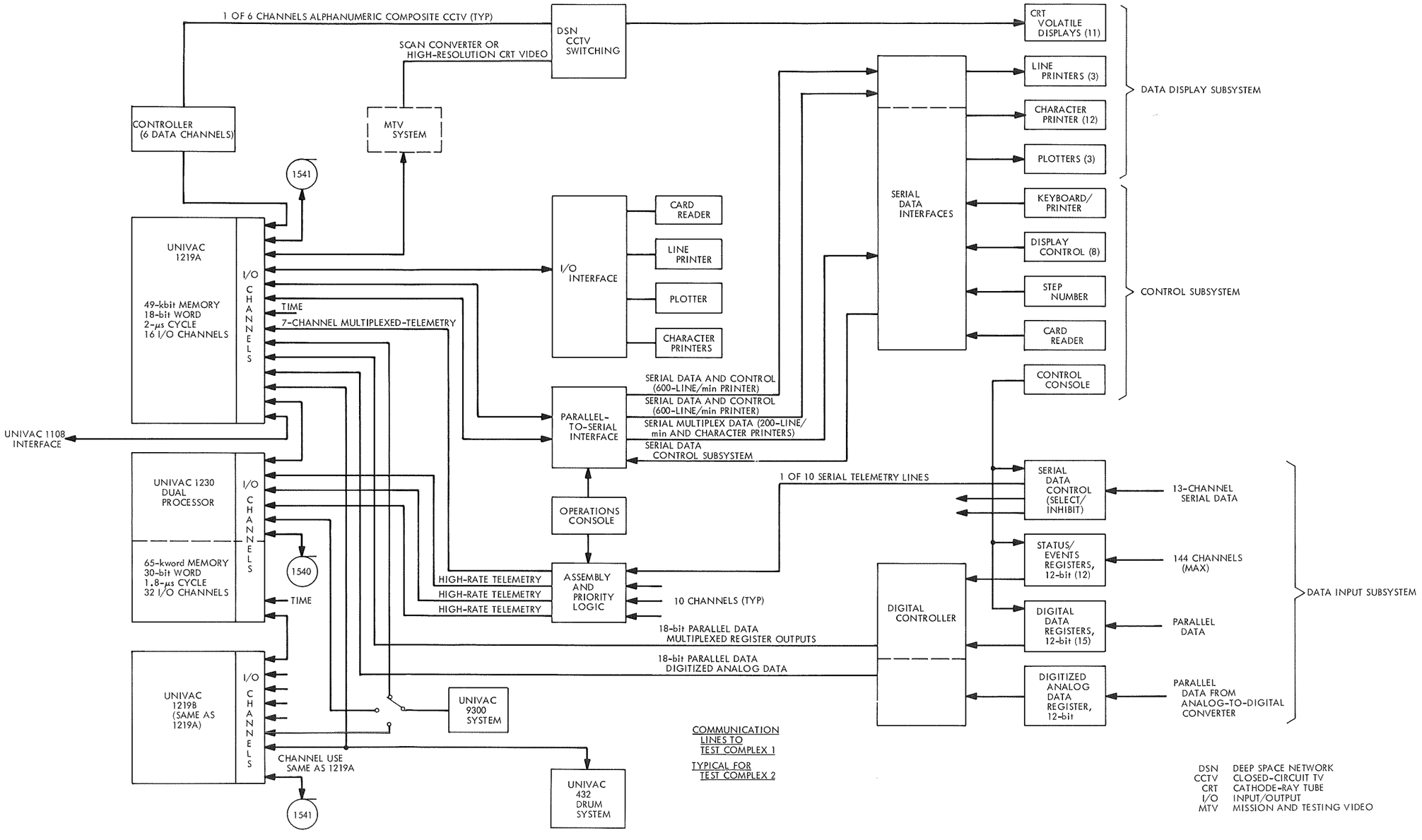

Fig. 3. Typical equipment at test complex and typical central computer area equipment serving test complex

Data input subsystem:

(1) Status and event channel registers; for entering spacecraft support equipment on–off status information and event occurrences to the computer.

(2) Digital data registers; for entering parallel digital data from counters or analog-to-digital converters into the computer.

(3) Line drivers and terminators; for transmitting serial telemetry data and parallel register output data to the computer, and receiving serial data for the display and control subsystem.

(4) Digital controller and priority logic; for controlling the sequence of data entry to the computer and identifying data with source codes.

Data display subsystem:

(1) Line printers (3); for listing spacecraft system data and science engineering and payload data (one 600-line/min and two 200- or 600-line/min printers).

(2) Character printers (12); for listing spacecraft and science payload data by subsystem (30 characters/s max rate).

(3) Cathode-ray tube volatile displays (6 separate data channels, 11 closed-circuit TV monitors); for providing five display modes (via the Space Flight Operations Facility (SFOF) closed-circuit TV distribution system, when at JPL), page display, data channel alarm messages, data channel suppressed data messages, command listing, or data plot mode.

(4) Plotters; 1–10-in. incremental plotter for science real-time time-based plots or nonreal-time channel correlation plots, 1 analog plotter for plotting real-time UV spectrometer/IR interferometer spectrometer data, and one 29-in. incremental plotter for system data plotting.

The central computer area in the SFOF contains the following equipment (Fig. 3):

(1) Univac MTC 1230 dual processor; 30-bit word, 32-kbit memory and 16 input/output channels per processor, 1.8-μs memory cycle, 4 tape units.

(2) Univac 1219 computers (2); 18-bit word, 49-k word memory and 16 input/output channels, 2-μs memory cycle, 4 tape units.

(3) Univac 1218 computer; 18-bit word, 32-k word memory and 8 input/output channels, 4-μs memory cycle, 4 tape units; utilized for nonreal-time processing and program development (not shown in Fig. 3).

(4) Univac 9300 computer terminal; 8-kbyte memory, 600-ns memory cycle, 600-cpm card reader, card punch, 600-line/min line printer; for program loading, data dumps, assemblies, operational data printout, etc.

(5) Univac 432 drum system; for storage of programs, tables of coefficients and limits, etc.

(6) Peripheral equipment; Burroughs card reader, 600-line/min printer, incremental plotter, and character printers; for data system status printouts, program development, operational backup, offline data printout, etc.

(7) Operations control console; for assigning serial data inputs to assemblers, configuring assemblers to match input signal and computer channel characteristics, and switching local computer-area or remote system test complex display and control equipment to any desired computer channel.

(8) Cable termination and switching equipment; not shown in Fig. 3 is equipment for terminating interbuilding cables, and cable switching racks which permit flexible interconnection of computers, peripheral equipment, and data interface, assembly, and logic equipment.

All spacecraft telemetry data transmission is serial digital between the test complex data sources and the computer system. Computer output data to the line printers, character printers, and plotters is also serial digital, which reduces the data bit skew and noise difficulties which were encountered in previous projects using parallel-digital longline communications. Additionally, this design permits Dataphone or wideband data line (WBDL) transmission for remote communication if required. For example, it will be feasible to drive display equipment in the JPL SFOF while the MTC system is located at the Air Force Eastern Test Range during prelaunch test operations. A 50-kbits/s WBDL will provide capability for driving, via a hardware demultiplexer, the following displays at JPL: two 200-line/min line printers, twelve channels of 30-character/s character printers, two channels of cathode-ray tube display, and data processing request equipment if necessary, consisting of a card reader, print request box, and control keyboard.

The responsibility for MTC system development for spacecraft testing is assigned to the *Mariner* Mars 1971 mission operations system. The capability developed for system test will also be available for mission operations and the current system design considers the mission operations aspects of data acquisition, processing, and display insofar as feasible.

The interface of the MTC system with the mission and testing video (MTV) system, formerly the *Surveyor* spacecraft TV ground data handling system, provides data for the production of negatives, positives, prints, and enlargements of TV data, and plots of science data. The MTV system will also include high-resolution TV monitors with hardcopy output capability, and the interface to deliver video or alphanumeric data output to the SFOF closed-circuit TV system. All of this capability will be utilized for spacecraft system test, as well as mission operations.

The engineering and science general data processing requirements were defined and documented in functional requirement form, and a version of the engineering special processing requirements was also completed. General processing includes the functions of attaching source codes and time tags to data samples, logging data in raw form, decommutating all data formats, and storing the identified data samples in buffers. Subsequently, the sample values for each measurement are subjected to standard processing, which consists of alarm-limit testing and suppression of printout of redundant samples, averaging and other statistical calculations, conversion to engineering units, and output formatting and buffering for the numerous display types. Special processing consists of calculations performed to aid in evaluating the performance of specific subsystems, and is peculiar to the individual spacecraft subsystems.

2. Mission Operations System Software[2]

The mission operations system (MOS) is responsible for development of mission-dependent computer programs required for mission operations, simulation, and spacecraft checkout, except for the mission-dependent software in the Deep Space Instrumentation Facility (DSIF) telemetry and command processor (TCP), which is provided by the tracking and data system (TDS). The *Mariner* Mars 1971 MOS software system operates in the Univac 1108 or IBM 360/75 Space Flight Operations Facility (SFOF) computers. The mission-independent software, which operates in the DSIF TCP is not described, nor are any other Deep Space Network (DSN) programs, or the operating system software in any of the computers in the DSIF, Ground Communications Facility, or SFOF systems.

A list of the presently defined MOS programs, a capsule description of the program function, and the computer in which each program is currently planned to operate are shown in Table 2. Several programs originally scheduled for development in the Univac 1108 system have been transferred to the IBM 360/75 to improve software system efficiency from an operational standpoint and to reduce the number of computers required to be online for running the operations support category of programs. Approval for transfer of several operations support programs (COMGEN, SCISIM, and SOEGEN) was received, and approval is pending for transferring the one remaining operations support program (SPOP), as well as the science support programs (SCILIB and UVS/IRR display).

Software functional requirements were developed, together with functional specifications for the ground data processing systems. The original specifications contained block diagrams of specific data system configurations, which were modified to a functional block diagram type as the *Mariner* Mars 1971 data processing system design evolved. The IBM 7044 real-time processor systems used in *Mariner* Mars 1969 were succeeded by two IBM 360/75 systems, in which the real-time-oriented MOS-type programs indicated in Table 2 will operate. The IBM 7094 systems were replaced with a Univac 1108 dual-processor system, which was subsequently reconfigured to provide two separate systems; the 1108A is primarily intended for scientific or general-purpose JPL computing, and the 1108B system is for support of *Mariner* Mars 1971 program development and integration, operational testing, and the support of flight operations. Each 1108 system can serve as backup to the other, although the configurations are somewhat different.

The Univac 1108 programs are primarily associated with spacecraft navigation, although there are several so-called category 2 programs assigned to the 1108. Category 2 programs are not considered essential for mission accomplishment, but are nevertheless of sufficient importance to be developed under MOS software implementation procedures. The mission support area peripheral equipment for the IBM 360/75 and Univac 1108 replaces all the IBM 7044/7094 control, display, and

[2]The software for spacecraft checkout is described in the previous article (*Subsection 1*).

Table 2. *Mariner* Mars 1971 mission operations system software

Program name	Computer	Functional description
Navigation		
Orbit data editor (ODE)	1108	Prepares double-precision orbit data file from the real-time tracking data master file by selection, compression, correction, or calibration, etc.
Double-precision trajectory (DPTRAJ)	1108	Integrates equations of spacecraft motion from epoch to desired point, using input from ODE, ICG, or nominal data. Provides listings and a tape of position, velocity, look angles, Deep Space Station (DSS) view periods, etc.
Injection conditions generator (ICG)	1108	Computes injection time, velocity, radius, coordinates, flight path angle, and launch azimuth, using launch time and a polynomial approximation equation.
Double-precision orbit determination (DPODP)	1108	Calculates best orbit from ODE file date, using weighted least-squares trajectory fit. Maps statistical errors to encounter. Also may solve for physical constants, DSS locations, perturbing forces, etc.
Satellite orbit determination (SATODP)	1108	Calculates and maps trajectory and errors, as above, from orbital data located in the ODE file.
Maneuver operations system (MOPS)	1108	Calculates maneuver capabilities, maneuver values and commands required for midcourse maneuver, orbit insertion, and orbit trim.
Planetary observation geometry and science instrumentation sequence (POGASIS)	1108	Computes sequences (time and platform orientation) required to observe specified surface positions, subject to observation criteria, using DPTRAJ or conic trajectory data. Conversely, computes actual coverage and observation conditions based on data received from SPOP (platform orientation and time).
Operations support		
Command generation (COMGEN)	360-75	Assembles and checks central computer and sequencer (CC&S) programs, simulates the CC&S action on the program, and forms spacecraft command messages for loading CC&S memory from this assembly or other sequences provided by SCISIM and SPOP.
Science subsystem event simulator (SCISIM)	360-75	Generates flight command subsystem and CC&S commands and timing for COMGEN to accomplish specified data automation subsystem (DAS) sequences; simulates DAS sequencing, and predicts time of occurrences of actual science events in any specified time base.
Sequence of events generator (SOEGEN)	360-75	Generates and displays a time-ordered sequence of events from file or card input, with capability to display or output by mission, DSS number, "report to or by," etc.
Scan platform operations (SPOP)	360-75	Provides commands to COMGEN based on data received from SCALP or POGASIS. Also determines best estimate of platform positioning angles from data received from SCALP.
Spacecraft support		
Propulsion subsystem operations and performance (PSOP)	1108	Provides prediction of subsystem performance based on propellant/pressurant system analysis, spacecraft mass distribution, and thrust vector orientation based on gimbal actuator data.
Telecommunications analysis (TPAP)	1108	Computes predicted channel performance from antenna pattern data, spacecraft and ground system characteristics, and trajectory data. Computes actual performance from real-time telemetry data and DSIF ground system data, and compares the computation with predicted data.
Celestial reference (CELREF)	1108	Computes sensor performance versus clock angle; lists acquirable objects using sensor characteristics and trajectory data. Calculates spacecraft attitude relative to sun, planets, or selected stars, and ouputs cone and clock angles of celestial objects.
Scan calibration (SCALP)	1108	Provides corrections to SPOP for improving accuracy of PEGASIS platform sequences based on SCALP and other calibration data. Also provides corrections to actual platform pointing direction based on calibration data, telemetry, and preceding history.

Table 2 (contd)

Program name	Computer	Functional description
Science support		
IRIS fourier transform	360-75	Accepts IR interferometer system (IRIS) EDR tape of engineering and interferogram data, processes data and parity information to provide spectral plots and listings, instrument coverage, and performance.
Science library (SCILIB)	360-75	Provides record of planetary coverage by all instruments, including slant range and illumination angle descriptors.
UVS/IRR display	360-75	Provides calibration and formatting of UV spectrometer (UVS) and IR radiometer (IRR) science telemetry data for display purposes.
Simulation		
Spacecraft subsystem mathematical model	1108	Provides realistic, command-responsive spacecraft engineering telemetry data streams for operational tests that simulate up to two independent spacecraft.

printout devices used in *Mariner* Mars 1969. A significant addition is the availability of graphics terminals for the Univac 1108, which will permit interactive communication between the user and programs, such as POGASIS, to obtain maps of the spacecraft instrument coverage for mission planning.

Phase A programs are scheduled to be integrated into their associated operating systems and available for use in MOS training by January 1971. Facility tests in the SFOF will be completed in November 1970 and DSN network system tests will be completed during December 1970. Transfer from DSN development to operations will then occur to permit MOS testing in early 1971. Four programs also have Phase B development versions, which provide desirable but not mandatory capabilities for the conduct of orbital operations.

Preliminary design of the MOS software system is completed and published in the MOS Implementation Plan. The design is concerned with a description of the operational functional requirements, detailed external and internal interfaces, and file detail design of the five following program sequences:

(1) Adaptive mode planning sequence: POGASIS, SPOP, SCALP, COMGEN, SOEGEN, SCISIM, and the DSN program PREDIX which provides expected values for DSIF-received doppler, range, and angles.

(2) Science library index sequence; SCISIM, SPOP, POGASIS, SCILIB, UVS/IRR, IRIS, and the DSN-provided science engineering data record (EDR) generation program in the 360/75.

(3) Scan calibration sequence; SPOP, CELREF, and SCALP.

(4) Orbit determination sequence; ODE, DPODP, and the DSN tracking data editor program in the 360/75.

(5) Maneuver determination sequence; DPODP, MOPS, DPTRAJ, and COMGEN.

C. Guidance and Control

1. Solar Panel–Battery Power Analysis

This article is a continuation of the presentation of the *Mariner* Mars 1971 solar panel shadow analysis program reported in SPS 37-59, Vol. I, pp. 24–28.

The shadow-casting computer program was used to provide a set of plots at 5-deg increments in both directions of yaw, and an initial analysis was made of the effect on the panel output power. It appeared that the reduction in power would be nearly a step function as each section was shadowed, and that the shadow of the thermal shield was nearly a straight line along its leading edge.

It was decided that photographs of a spacecraft model would be useful in confirming the initial data of the shadow casting program, and determining what addi-

tional points might be necessary to more accurately define the geometry of the shadows cast.

In January 1970, a spacecraft model was borrowed from the Engineering Mechanics Division and photographs were taken in the Celestarium building of the model for turns along the + and − yaw axis. Since these photographs were to be used only as a verification of the results from the computer program, pictures were taken for 0-deg yaw and in increments of 10 deg between +20- to +70-deg and −20- to −70-deg yaw.

A comparison of the spacecraft photograph (Fig. 4) and the computer plot (Fig. 5) for 30-deg yaw turn shows a reasonable correlation. However, the computer plot lacks some detail in the curvature of the thermal shield. Also, the $-X$ panel in the photograph is being slightly shadowed by the tip latch mechanism. These were not accounted for in the original inputs of the shadow-casting program.

Although the results of the spacecraft model photograph analysis have not been factored into the shadow-casting program, it is planned to complete this effort by late 1970 and incorporate the capability to predict array power at the various angles, considering both reduction due to the off-sun angle and the shadow.

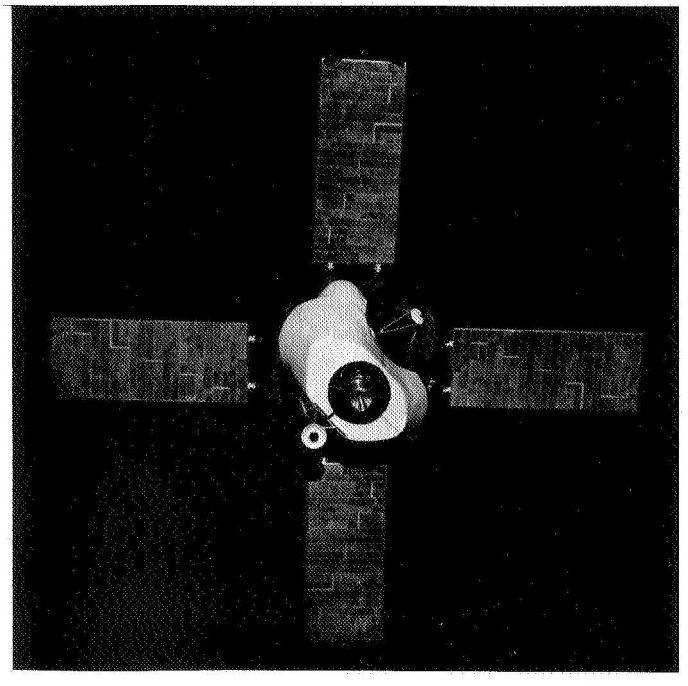

Fig. 4. Spacecraft model photograph for +30-deg yaw turn

The photographs of Fig. 6 provide a representative selection of the set of pictures taken. The propulsion structure shadow begins to affect the panels at about 25-deg yaw turn, but the tip latch shadow appears to be covering a part of the cells in the +20- and −20-deg yaw pictures of Figs. 6a and b.

2. Scan Platform Motion Effects on Attitude Control System

a. Introduction. This article presents the effects of scan platform stepping motion on the *Mariner* Mars 1971 attitude control system. Satisfactory TV pictures can be achieved when the maximum incident angle is limited to within 20 deg of the local vertical. Under this constraint, only two or three scan platform position changes are required. During these position changes, disturbing torques are applied to the spacecraft as a result of the law of conservation of momentum. The effects of these disturbing torques on the *Mariner* Mars 1971 spacecraft attitude control system are determined and the corresponding gas consumption to stabilize the spacecraft is estimated. Two cases with stepping rates of 1 deg/s and 0.25 deg/s are considered. Digital computer simulations were developed to aid in obtaining the results.

b. Simulation. A six-degree-of-freedom spacecraft attitude control system was programmed on the 7094, using DSL/90 language. The following items were considered in the simulation.

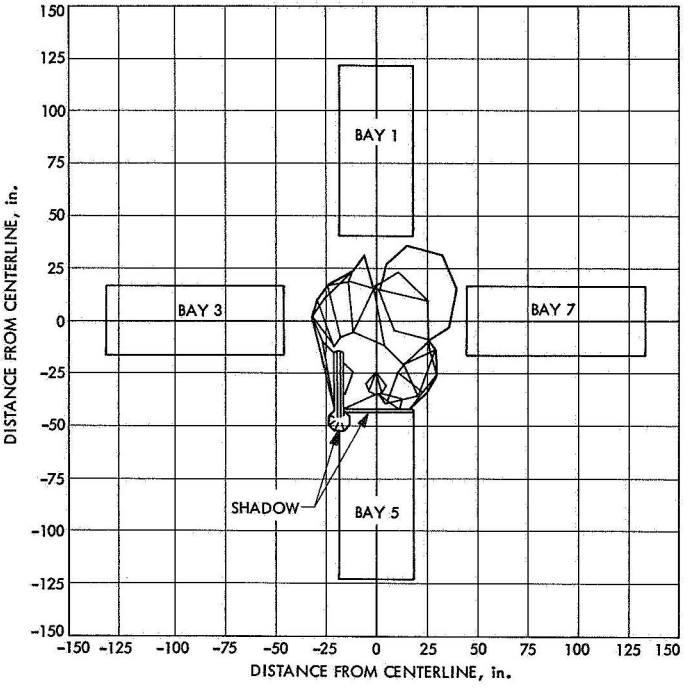

Fig. 5. Computer program plot for 30-deg yaw turn

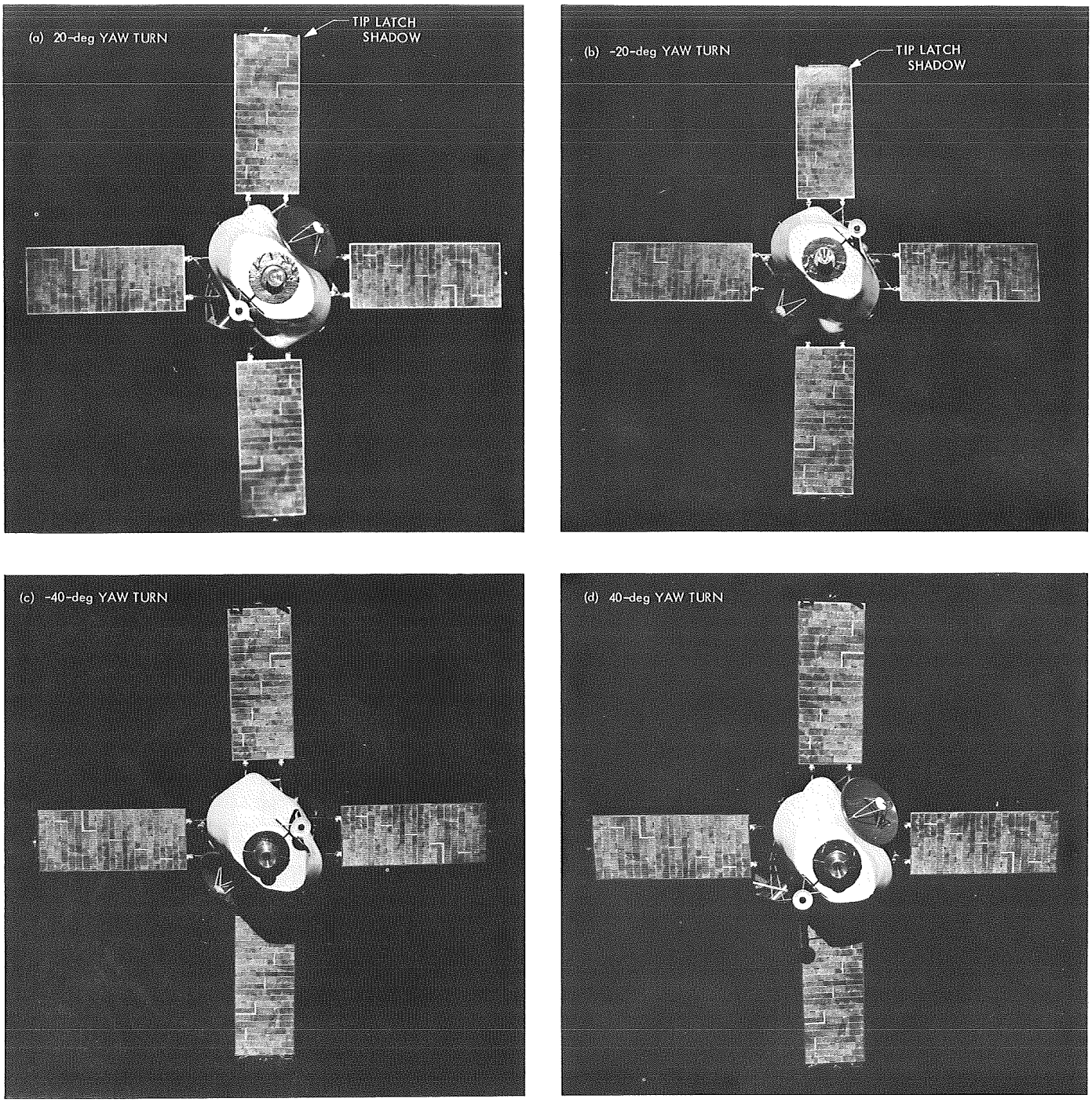

Fig. 6. Spacecraft model photographs at various yaw angles

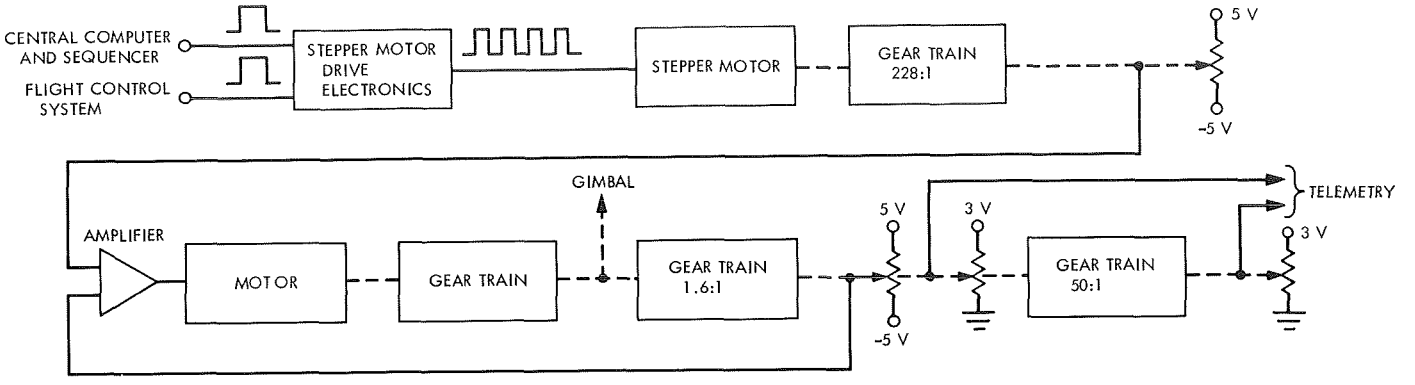

Fig. 7. Single-axis block diagram for scan platform mechanism

Scan platform stepping mechanism. A fairly elaborate model of the scan platform mechanism was used to accurately simulate the proper disturbing torques. A single-axis block diagram for the scan platform mechanism is shown in Fig. 7. The scan platform stepping motion is initiated by either a central computer and sequencer or a flight control system command. Upon receiving one of these command signals, the stepper motor drive electronics will convert the signal into a sequence of four 35-ms pulses with a period of 100 ms. Each of these pulses will rotate the stepper motor in either a clockwise or counter clockwise direction by 90 deg, which in turn will produce a change in the input voltage to the amplifier of ± 0.01095 V (for the case of stepping rate 1 deg/s). Thus, corresponding to each input command, there will be an input to the amplifier of the following form:

$$V_{in} = \sum_{K=0}^{3} U(t - 0.1K) \times 0.01095 \qquad (1)$$

where $U(t)$ is the unit step function defined by

$$U(t) = \begin{cases} 0, & t < 0 \\ 1, & t \geq 0 \end{cases} \qquad (2)$$

The block diagram of the scan platform control system about the cone and the clock axes is shown in Fig. 8. In this figure, K_t', K_w', and J are the effective motor torque constant, effective back-electromotive-force constant, and effective total moment of inertia of the motor and scan platform set, respectively. These parameters are given by

$$\left.\begin{aligned} K_t' &= NK_t \\ K_w' &= N^2K_w \\ J &= I_MN^2 + I_S \end{aligned}\right\} \qquad (3)$$

where

K_t = motor torque constant

K_w = motor back-electromotive-force constant

N = gear ratio

I_S = moment of inertia of the scan platform (cone or clock axis)

I_M = moment of inertia of the motor

It should be noted that a second-order transfer function of the form

$$\frac{w_n^2}{S^2 + 2\eta w_n S + w_n^2}$$

is introduced in the feedback loop of the clock axis control system. This function results from a slightly different mechanism in scan platform cone and clock axes.

The disturbing torques due to scan platform stepping can be calculated.

$$\begin{aligned} T_d &= I_s\ddot{\theta}_L \pm I_M\ddot{\theta}_M \\ &\cong I_s\ddot{\theta}_L \end{aligned} \qquad (4)$$

The sign of the term $I_M\ddot{\theta}_M$ will depend on the direction of rotation of the scan platform and the motor. However, since this term is much smaller in magnitude than the $I_s\ddot{\theta}_L$ term, it can be neglected. The parameters of the scan platform are summarized in Table 3.

Table 3. Scan platform parameters

Parameter	Value
Motor torque constant K_t, ft-lb/V	2.55×10^{-4}
Motor back-electromotive-force constant K_w, ft-lb/V	1.74×10^{-6}
Motor moment of inertia I_M, slug-ft^2	$50/N^2$
Gear ratio between motor and scan platform N	27,000
Moment of inertia of scan platform about cone axis I_{CO}, slug-ft^2	6.27
Moment of inertia of scan platform about clock axis I_{CLK}, slug-ft^2	5.16

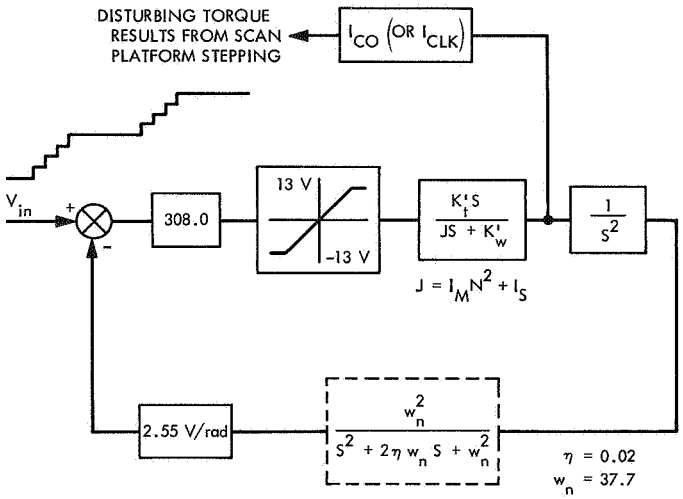

Fig. 8. Scan platform cone (or clock) axis control system

Scan platform stepping requirements. The scan platform cone and clock angles should satisfy the following constraints during each orbit of the 90-day normal orbiting mission.

Position in orbit	Cone angle, deg	Clock angle, deg
1	127	233
2	112	251
3	96	265

As the spacecraft moves through its orbit, the cone and clock angles are adjusted to the above values. In changing from one position to the next, both 1 deg/s and 0.25 deg/s scan platform stepping rates are considered in this simulation. Due to power limitations, the cone and clock stepping motions cannot be actuated at the same time. It is assumed that the cone stepping motion will always be performed first and will then be followed by the clock stepping motion.

Worst-case initial conditions. It is desirable to determine the maximum gas consumption that will be required to stabilize the spacecraft. Since the positioning of the scan platform produces no net change in torque on the spacecraft, it is conceivable that if the initial roll, pitch, and yaw angles are well within their respective deadbands, the transient positioning torques will not require any stabilizing gas. The worst-case conditions which will require the greatest amount of stabilizing gas correspond to starting the stepping motion when the roll, pitch, and yaw angles of the spacecraft are all approximately on their deadband edges and the disturbing torques have the tendency to drive these angles outside their respective deadbands. These worst-case initial conditions are summarized as follows:

Position change	θ_x, mrad	θ_y, mrad	θ_z, mrad	w_x, μrad/s	w_y, μrad/s	w_z, μrad/s
1–2	−4.3	−4.3	−4.3	9	9	9
2–3	−4.3	−4.3	−4.3	9	9	9
3–1	4.3	−4.3	−4.3	−9	−9	−9

where θ_x, w_x, θ_y, w_y, θ_z, and w_z are the angular positions and rates of the spacecraft pitch, yaw, and roll axes, respectively.

c. Simulation results. Many curves were generated from the simulation; of these, 5 typical curves are shown in Figs. 9 to 13 to illustrate the major results. In Fig. 9, the disturbing torques due to a 5-deg position change in clock direction with a stepping rate of 1 deg/s are demonstrated. It is interesting to note that the disturbing torques on the spacecraft, as shown in Fig. 9, are periodic in nature. This periodicity is a result of the fast response time of the scan platform to the positioning torques. Since there are no net scan platform disturbing torques on the spacecraft, once the gas jet system is fired to counterbalance one part of the disturbing torque it must be fired a second time to reduce the net torque in the system to zero. Thus, in general, there will always be an even number of gas jet firings. This fact is clearly indicated in the "total switching amplifier (swamp) on time" curves

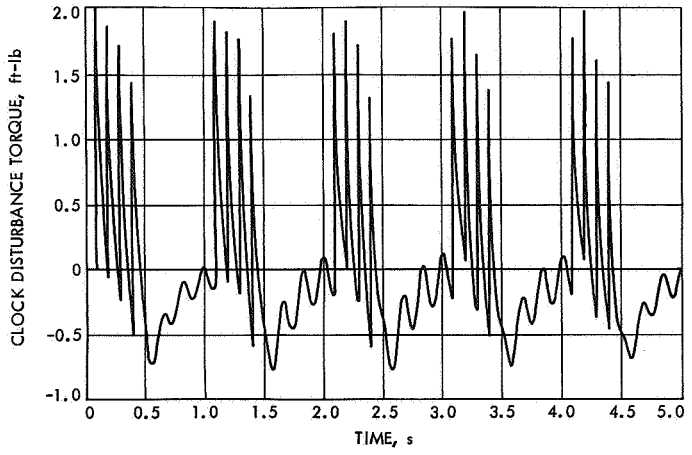

Fig. 9. Disturbing torques

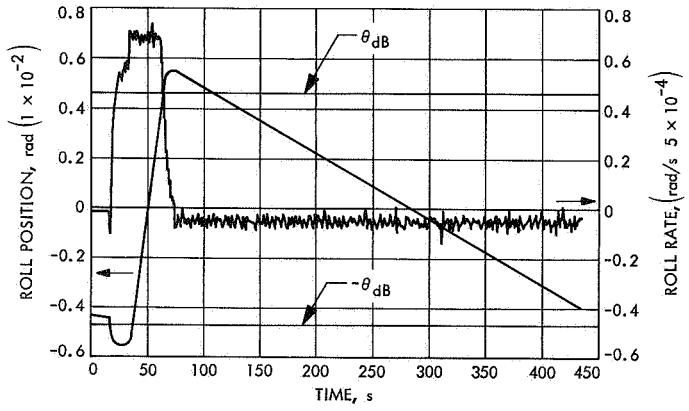

Fig. 10. Roll position and rate vs time (stepping rate of 1 deg/s)

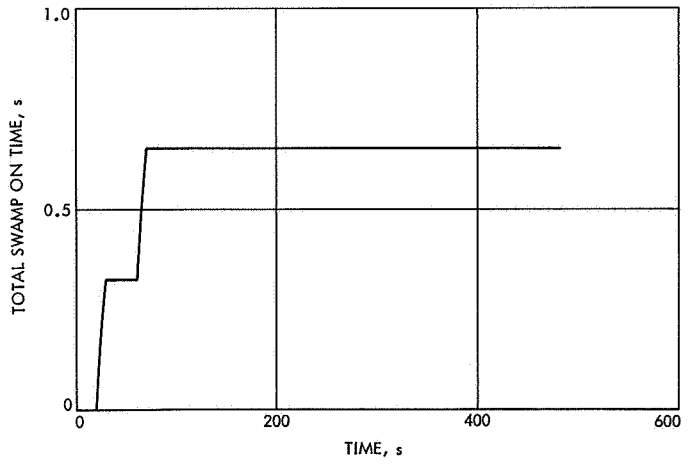

Fig. 11. Roll axis switching amplifier on time (stepping rate of 1 deg/s)

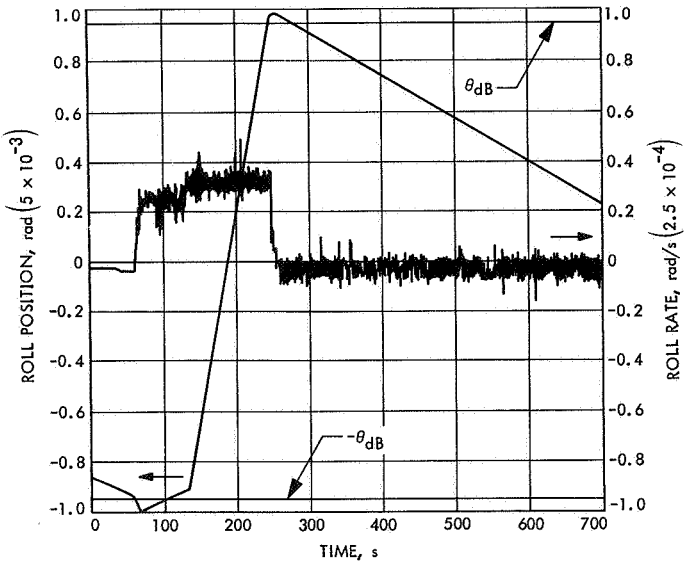

Fig. 12. Roll position and rate vs time (stepping rate of 0.25 deg/s)

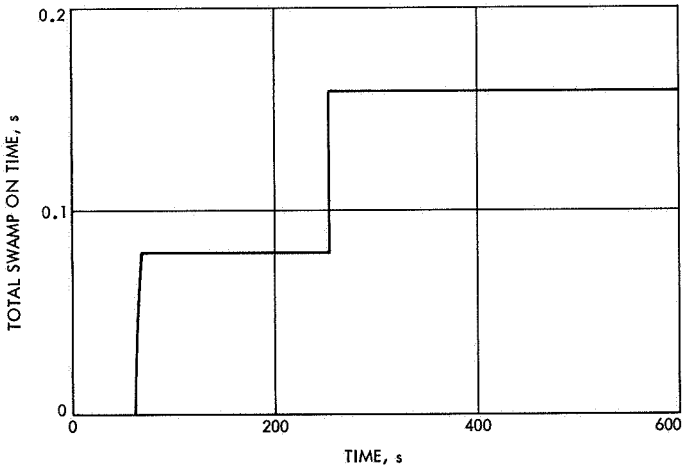

Fig. 13. Roll axis switching amplifier on time (stepping rate of 0.25 deg/s)

(Figs. 11 and 13). A summary of the effects of scan platform stepping motion on the *Mariner* Mars 1971 spacecraft attitude control system is given in Table 4.

d. Conclusion. From the simulation results, it was concluded that the scan platform with a stepping rate of 1 deg/s will require more gas consumption, but less settling time, than the platform with a stepping rate of 0.25 deg/s. In general, neither of the above cases will impose any serious limitation on the *Mariner* Mars 1971 attitude control system.

Table 4. Effects of scan platform stepping motion on attitude control system

Spacecraft axis	Spacecraft position change in orbit	Scan platform position change		Stepping rate, deg/s	Swamp on time, s	Approximate settling time, s	Rate at settling time, μrad/s
		Δ cone, deg	Δ clock, deg				
Roll	1–2	−15	18	1	0.64 (Fig. 11)	130 (Fig. 10)	−16.78
Pitch					2.0	65	−53.30
Yaw					0.8	65	−28.51
Roll	2–3	−16	14	1	0.65	120	−20.20
Pitch					1.97	55	−60.10
Yaw					0.77	55	−22.76
Roll	3–1	31	−32	1	0.73	130	39.61
Pitch					1.87	75	69.80
Yaw					1.51	75	−28.25
Roll	1–2	−15	18	0.25	0.16 (Fig. 13)	270 (Fig. 12)	1.37
Pitch					0.81	90	−31.23
Yaw					0.70	60	−18.06

3. Scan Platform Motion Effects on Attitude Control Gas Consumption

a. Introduction. This article presents the results of an analysis that was made to determine the effects on *Mariner* Mars 1971 attitude control gas consumption from scan platform motion during the orbital phase of the mission. In addition, a reexamination of the gas storage requirements outlined in SPS 37-58, Vol. I, pp. 44–47, was made; these requirements are based on the most current definition of the vehicle configuration and the mission requirements which affect gas consumption.

b. Analysis and results. The various operating modes of the *Mariner* Mars 1971 attitude control system which affect gas consumption are described in SPS 37-58, Vol. I. Through the use of a computer program, described in SPS 37-58, Vol. I, the *Mariner* Mars 1971 attitude control gas consumption was determined for the following revised conditions during the mission:

(1) Initial rate removal: 0.2 deg/s (each axis).

(2) 6 roll searches ($\dot{\theta}_s$ = 3.5 mrad/s).

(3) 50 roll overrides.

(4) 6 acquisitions ($\dot{\theta}_a$ = 3.5 mrad/s).

(5) 2 roll-yaw midcourse commanded turns with unwinds.

(6) 1 roll-yaw orbit insertion commanded turn with unwinds.

(7) 2 roll-yaw orbit trim commanded turns with unwinds.

(8) Total motor-burn duration for maneuvers: 20 min (roll control via gas system).

(9) Roll axis disturbance torque during motor burns: 0.1 in-lb.

(10) Maximum transit cruise duration: 200 days.

(11) Orbital cruise duration: 90 days.

(12) Orbital periods: 12 h (mission A), 32.8 h (mission B).

(13) Stray light operations (roll inertial hold): once per orbit, 3 h in duration (mission A only).

(14) Continuous one-sided disturbance torque: 50 dyne-cm about pitch and yaw, 10 dyne-cm about roll.

(15) Maximum gas valve leakage rate: 3 cm³/h/valve.

(16) Scan platform motion to accommodate a given set of pointing requirements: 10 per orbit.

The following revised inertial properties were used:

Launch-to-orbit insertion, slug-ft²	
I_{xx}	324
I_{yy}	342
I_{zz}	401
Orbital phase, slug-ft²	
I_{xx}	264
I_{yy}	279
I_{zz}	340

The attitude control system parameters are the same as were given in SPS 37-58, Vol. I.

The effect of scan platform motion on attitude control gas consumption is shown in Figs. 14 and 15. These curves, based on an initial storage weight of 5.4 lbs, show the maximum number of scan platform slews (N) (1 slew is motion about both scan clock and cone) as a function of time of a possible half gas system failure (t_f) from launch for mission A and mission B. The data in Tables 5 and 6 were used to prepare the data in Table 7, from which Figs. 14 and 15 were plotted. Table 7 and Figs. 14 and 15 reflect two possible failure conditions at the beginning of the mission. An immediate failure at the beginning of the mission (launch), designated as $t_f = 0^-$, represents the worst possible case in which two-thirds of the initially stored gas (5.4 lb) is lost, leaving 1.8 lb for completing the mission. In this case, as many as 9 scan slews per orbit for mission A and 24 scan slews per orbit for mission B can be guaranteed without any initial sacrifice of redundancy. A second possible failure at the beginning of the mission, designated as $t_f = 0^+$, represents the case in which a failure occurs several days after launch, and after half of the discrete events (initial rate reduction, acquisition, first midcourse maneuver) have been completed. This case, while still considered a failure at the beginning of the mission, leaves somewhat more attitude control gas available for science pointing in that 11 slews per orbit for mission A and 30 slews per

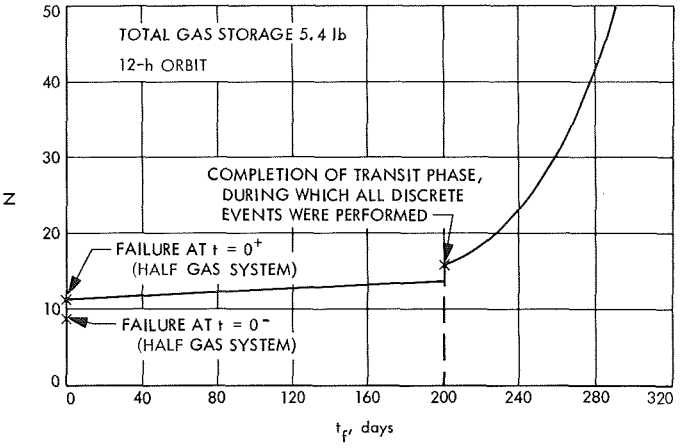

Fig. 14. Number of scan slews per orbit vs time of possible half gas system failure (mission A)

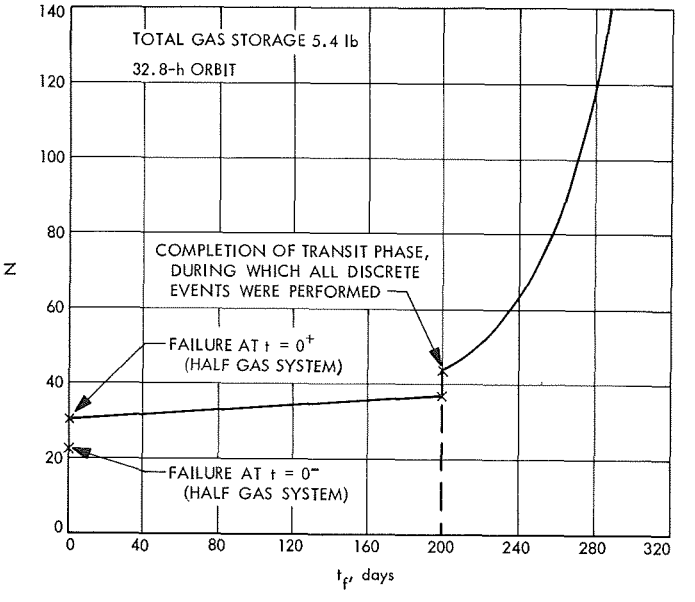

Fig. 15. Number of scan slews per orbit vs time of possible half gas system failure (mission B)

orbit for mission B could be accommodated. In any case, the farther the mission progresses without a failure, particularly after orbit insertion, the greater the amount of gas available to accommodate science pointing.

Figures 16 and 17 show nominal full gas consumption for mission A and mission B. For convenience, gas consumption due to the discrete events is shown initially at day zero. Gas consumption during the 90-day orbital phase is based on 10 scan slews per orbit. Gas consumption for mission A is higher because of the greater num-

ber of scan slews due to the greater number of orbits during the 90-day orbital phase.

c. Conclusion. Gas consumption for mission A and mission B, based on 10 scan slews per orbit, is summarized in Tables 5 and 6. The minimum gas storage for the dual redundant gas system is three times the half gas system consumption. Mission A, which is the worst case, would require an initial storage of at least 3 times 1.88 lb, or 5.64 lb of gas. It is interesting to note that the largest single source of gas consumption in this case is from scan platform stepping (10 slews per orbit). Half gas system consumption for scan platform stepping is 0.708 lb, which means that 2.1 lb of the minimum required initial storage weight is for this function.

The initial gas storage weight for the *Mariner* Mars 1971 attitude control gas system, consistent with safety requirements, is 5.4 lb. This weight of gas represents the maximum storage capability of the existing *Mariner* Mars 1969 tank design. Full redundancy from launch for mission A can only be guaranteed for science pointing operations requiring, on the average, less than 10 scan slews per orbit. If the scan stepping requirements for mission A become more ambitious than 10 slews per orbit, the initial storage capability of these tanks will not be sufficient to guarantee full redundancy from the beginning of the mission (Fig. 14 and Table 7).

With regard to extended mission operations, computed nominal full gas system consumption is 2.46 lb for mission A and 1.93 lb for mission B. This means that, based on an initial storage weight of 5.4 lb, 3.04 lb of gas remain at the end of mission A and 3.47 lb at the end of mission B. Average daily consumptions during the orbital phases of the missions are 0.014 lb/day for mission A and 0.009 lb/day for mission B. This means that under nominal conditions, attitude control could be theoretically maintained for an additional 217 days for mission A and 386 days for mission B.

Table 5. *Mariner* Mars 1971 attitude control gas system requirements for a 12-h orbit mission (mission A)

Events	Full gas system		Half gas system	
	Daily usage, lb/day	Gas weight, lb	Daily usage, lb/day	Gas weight, lb
Cruise				
Limit cycling				
Transit (200 days)	0.00184	0.368	0.00111	0.222
Orbit (90 days)	0.00151	0.136	0.000868	0.0781
Stray light operations	0.000909	0.0818	0.000227	0.0204
Gravity gradient	0.00051	0.0459	0.00051	0.0459
Scan platform stepping (10 slews per orbit)	0.00787	0.708	0.00787	0.708
Leakage	0.00226	0.655	0.00113	0.328
		1.995		1.402
Discrete				
Initial rate reduction		0.00563		0.00563
Acquisitions (6)		0.0264		0.0264
Roll searches (6)		0.0231		0.0231
Roll overrides (50)		0.193		0.193
Roll-yaw commanded turns (6)		0.0770		0.0893
Motor burns		0.137		0.137
		0.462		0.474
		Total 2.46		Total 1.88[a]

[a]Minimum required initial gas storage weight is three times the half system requirement.

Table 6. *Mariner* Mars 1971 attitude control gas system requirements for a 32.8-h orbit mission (mission B)

Events	Full gas system		Half gas system	
	Daily usage, lb/day	Gas weight, lb	Daily usage, lb/day	Gas weight, lb
Cruise				
Limit cycling				
Transit (200 days)	0.00184	0.368	0.00111	0.222
Orbit (90 days)	0.00201	0.181	0.00116	0.104
Stray light operations	0.00	0.00	0.00	0.00
Gravity gradient	0.00051	0.0459	0.00051	0.0459
Scan platform stepping (10 slews per orbit)	0.00288	0.259	0.00288	0.259
Leakage	0.00226	0.655	0.00113	0.328
		1.463		0.959
Discrete				
Initial rate reduction		0.00563		0.00563
Acquisitions (6)		0.0264		0.0264
Roll searches (6)		0.0231		0.0231
Roll overrides (50)		0.193		0.193
Roll-yaw commanded turns (6)		0.0770		0.0893
Motor burns		0.137		0.137
		0.462		0.474
		Total 1.93		Total 1.43[a]

[a]Minimum required initial gas storage weight is three times the half system requirement.

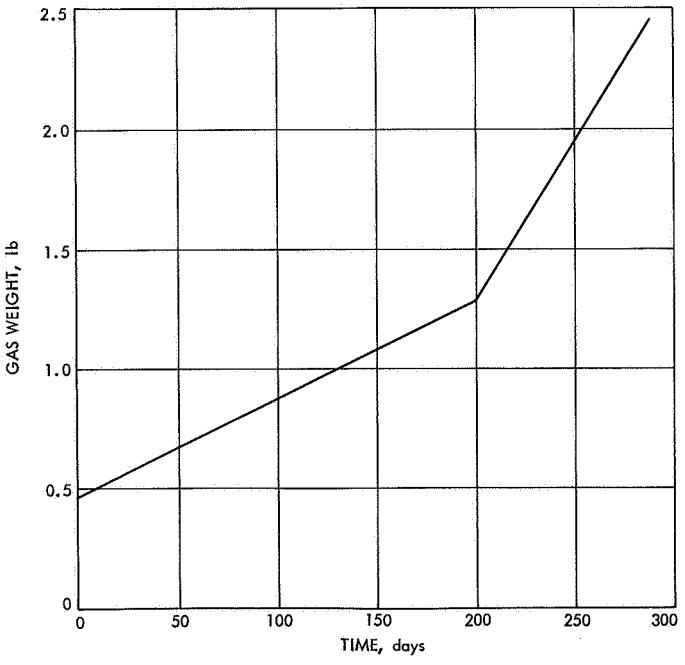

Fig. 16. Total gas weight vs time (mission A)

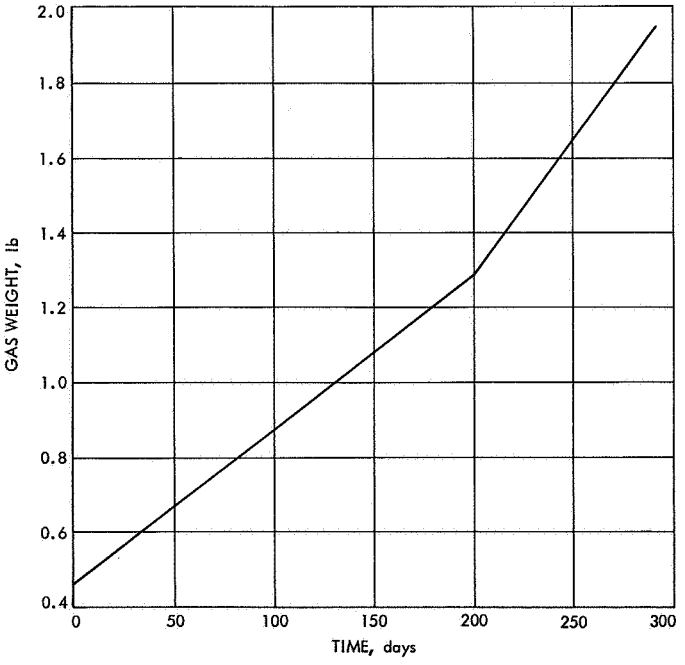

Fig. 17. Total gas weight vs time (mission B)

Table 7. Number of scan slews per orbit[a] as a function of half gas system failure

t_f		0⁻	0⁺	20	40	60	80	100	120	140	160	180	200	200⁺	220	240	260	280	290
N	12-h orbit	8.93	11.19	11.44	11.68	11.85	12.10	12.34	12.59	12.84	13.17	13.41	13.66	15.92	19.03	23.44	31.20	41.88	51.61
	32.8-h orbit	24.17	30.36	31.04	31.71	32.39	33.06	33.74	34.41	35.06	35.76	36.44	37.11	43.30	51.93	64.18	82.98	115.44	142.49

[a]12-h orbit (mission A):

$$5.4 = 0.2311 + 0.0041\, t_f + 3\left[0.2372 + 0.00224\,(200 - t_f) + 90\left(0.002735 + 0.000393\, N \cdot \frac{24}{12}\right)\right], \quad t_f < 200$$

$$5.4 = 0.462 + 0.0041 \times 200 + \left(0.00519 + 0.000393\, N \cdot \frac{24}{12}\right)(t_f - 200) + 3\left[0.002735 + 0.000393\, N \cdot \frac{24}{12}\right](290 - t_f), \quad t_f \geq 200$$

32.8-h orbit (mission B):

$$5.4 = 0.2311 + 0.0041\, t_f + 3\left[0.2372 + 0.00224\,(200 - t_f) + 90\left(0.00280 + 0.000393\, N \cdot \frac{24}{32.8}\right)\right], \quad t_f < 200$$

$$5.4 = 0.462 + 0.0041 \times 200 + \left(0.00478 + 0.000393\, N \cdot \frac{24}{32.8}\right)(t_f - 200) + 3\left(0.00280 + 0.000393\, N \cdot \frac{24}{32.8}\right)(290 - t_f), \quad t_f \geq 200$$

4. Modifications to the Logic Mechanization of the Attitude Control Subsystem

Recently conducted integration tests of the attitude control subsystem have brought to light an anomalous logic state of the subsystem not anticipated during the design phase. The logic equations were modified to correct this condition and the hardware was reworked to reflect the changes to the logic.

The attitude control subsystem is designed to provide gyro damping about the roll axis in the absence of a celestial reference (star Canopus). The acquisition of Canopus (logic condition CA = 1) normally results in shutting off the gyros after a 3-min delay. This is effected through the presence of the $\overline{CA}$ term in the gyro power equation:

$$\text{gyro power} = \cdots + \overline{CA} \cdots \quad (1)$$

The end circuitry in the Canopus sensor, where the CA signal is generated, is shown in Fig. 18. Thus, for CA = 1, the Canopus tracker is in an acquired state and Q1 is off. Conversely, CA = 0 for Q1 on and the tracker is in a nonacquired mode.

Because of the corona breakdown problem, the tracker is turned on some 4 h after launch, which is typically 2 h after sun acquisition. Thus, after sun acquisition the attitude control subsystem logic looking at the CA interface (Fig. 18) sees a de-energized Canopus tracker with Q1 off and the CA line characterized by an impedance of several K to ground. This looks like a "1" input to the Signetics 480J logic integrated circuit. Therefore, the gyros may be shut down prior to Canopus acquisition, contrary to the design intent.

The easiest way of correcting for this anomaly is through modifying the logic. Since it is the attitude control electronics logic that defines the turn-on time of the Canopus tracker, that information can be used to weigh the validity of the CA information, i.e., before the tracker is on the logic can be forced to disregard the state of CA and unconditionally judge Canopus to be not acquired. Only after the tracker is turned on shall the state of CA be judged to contain information. Thus, using the existing logic state of CA_p (Canopus power on), the gyro power equation can be modified to read

$$\text{gyro power} = \cdots + \overline{CA}_p + \overline{CA} + \cdots \quad (2)$$

In Eq. (2), for gyro power to become true (gyros are on) *either* the Canopus tracker power must be off *or* the CA signal must read 0.

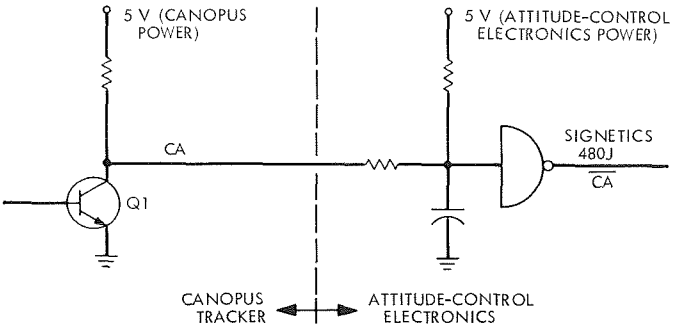

Fig. 18. Initial Canopus sensor/attitude control electronics circuitry

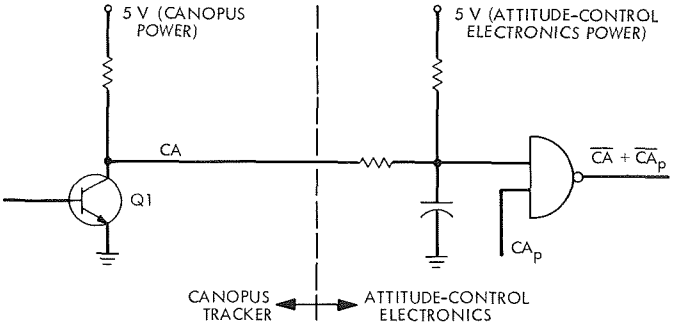

Fig. 19. Modified Canopus sensor/attitude control electronics circuitry

Figure 19 shows the changes made to the circuitry of Fig. 18 to implement the modified logic. The attitude control electronics proof test model was reworked to reflect the changes.

5. Integration Testing of Attitude Control Subsystem

Prior to delivery to the Spacecraft Assembly Facility and at the earliest availability of representative hardware, a series of integration tests are conducted on the attitude control subsystem to verify the following items:

(1) Compatibility of interfaces within the attitude control subsystem.

(2) Phasing of the subsystem, from the sensors to the actuators.

(3) Compatibility of the support equipment with the flight components and the required stimuli (celestial sensor hoods).

(4) An exercising of all elements (including peripheral equipment) at one time to establish confidence in all phases of the flight equipment/support equipment task.

To date in the *Mariner* Mars 1971 program, the first of the integration tests have been performed as follows:

(1) The production prototype attitude control electronics (ACE) was integrated and tested with the lab test set (LTS). All of the support equipment monitors, controls, and testing schemes were evaluated. This is of value since the monitoring and testing schemes implemented on the LTS are identical to the ones utilized in the Spacecraft Assembly Facility testing complex.

(2) The remaining attitude control components were integrated into the ACE/LTS system, one at a time, and its ACE/LTS interfaces was evaluated.

(3) A subsystem test was performed. This test procedure follows the spacecraft flight sequence and the various backup modes for nonstandard operation.

A view of the attitude control subsystem testing area (Fig. 20) includes the LTS, the bay III assembly with the ACE and inertial reference unit, a Canopus sensor, one half of the proof test model gas system, and one gimbal actuator. The sun sensors and the second gimbal actuator, which are normally part of the system, have been released from the test area and were simulated in the LTS for the test. Bay III (without the central computer and sequencer subassemblies) and the Canopus sensor are shown in Fig. 21, and the half gas system and gimbal actuator are shown in Fig. 22.

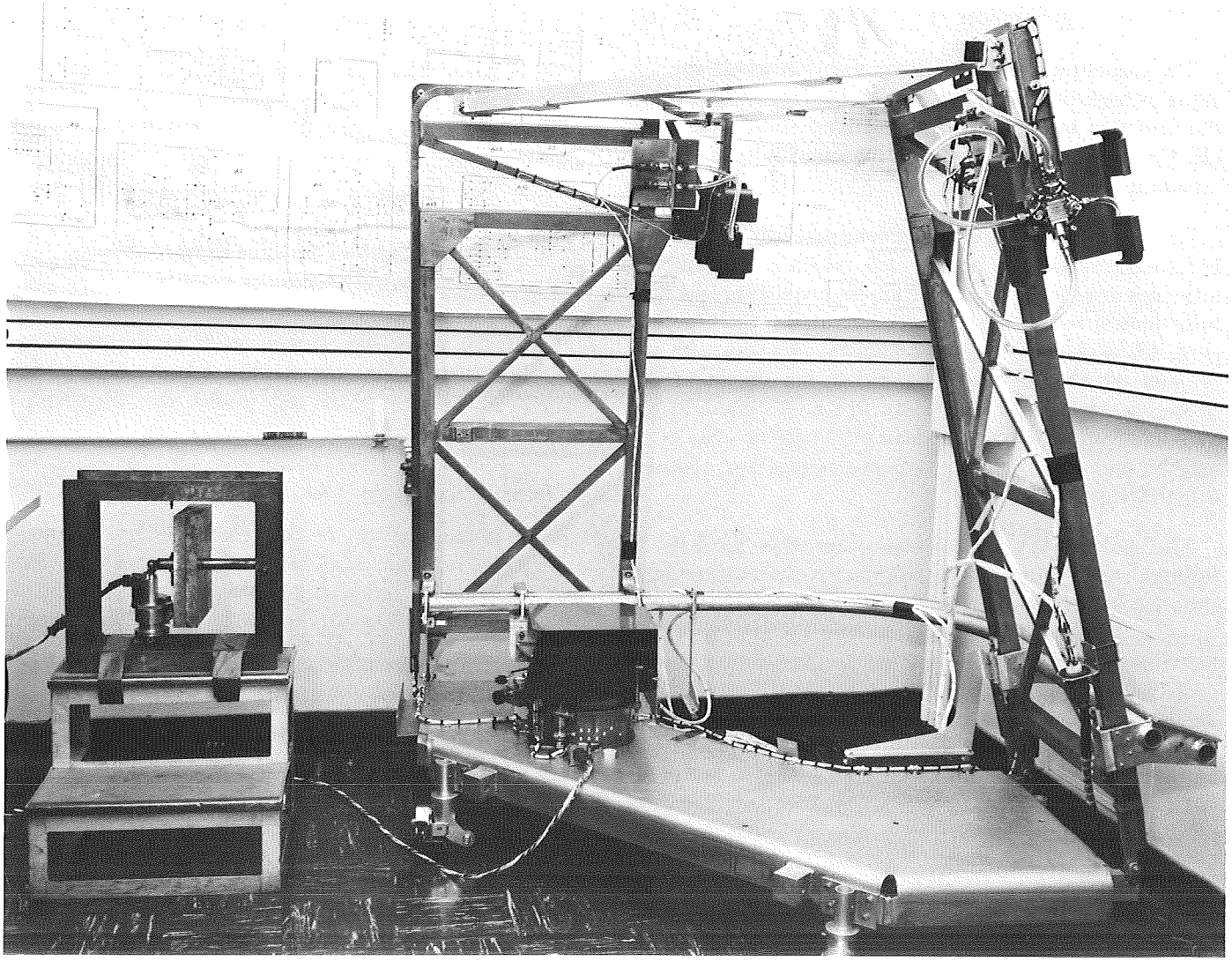

Fig. 20. Attitude control subsystem testing area

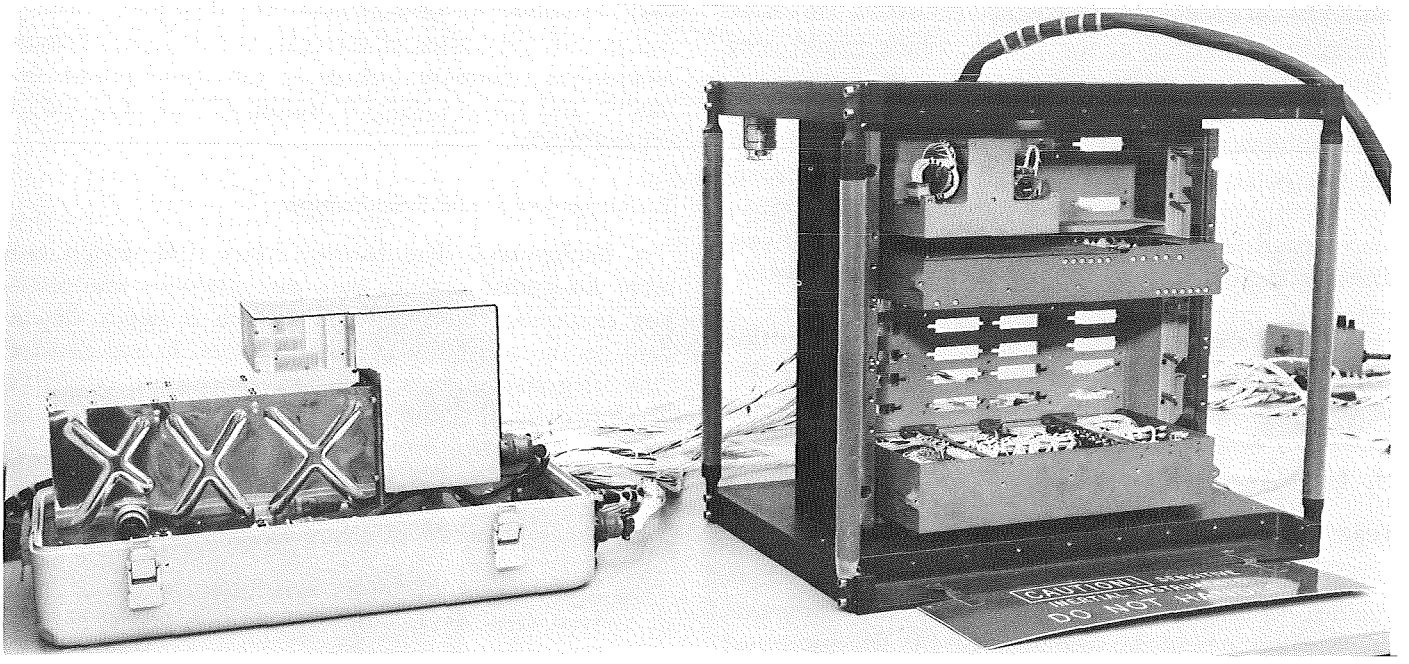

Fig. 21. Bay III assembly (without central computer and sequencer subassemblies) and Canopus sensor

As a result of the first test, some changes have been implemented in the support equipment to improve its compatibility with the flight equipment and its associated stimuli (hoods). Also, a change in the attitude control subsystem logic was made to resolve a discrepancy in the Canopus acquisition signal when the Canopus sensor was not powered. The second integration test, with the proof test model hardware and all the associated flight/LTS changes, is scheduled prior to flight equipment delivery to the Spacecraft Assembly Facility.

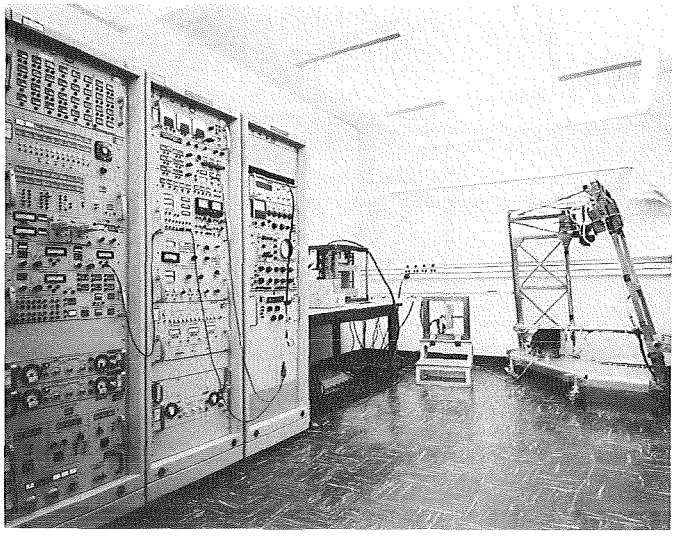

Fig. 22. Half gas system and gimbal actuator

6. Stabilization of the Autopilot in a Nonflight Environment

a. Introduction. Because of the inherent instability of the *Mariner* Mars autopilot (A/P), when operated in a ground environment (open loop), a circuit has been designed and incorporated into the lab and system test sets to stabilize the A/P for test purposes and to prevent driving the engine gimbal actuators to their mechanical stops.

b. Path guidance test stabilization. The portion of the A/P which causes instability in a ground test mode performs the path guidance function in flight. The purpose of path guidance is to correct for offsets of the center of gravity from a line from the aiming point to the center of thrust. The path guidance circuit consists of a positive feedback loop, with a large lag, around the mix amplifier. By integrating the output of the mix amplifier and feeding it back, a bias is introduced in the mixing which compensates for the CG offset and forces the aiming point, CG, and center of thrust to become aligned.

It was decided to correct the instability in the minor loop, rather than simulate a space environment by torquing the gyros. If the latter had been done, there

would be an oscillatory or dynamic condition, contained within the deadband of the system, which would complicate testing.

To stabilize the A/P, a circuit was added to two existing test points, which changes the path guidance feedback from positive to negative. By stabilizing this minor loop, a good deal of complexity is avoided and a static condition is created in the system, which facilitates testing.

Figure 23 shows one axis of the path guidance portion of the A/P and the basic stabilization circuit as mechanized in the system and lab test sets.

D. Engineering Mechanics

1. Introduction

During the reporting period, most of the structure, cabling, and mechanical devices subsystem equipment for the proof test model were delivered to the Spacecraft Assembly Facility. The effort is now concentrated on completion of flight equipment and support of problem areas in the subsystems. The following subsections report activities in procurement of integrated circuits, design and fabrication of the solar panel deploy/damper mechanism, vibration testing of the development test model, and space simulator testing of the temperature control model.

2. Integrated Circuit Procurement

a. Background. The *Mariner* Mars 1971 design uses more integrated circuits than any previous interplanetary spacecraft. Since mission success is highly dependent on the reliability of these devices, it was decided that integrated circuits, with few exceptions, would be purchased by JPL and supplied to the subsystem contractors. A central buy of integrated circuits had the following benefits:

(1) Central control of many mission critical devices.

(2) Procurement of larger quantities of devices per type, resulting in cost minimization and maximization of vendor attention.

(3) Uniform reliability and quality practices for all devices.

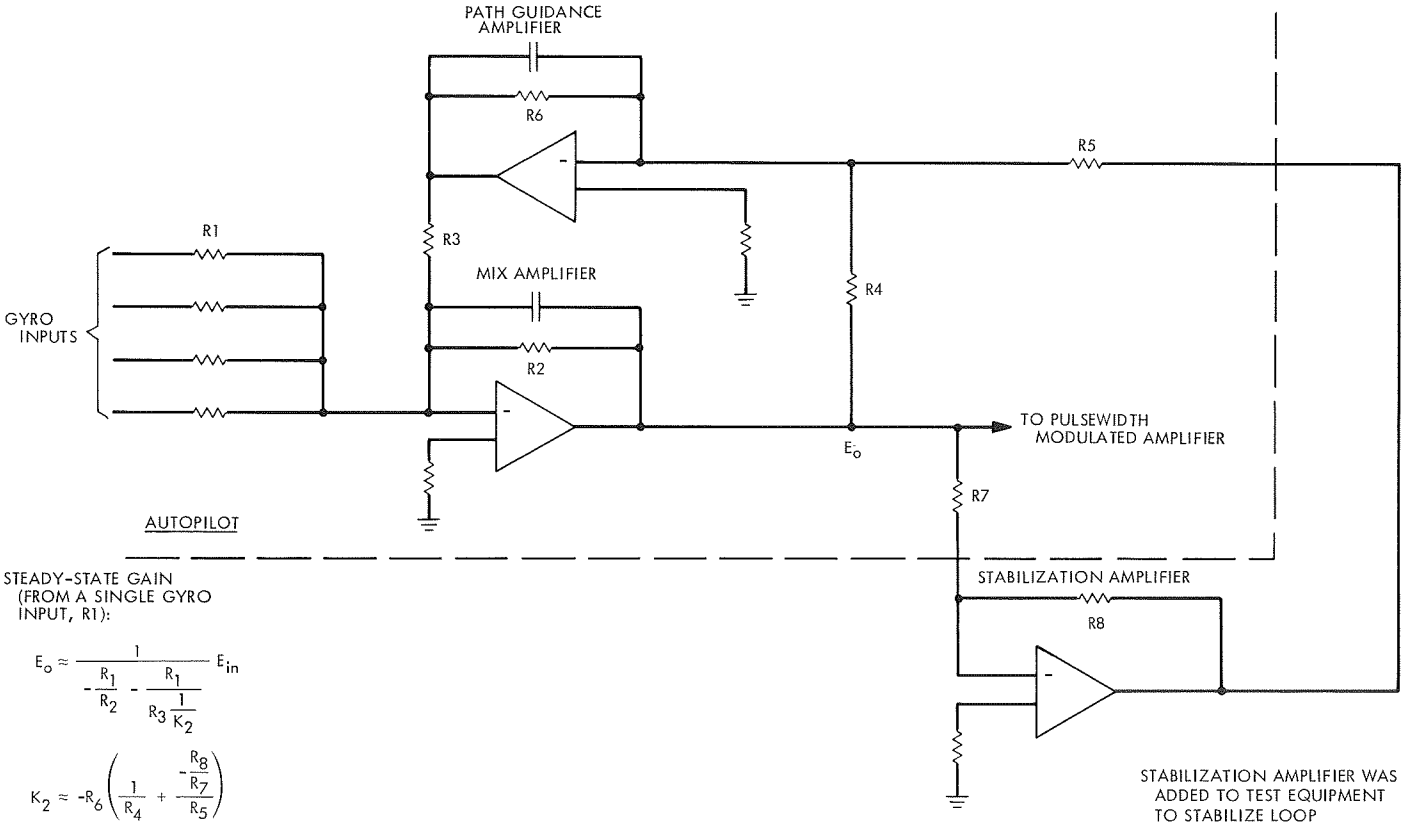

Fig. 23. A/P stabilization implementation

(4) Rapid feedback to project on schedule or reliability problems.

(5) No competing orders for integrated circuits by subsystem contractors.

b. Approach. Integrated circuit procurement specifications defined the performance requirements for the devices and also specified both the environmental and electrical screening regimen to which the devices were to be subjected. In addition, a rigorous 100% preseal visual inspection somewhat more stringent than that of MIL-STD-883 condition A was required.

In general, the devices purchased for *Mariner* Mars 1971 were of a normal commercially available structure but were subjected to special inspections and screens. For the most part, linear integrated circuits were contained in TO-5 type cans and digital circuits were in flat packages. In the case of one digital circuit supplier, a ceramic flat package and aluminum wire internal connections were utilized in lieu of a glass flat package and gold wire interconnects used in normal commercial production. This choice was made to preclude problems observed on previous programs, namely, bond failure due to gold–aluminum intermetallic formation (purple plague) at the silicon die and hermeticity problems due to cracked glass packages.

c. Conclusion. All integrated circuits required for *Mariner* Mars 1971 have been delivered and the majority of the devices have been incorporated into subsystems. Thus far, of the approximately 10,000 integrated circuits delivered, there have been four proven legitimate failures, i.e., devices not destroyed by wiring error, testing error, etc. This incidence of integrated circuit failure is far below that encountered on previous *Mariner* projects at an equivalent stage of maturity.

3. Solar Panel Deployment/Damper Mechanism

a. Introduction. The positioning of the solar panels on outriggers and the reorientation of the rocket engine thrust vector necessitated a redesign of the solar panel deployment and damper mechanism for *Mariner* Mars 1971. Unlike previous *Mariners* (1964, 1967, and 1969), where the rocket engine thrust vector was approximately parallel to the plane of the deployed solar panels, the *Mariner* Mars 1971 spacecraft is configured with the rocket engine thrust vector perpendicular to the plane of the deployed panels. As a result of this reorientation, a torque of 360 in.-lb (corresponding to 1/4 g) can be generated about the solar panel hinge axis during engine firing. The resulting torque tends to rotate the panels to the launch configuration. A latching mechanism had to be designed which would accommodate the panel loads and remain insensitive to panel deflections. The geometry and mounting restrictions imposed by positioning the solar panels on outriggers also called for significant design changes.

b. Description. One deployment/damper mechanism is positioned on each outrigger inboard of the solar panel hinge axis (Fig. 24). The axis of rotation of the mechanism is parallel to that of the solar panel. The asymmetric bolt pattern in the base of the mechanism matches a press nut pattern on the side of each outrigger. This arrangement greatly simplifies installation and removal. A turnbuckle, with monoballs at each end to accommodate misalignments, links the mechanism to the solar panel and provides a simple means of adjusting the cruise position of the panels after they are installed. The latch portion of the device consists of two spring-loaded, tapered, stainless steel pins which mate with two similarly tapered holes in the spring arbor.

Basically, the mechanism is a rotary-vane-type dashpot with separate springs for the deployment and cruise functions (Figs. 25 and 26). Although solar panel damping is only required during the cruise and orbit insertion phases of the mission, it would have been very difficult to separate the damping from the deployment phase. Consequently, a damping force is generated throughout the cruise and deployment phases. This functional characteristic, however, permits the use of a high-energy deployment spring without introducing the problem of absorbing excessive kinetic energy at the end of the deployment cycle. The mechanism also incorporates a means of monitoring latch engagement.

c. Damping. The viscous damping for the device is obtained by forcing silicone oil (200,000 centistokes) through two segments of a cylindrical annulus. The annulus, as defined by the integral vanes of the stationary rotor and the inside diameter of the stator, has a radial clearance of 0.030 in. The damping constant for the mechanism varies linearly with the viscosity and, as an approximation, inversely with the cube of the radial clearance. An attempt was made to keep the annular clearance as large as possible to minimize the effect of dimensional variations. The primary restriction on this approach was that the required viscosity be obtainable in a readily worked fluid. The solution of a 0.030-in. gap

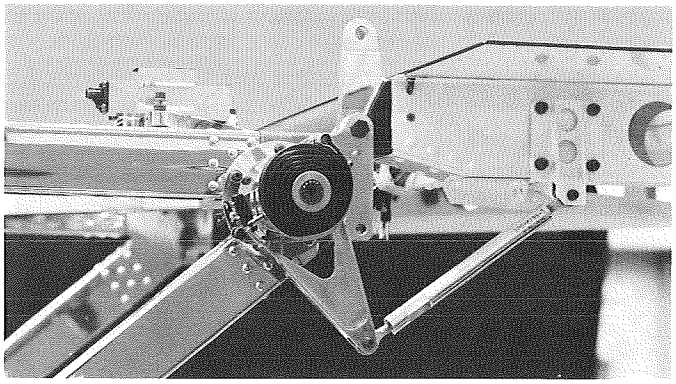

Fig. 24. Deploy/damper mounted to outrigger in panel deployed position

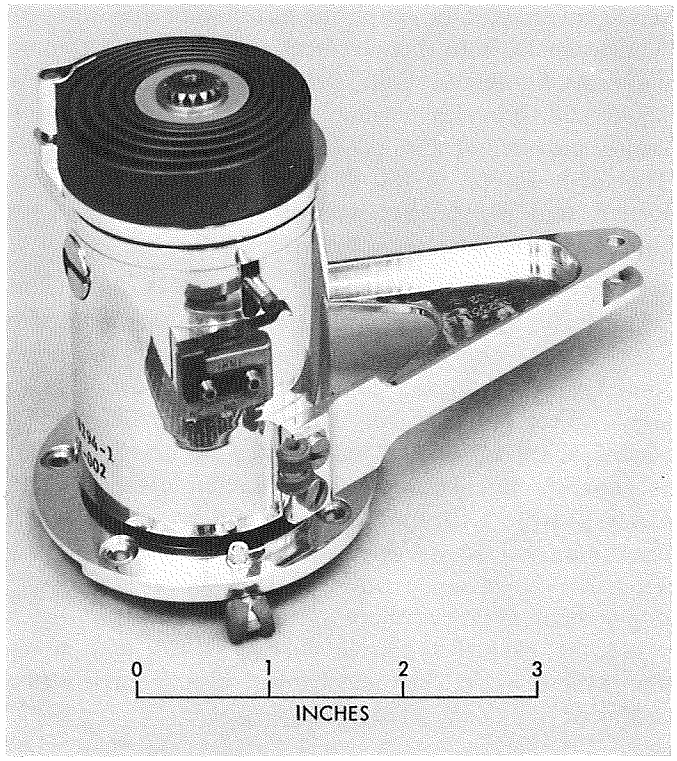

Fig. 25. Panel deploy/damper mechanism

with a 200,000-centistoke fluid is very satisfactory. All other clearances within the mechanism are held to 0.003/0.005 in. to minimize leakage away from the working annulus. The damping constant for the mechanism is calculated to be 33 in-lb-s. Tests were run on a prototype unit and four flight units by applying a constant torque to the devices and computing the average velocity through seven 10-deg increments. The experimental values were very closely grouped about 31 in.-lb-s/deg.

d. Deployment. The presence of viscous damping during the deployment cycle permits use of a high-torque deployment spring to overcome the initially small mechanical advantage and any inherent friction. The ratio of torque-in at the mechanism to torque-out at the panel axis varies from approximately ⅓ in the stowed position to one in the fully deployed position. The *Mariner* Mars 1969 outset deployment torque was on the order of 20 in.-lb. With this reference point, a clock spring with a maximum torque of 80 in.-lb was designed to supply the deployment energy. Because of the geometry factors, the initial deployment torque on the panel is 26 in-lb. In the interest of efficiency, weight, and reliability, a high-strength 18% nickel maraging steel was selected for the spring material. The deployment spring, through a hole in the inner leaf, is held in place by a dowel pin pressed into the spring arbor. The torsion bar (used as the damping spring during cruise) is one thousand times stiffer than the deployment spring, so the series spring arrangement has a negligible effect on the available deployment torque. As the panel deploys, the decreasing deployment torque is offset by the increasing mechanical advantage of the linkage.

Attention was given to reducing friction at all moving points in the system. All surfaces of the finished deployment spring were electrofilmed to reduce sliding friction between adjacent segments. The two dynamic seals in the mechanism are Teflon omniseals impregnated with molybdenum disulfide to reduce breakout force and slid-

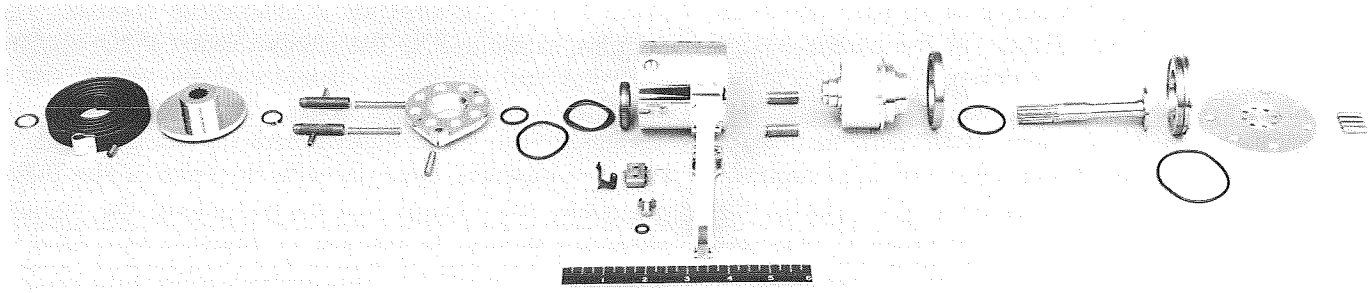

Fig. 26. Panel deploy/damper mechanism (exploded view)

ing friction. The mechanism itself rotates on two high-precision ball bearings which are contained within the working fluid. Since there is an area imbalance between the two ends of the mechanism, the larger bearing is an angular contact bearing to react the thrust loads which arise as the internal pressure increases. The hinge points on the turnbuckle and solar panel are fitted with close-tolerance electrofilmed bolts.

Numerous tests have shown that the panel rotates through 105 deg (a 75-deg rotation of the mechanism) in 30 s. The deployment and latching are very smooth with very little over-shoot after lock-up.

e. Latching mechanism. The latch within the mechanism has two functions: (1) lock the panels in the cruise position to prevent catastrophic refolding during engine firing; (2) link the cruise spring (torsion bar) in parallel with the dashpot portion of the mechanism. The latch consists of two spring-loaded, tapered steel pins housed in cylindrical cavities within the stator. The pins ride against the spring arbor, which is splined onto the torsion bar and held in place by snap rings. The sliding ends of the lock pins are tipped with Vespel SP-3 to reduce friction; the surface of the spring arbor is stabilized with an anodic coating. In addition to its excellent machining characteristics, the Vespel has demonstrated outstanding wear resistance under the 4- to 5-psi spring loads. The lock pins, except for the tapered surfaces, are electrofilmed.

As the device rotates to the cruise position, the lock pins are seated into matching tapered holes in the spring arbor by the force of the latch compression springs. The motion of one of the lockpins is monitored by a microswitch. In addition to actuating the microswitch, the retraction pins permit disengagement of the lock pins and recocking of the mechanism. Prior to final assembly, the lock pin holes are line-drilled and positioned such that the internal vanes are 2 deg from bottoming at final lock-up. The 2-deg back step protects the latch and torsion bar from accidental overload in this direction. The Vespel tips of the pins are allowed to protrude through the spring arbor so that these pads are not subjected to bearing loads. The engagement of one pin is sufficient for latching. Throughout the course of testing, the latch has worked smoothly and flawlessly.

f. Cruise. When the device is latched, the damper and the torsion bar are linked in parallel. The torsion bar is 17-4 Ph stainless steel in the H900 condition and is attached to the base plate by four dowel pins. The bar is splined to mate with the broached spring arbor. The stiffness of the torsion bar is 260 in.-lb/deg, which gives a panel undamped natural frequency of approximately 1.3 Hz (minimum allowable, 1 Hz). The required panel damping is a critical damping ratio of 0.20 or greater, with the added restriction that any pair of devices on a common axis be matched within an absolute difference of 0.3. A design goal of 0.5 was set so that temperature variations would not lead to unacceptable performance.

Two bellows are used to compensate for changes in volume of the damping fluid with temperature. These compensators are housed in holes in the vanes of the rotor. The bellows are evacuated and sealed so that the only spring force available is that of the bellows itself. As a result, the bellows can be set by atmospheric pressure to provide compensation over a temperature range of approximately 110°F. The limits of this range can be varied by altering the temperature at which the mechanism is filled and sealed. A bellows can be checked for leakage by simply checking the length of the compensator in 1 atm.

Although the damping constant for several devices has fallen very close to the design goal, the desired damping of 50% of critical for a solar panel has proved to be quite elusive. It is important to remember that the damping constant for the device was an average computed over the full stroke of the mechanism while solar panel damping takes place at the end of travel where the amplitude is on the order of 2 or 3 deg. Early tests with the panel hinge axis vertical to eliminate gravity effects gave critical damping ratios of 0.45 to 0.50 in excellent support of the design goal. Further tests with the hinge axis horizontal and the mechanism-panel system tilted 14½-deg off vertical to simulate a 1/4-*g* impulse, however, gave critical damping ratios on the order of 0.15 to 0.25. A decrease of this magnitude cannot be attributed to the pendulum effect. Incomplete filling with the subsequent formation of a void or entrapment of air is felt to be responsible. It should be noted also that the orientation of the vanes in the 1/4-*g* test is such that a void or bubble would be particularly damaging—the "bubble" would form over the surface of one of the vanes. Refined vacuum filling techniques have resulted in values of 0.30 to 0.34 in the 1/4-*g* simulation test. Testing is being continued with attention being given to pressure filling, bellows interaction, and higher viscosity fluids.

4. Developmental Test Model Forced Vibration Test

a. Test objectives. The primary purposes of the developmental test model (DTM) forced vibration test program were:

(1) To obtain dynamic response information for correlation with the analytical results obtained from the spacecraft composite analysis.

(2) To verify the structural adequacy of the *Mariner* Mars 1971 DTM when subjected to qualification and design-ultimate load levels.

(3) To develop test control techniques, including load suppression, and test procedures required for future system level tests.

(4) To investigate the effects of varying propellant tank pressures on the response characteristics of the structure.

b. Level of testing. The DTM was subjected to sinusoidal vibration at frequencies between 5 and 2000 Hz (Table 8). Approximately 77 test runs and 15 working days were required to implement the schedule.

c. Test control. Control of the input acceleration level was accomplished with a 12-channel "peak select" system. The amplitudes of the control points were sampled by an automatic sensing device. The device selected the maximum acceleration and controlled it to the specified test level.

Verification of control levels was provided by O-graph plots and a near-real-time computer printout. The computer printed the frequency and amplitude of the control channels, identified the controlling accelerometer, compared its reading with the specification level, and printed the deviation.

d. Test configurations. The typical DTM configuration for all axes of low-frequency testing plus Z-axis high-frequency testing is shown in Fig. 27. The DTM was mounted on its adapter with a flight type V-band. The entire assembly was then mated to the *Centaur* adapter and mounted on the appropriate shake fixture. The lateral-axis high-frequency testing was accomplished *without* the *Centaur* adapter.

The DTM propellant tanks were filled with referee fluids. The oxidizer tank was loaded with freon TF to an

Table 8. DTM vibration test levels

Test loads category	Test axis	Test loading, g rms			
		5–120 Hz	120–250 Hz	250–400 Hz	400–2000 Hz
Low-level checkout	Lateral (XY, −XY)	0.25	0.25	1.00	1.00
	Axial	0.25	0.25	1.00	1.00
Flight-acceptance test	Lateral (XY, −XY, Y) (XY) (−XY)	0.50	12 dB/octave	12 dB/octave 12 dB/octave	2.0[a]
	Axial	0.50	12 dB/octave	12 dB/octave	5.5
Type-approval test	Lateral (XY, −XY, Y)	0.75	12 dB/octave		
	Axial	0.75	12 dB/octave		
Design-ultimate test	Lateral (XY, −XY)	0.90			
	Axial	0.90			

[a]Abortive flight-acceptance-test attempts—shaker system capability limited.

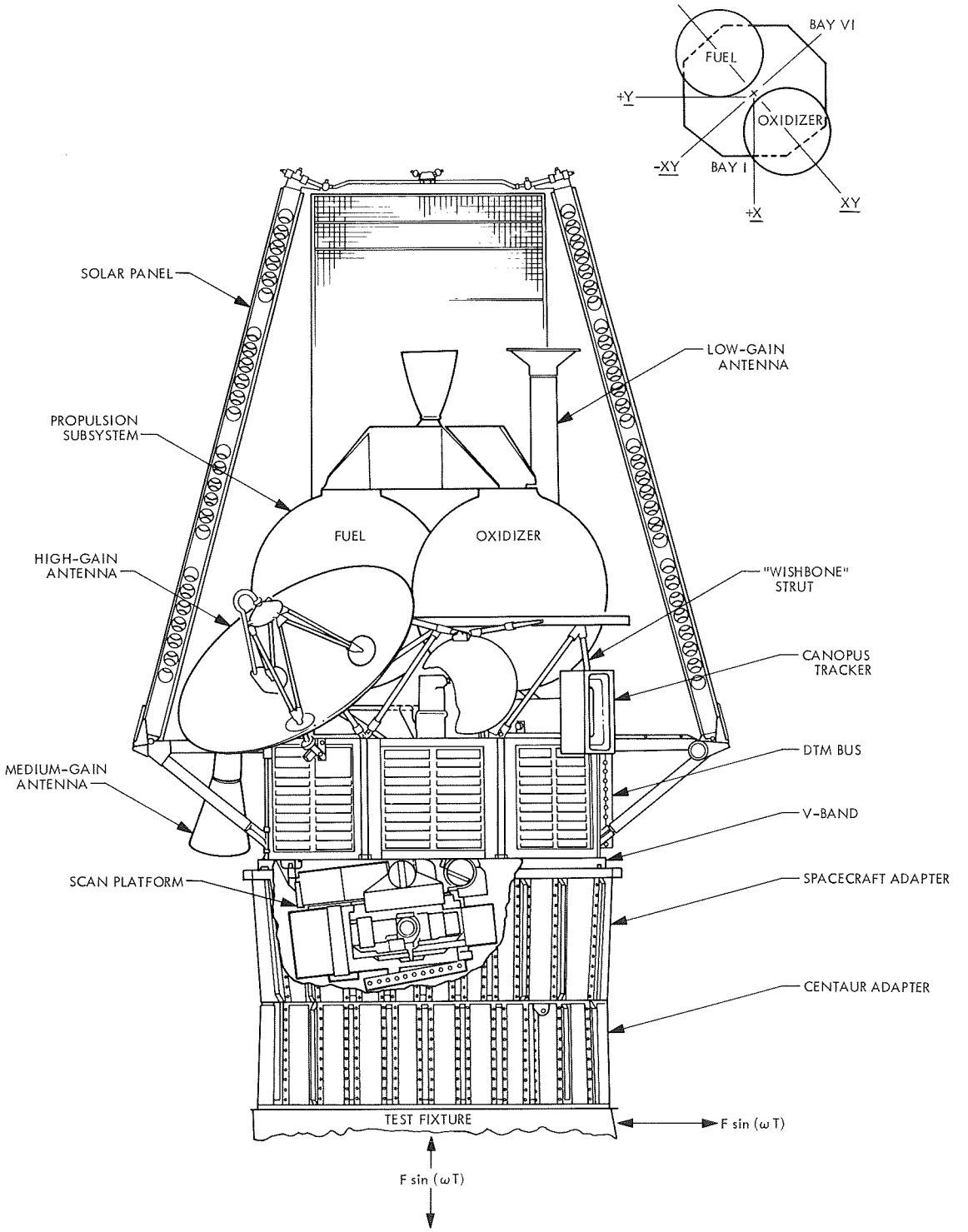

Fig. 27. DTM low-frequency Z-axis high-frequency test configuration

ullage of 9.8%, while the fuel tank utilized alcohol with an ullage of 5.0%. The ullage for both tanks was *outside* the bladder. The tanks were pressurized to 50 psig for all qualification and design-ultimate test runs.

e. Instrumentation and data reduction. Control and response accelerations of the test structure were measured with piezoelectric accelerometers. Dynamic loads were obtained with strain gages located on the spacecraft adapter, the beryllium support truss, propellant tank tabs, and on one set of solar panel dampers.

The signals of approximately 24 strain gages and 50 accelerometers were recorded on electromagnetic tape during the low-frequency test runs. Over 70 accelerometers were recorded for the high-frequency test runs. During the low-frequency test run, 12 channels of dynamic strain from the truss and adapter and 12 channels of acceleration from the control and response limit system were displayed in real time on oscillographs and visually monitored for anomalies. Selected channels of dynamic strain and response limit acceleration versus input acceleration were hand-plotted immediately after each test run. These plots were then compared to analytically derived predictions. In this manner, the allowable rms acceleration values used to limit the response of the spacecraft were predetermined.

f. Results. The primary structural response frequencies agreed well with the analytically predicted values. A summary of the major structural frequencies is presented in Table 9. Due to the damping characteristics of the test configuration, response limiting of the DTM was not required—even for design-ultimate input levels. A plot of adapter strain versus input acceleration (Fig. 28) shows typical DTM system behavior.

During the Z-axis type-approval downsweep, the upper magnesium fitting of the oxidizer tank "wishbone" strut fractured. Metallurgical examination revealed that the failure was of a fatigue nature. Dye-penetrant[3] examination of the failed fitting's counterpart 180-deg away was inconclusive. The strut assembly with the fractured fitting was, therefore, replaced and type-approval and design-ultimate testing completed. Disassembly of the subsystem, following the high-frequency and acoustic testing, revealed tightly closed cracks in the fittings of *both* wishbone struts.

[3]The "wishbone" magnesium fittings and other accessible fittings were penetrant-examined after each phase of testing, including high-frequency and acoustic. Results were inconclusive.

Table 9. DTM major structural frequencies

Test axis	Approximate frequency, Hz	Remarks
+XY	17.0	First bending about −XY axis
−XY	23.0	First bending about +XY axis
Y	15.0	Bending about −XY axis
Y	22.0	Bending about +XY axis
Z	28.0	Oxidizer tank bounce
Z	36.0	Fuel tank bounce

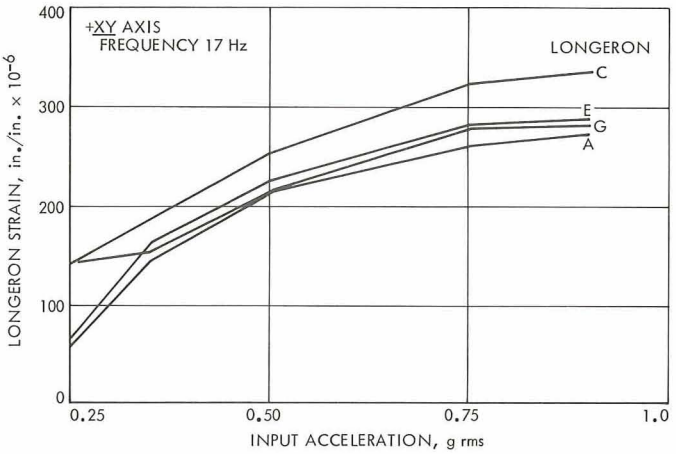

Fig. 28. Adapter longeron strain vs input acceleration

g. Conclusions. Results of the DTM forced vibration test indicated that:

(1) The *Mariner* Mars 1971 DTM structural adequacy for exposure to qualification and design-ultimate sine sweep loads was partially verified.

(2) The DTM configurations tested displayed sufficient damping at type-approval and design-ultimate load levels[4] so that response limiting was not necessary.

(3) The test control method and test procedures would be adequate for future system level tests for the same propellant tank ullage configurations.

(4) Varying tank pressure from 100 to 50 psig had no apparent effect on the response characteristics of the structure.

(5) Correlation of test results and analysis was reasonable. Slosh damping was higher than anticipated.

[4]The propellant tanks were ullaged *outside* the bladder.

5. Temperature Control Model Testing

a. Introduction. The *Mariner* Mars 1971 temperature control model (TCM) test was completed on March 17, 1970, after approximately two weeks of testing in the 25-ft space simulator (Fig. 29). The test was performed in three phases of roughly equal duration, each requiring a pumpdown/warmup cycle of the simulator and each separated by an average chamber-open period of 21 h.

The primary objectives to be met with the TCM test were (1) verify the thermal design of the spacecraft (with an iterative test-modify procedure if necessary), (2) in the time allotted, gain as much insight as possible into the thermal interactions between individual spacecraft components and the thermal behavior of the spacecraft as a whole, and (3) obtain data under good vacuum conditions of the effect of a simulated rocket engine burn on the rest of the propulsion module.

The thermal design was verified by testing two internal power state/solar intensity combinations specifically designed to bracket all mission conditions of thermally significant duration. The results indicated that, with only superficial design changes to the temperature control subsystem, spacecraft temperatures could be maintained within acceptable limits throughout the mission.

The several parametric modes that were tested yielded valuable data concerning the coupling between the upper propulsion module and the bus, the solar sensitivity and power sensitivity of the total spacecraft, the thermal influence of the solar panels, and the effect of scan platform articulation through the full cone angle range. Data was also obtained regarding power and/or solar sensitivities of various science instruments, electronic bays, and appendages (sun sensor/sun gate package in particular).

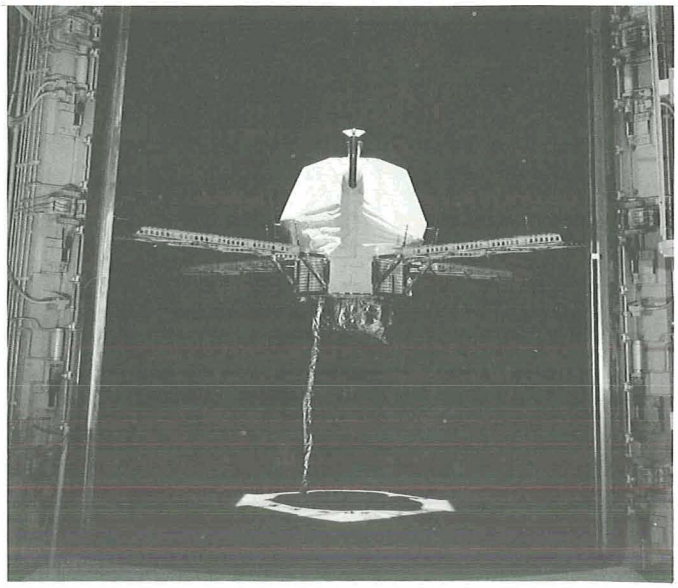

Fig. 29. TCM in 25-ft space simulator

Three simulated engine firings were performed: one nominal, one conservative (twice the total nominal energy applied to the thrust chamber), and one performed in a 6-torr environment to simulate a test firing under Edwards Test Station (ETS) conditions. The data indicated that a nominal soakback is much less severe than the ETS data for actual test firings.

b. TCM description. The TCM is a full-scale mockup of the flight spacecraft with particular attention given to duplication of significant thermal paths (conductive and radiative), significant internal radiation blockages, external configuration, and surface thermo-optical properties. The most significant difference between the TCM and the flight spacecraft is that the TCM contains no electronics subassemblies. The subassemblies in the bus are simulated by aluminum plates equipped with controllable resistive heaters. These plates are mounted to the radiating surfaces (shear plates) in each bay in the same manner as are the flight electronics modules (i.e., identical bolt patterns and torques). The use of simulated electronics modules allows for direct control and accurate measurement of power dissipation, less transient test time as a result of the reduction in thermal mass, and a more flexible test capability without the restrictions related to electronic component survival.

The TCM solar panels were full-scale mockups consisting of flightlike spar structures with rigid area heaters replacing the cell/substrate portion of the panel. Since the panels for the most part were not illuminated by the 8-ft-diameter beam, their temperatures could be controlled by means of the area heaters only and were not dependent on the solar intensity level.

The flightlike rocket engine used for the TCM included a specially constructed thrust chamber made from mild steel and equipped with 12 high-wattage electrical heaters of the cartridge type. The thermal mass of this thrust chamber was identical to the flight beryllium chamber to provide an accurate engine burn soakback simulation.

c. Discussion of results. The TCM test was performed in three phases with modifications made to the thermal design between each phase. The data listed in Table 10 for the cold, nominal, and hot verification modes was obtained in phase II after several changes had been made to the baseline design tested in phase I. The more significant modifications were (1) louvers were installed on bay III in place of the polished aluminum shield, (2) PV-100 white paint was applied to the TV-A optics housing and the TV-B camera head, then cutouts were made in the platform thermal blanket to expose appropriate areas of the white paint, and (3) cutouts were made in the upper thermal blanket above the high-gain antenna near the fuel propellant isolation assembly.

Bus/propulsion module. It was originally feared that the upper propulsion module and the bus would be so decoupled from one another that the upper module would become overly sensitive to small variations or uncertainties in either heater power or thermal blanket properties. Test results indicate that the two are relatively well coupled (approximately ⅔ W/°F) and that the maximum differential between the average bus temperature and the average tank top temperature should be no greater than 15°F for the quasi-steady-state portions of the mission.

Solar inputs at earth were found to be about 24 W in the propulsion module and an additional 36 W in the bus for a spacecraft total of 60 W. Although the solar input to the upper propulsion module was somewhat greater than expected, the sensitivity of the upper module was sufficiently low (about 1.5°F/W), due to the good coupling with the bus, that the temperature change over the mission as a result of the variation in solar intensity would be approximately 21°F without the 10-W propulsion module heater and 15°F with the heater (both assuming a constant bus temperature). In reality, the good coupling between the upper module and the bus causes the module to track the bus on a slightly less than 1 for 1 basis (i.e., 1°F change in the bus causes approximately a 0.8°F change in the upper propulsion module).

The characteristic temperature versus power curve for the total bus is shown in Fig. 30. The effectiveness of the louvers in attenuating the bus power sensitivity is clearly shown. Figure 30 assumes 6 bays equipped with "standard" louvers (55 to 82°F range). The possibility exists that, to depress the battery temperature, the Bay 8 louvers might be recalibrated to drop the range approximately 15°F. This would have slight effect on the characteristic curve shown in Fig. 30.

Table 10. TCM test results

Assembly	Temperature, °F		
	Cold mode	Nominal mode	Hot mode
Bay I (power)	63	70	87
Bay II (power/IR interferometer spectrometer/scan)	64	70	96
Bay III (central computer and sequencer and attitude control)	64	70	100
Bay IV (flight control subsystem/flight telemetry subsystem)	60	79	103
Bay V (data storage subsystem)	50	66	85
Bay VI (radio frequency subsystem)	56	80	118
Bay VII (data automation subsystem/TV)	39	62	94
Bay VIII (battery)	39	71	85
Canopus tracker	44	76	96
Clock motor	49	68	111
Bipropellant valve	63	110	126
Pressurant tank (Bay I/V)	47/48	69/70	92/96
Propellant tank (fuel/oxygen)	50/48	73/72	95/94
Maximum propellant tank gradient	9	7	6
Thrustplate	52	75	96
Low-gain antenna	2 to 41	85 to 101	102 to 106
High-gain antenna dish	15 to 54	122 to 176	123 to 178
Medium-gain antenna	−30 to 5	37 to 71	54 to 89
Solar panel damper (Bay III)	15	86	98
Cruise sun sensor/sun gate	14	98	102
Cone actuator	39	—	64
IR interferometer spectrometer optics	−11	—	−13
IR interferometer spectrometer base	29	—	67
TV-A vidicon	29	—	68
TV-B vidicon	41	—	74
Maximum TV-B optics gradient	3	—	1
IR radiometer	0	—	47
UV spectrometer	29	—	56

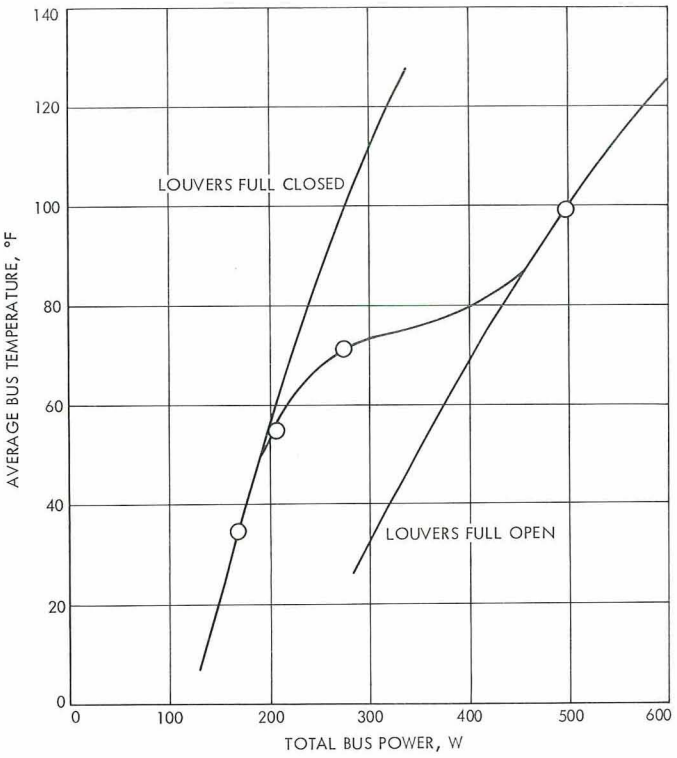

Fig. 30. Average bus temperature vs power (electronics and absorbed sun)

The total contribution of the solar panels to the heat balance of the bus/propulsion module is very small, perhaps 5 W total.

Figure 31 presents partial results of a simulated nominal engine burn and consequent soakback. For a basis of comparison, the bipropellant valve temperature recorded during an actual 15-min firing (test DD-405 at the Edwards Test Station) is included. The test DD-405 data has been normalized to the same initial temperature and shifted 15 min along the time scale to account for the difference in heating rates between the actual firing and the TCM-simulated firing.

Scan platform. The scan platform characteristic curve is shown in Fig. 32. Although the platform half-set of louvers is calibrated to open at 0°F and be fully closed at 30°F, the large thermal resistances within the blanketed platform cause the louver actuators to sense a temperature that is considerably lower than the average platform temperature. As a result of this temperature differential, the louvers open at an average platform temperature of approximately 7°F, and are fully closed at an average platform temperature of 60°F.

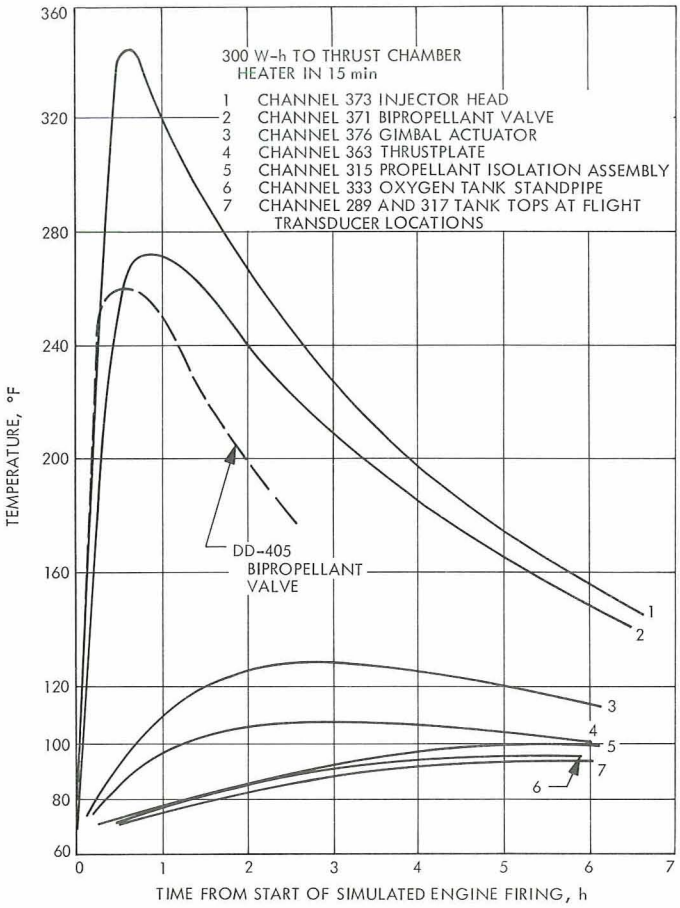

Fig. 31. TCM rocket engine nominal thermal soakback data

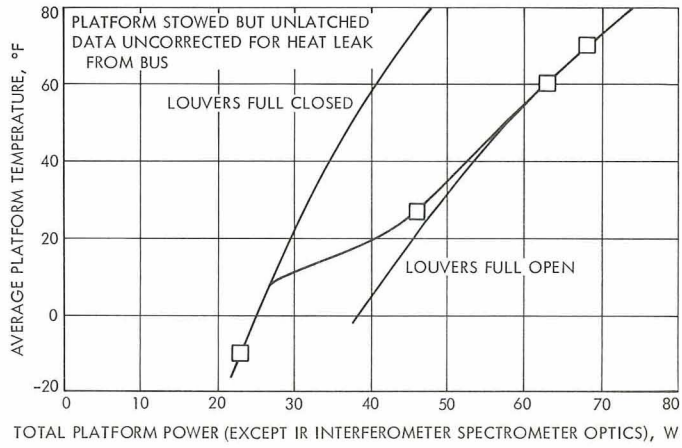

Fig. 32. TCM scan platform thermal performance

Within ±20 W of the science-on operating point, which is near the point at which the louvers are full open, the power sensitivity of the total platform remains

relatively constant at 2°F/W. The data indicates that each individual instrument's sensitivity to changes in its own power varies from about 9°F/W for the IR radiometer to approximately 4°F/W for the UV spectrometer. The TV sensitivities are about 6 and 7°F/W for the B and A camera heads, respectively. IR interferometer spectrometer sensitivity data was inconclusive due to an apparently large thermal resistance between the base and the perch tube mounts. All of the instruments except the IR radiometer have sensitivities to platform power variations external to themselves of about 1°F/W. The IR radiometer sensitivity to external changes is closer to 2°F/W.

Based on a determination of radiant inputs to the platform from the solar panels, the effect on the average platform temperature over the entire mission is expected to be less than 3°F. The effect of dropping the platform from the stowed/unlatched position to the full-cone position is greatest (5°F) with science on at Mars.

Appendages. The test data indicates that the sun sensor/sun gate heater is not required for the primary mission. Without the heater, the sun sensor/sun gate package becomes almost entirely sun-dependent due to the intentionally poor conductive coupling with the outrigger.

The solar panel cruise dampers are significantly coupled to the bus through the outrigger, thereby reducing the damper solar sensitivities to approximately 1°F/W/ft^2.

d. Impact of results on spacecraft design. Based on TCM test results, the following changes to the *Mariner* Mars 1971 baseline design are necessary:

(1) Replace the bay III polished aluminum shield with a standard louver set.

(2) Increase the emittance of the TV-B camera head and TV-A optics housing, preferably with the application of PV-100 white paint.

(3) Incorporate cutouts in the platform blanket to expose approximately 23 and 20 in.^{2} of this white paint on TV-A and B, respectively.

(4) Modify the upper thermal blanket to increase the effective emittance in the vicinity of the thrust plate.

(5) Size the TV-B optics heater to dissipate 10 W at 45 V.

Optional changes to the baseline design are:

(1) Delete the platform heater (5 W).

(2) Delete the sun sensor/sun gate heater.

(3) Install nonstandard louvers on Bay 8 to depress the long-term battery temperature.

The thermal resistance between the IR interferometer spectrometer electronics base and the perch tube mounting pads was found to be much greater than expected. As a result, the amount of replacement power (applied to the mounts) required to maintain the temperature of the base within limits was correspondingly greater. The anomalous nature of this high resistance is being investigated.

E. Propulsion

1. Propulsion Subsystem Sequence Failure Mode Analysis

a. Introduction. The *Mariner* Mars 1971 propulsion subsystem must perform a midcourse maneuver near earth and four or more maneuvers near Mars (Table 11). The propulsion subsystem has an electrically operated bipropellant valve and a gaseous nitrogen pressure regulator which nominally prevent fluid leakage during nonfiring periods. Concern over the possible leakage of these components during the 6-mo duty cycle caused three groups of pyrotechnic-actuated valves to be placed in the system. For a nominal sequence, the first midcourse maneuver and the four maneuvers near Mars are treated as two maneuver sets. The pressurant and propellant lines will nominally be opened and closed before and after each set. A fifth valve in each line provides redundancy and/or extended mission capability.

b. Leakage failure tree. Figure 33 illustrates the mission sequences which would be implemented if a pressurant or propellant leak occurred at various phases of the mission. The nominal sequence is in the center of Fig. 33, propellant leaks cause a translation to the right, and pressurant leak sequences are represented on the left. Inherent in the logic tree is the assumption that the leaks are slow enough to allow time for corrective action without sufficient loss of fluid to destroy the system's functional capability. This assumption is generally valid for contamination-induced leaks, which are of greatest concern.

c. Pyrotechnic valve failure modes. Addition of pyrotechnic valves requires that additional failure modes induced by the valves be considered. Structural and

Table 11. Typical propulsion sequence

Maneuver (time)	Event	Time	Component actuated	Typical velocity change, mps	Typical burn duration, s
	Vent manifold	Separation + 2 days	Engine valve		
Midcourse 1 (launch + 1 wk)	Pressurize system and open propellant lines	Maneuver − 1 day	Valve P1, 01, F1		
	Execute engine burn	Engine burn	Engine valve	15	12
	Close pressurant line	Maneuver + 7 days	Valve P2		
	Close propellant lines	Maneuver + 7 days	Valves 02, F2		
Midcourse 2 (orbit insertion − 2 wk)	Open pressurant line	Maneuver − 1 day	Valve P3		
	Open propellant lines	Maneuver − 1 day	Valves 03, F3		
	Execute engine burn	Engine burn	Engine valve	5	4
Orbit insertion	Execute engine burn	Engine burn	Engine valve	1575	900
Orbit trim 1 (orbit insertion + 1 to 3 days)	Execute engine burn	Engine burn	Engine valve	25	11
Orbit trim 2 (orbit insertion + 3 to 5 days)	Execute engine burn	Engine burn	Engine valve	30	13
	Close pressurant line	Maneuver + 2 days	Valve P4		
	Close propellant lines	Maneuver + 2 days	Valves 04, F4		
			Total	1650	940

Table 12. Pyrotechnic valve actuation telemetry information

Command and/or event information	
Failure mode	**Information**
Command subsystem output	Event counter 1, 3, 4 ground command log
Central computer and sequencer output	Event counter 1, 2, 4 state of central computer and sequencer programs
Pyro silicon-controlled rectifier short	Event counter 1 or 4

Propulsion pressure indications			
Fluid	**Old state**	**New state**	**Telemetry indication**
Pressurant	Closed	Closed	None
		Open	Probable increase in tank pressures
	Open	Closed	No immediate change
		Open	None
Propellant	Closed	Closed	None
		Open	Line pressure equilibrium with tank pressure
	Open	Closed	Increase in line pressure due to valve closure
		Open	None

hydraulic effects of valve operation are amenable to design solution and test verification. The remaining items of concern are failure-to-fire and inadvertent operation.

Telemetry data available to verify electrical signal output and/or valve actuation are summarized in Table 12. These indications would be used to follow the various valve-no-fire sequences of Fig. 34, if required. Steps to be taken in the event of an inadvertent valve operation are summarized in Table 13.

Table 13. Pyro valve actions required if inadvertent firing is indicated

Old state	New state	Action
System closed	No change indicated	Leave system as is until next maneuver. Open valves as required to open system. Work problem, depending on state of mission and valves remaining.
System closed	Partially open (gas or propellant)	Leave system as is, but watch closely for indications of leakage. At next maneuver, fire only valves required to open system entirely.
System open	No change indicated	Fire no valves. Work problem at next maneuver. If orbit insertion is imminent, fire valves 05, F5, P5 to insure open system.
System open	Partially closed (gas or propellant)	Open valves when required for further maneuvers.

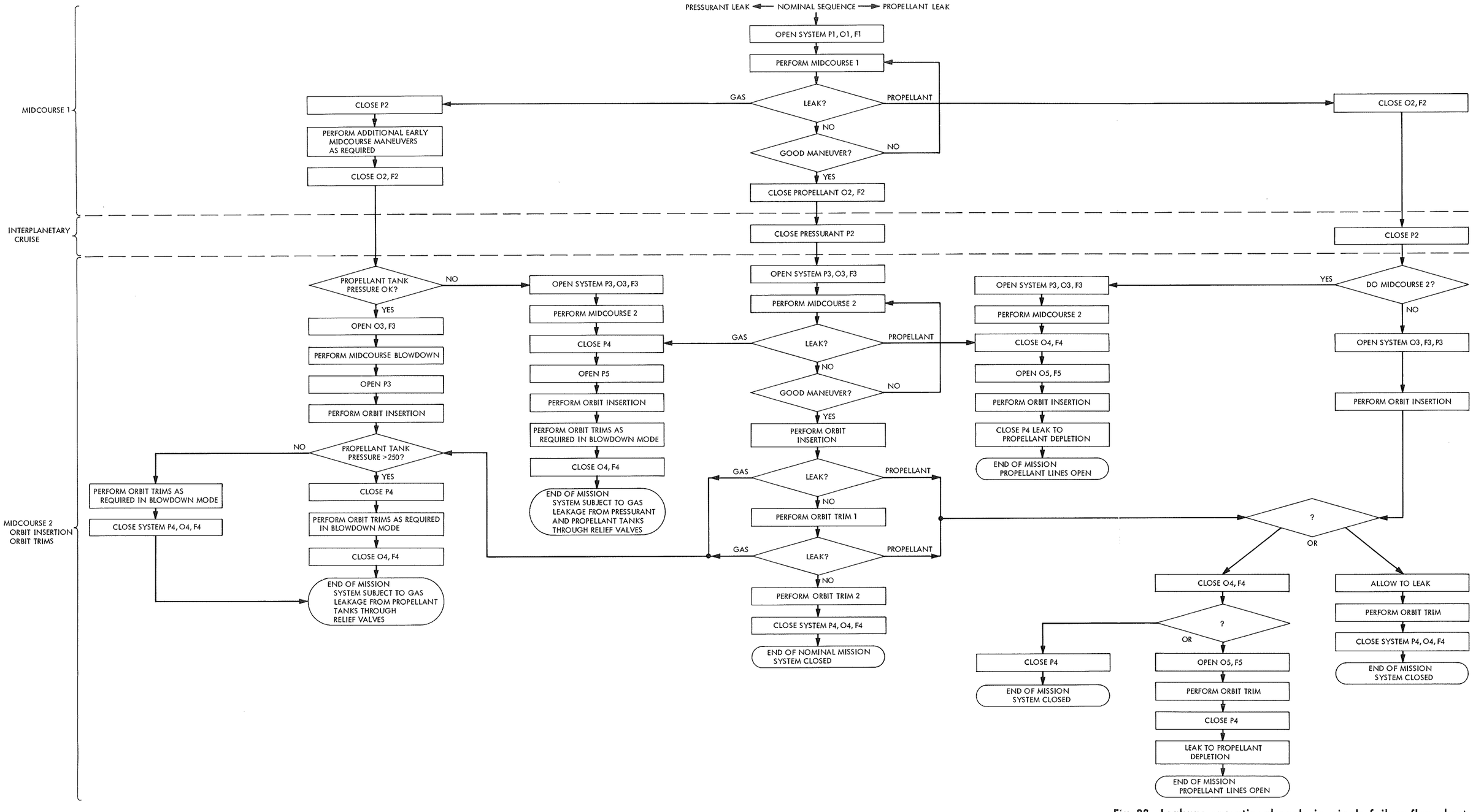

Fig. 33. Leakage operational analysis—single-failure flow chart

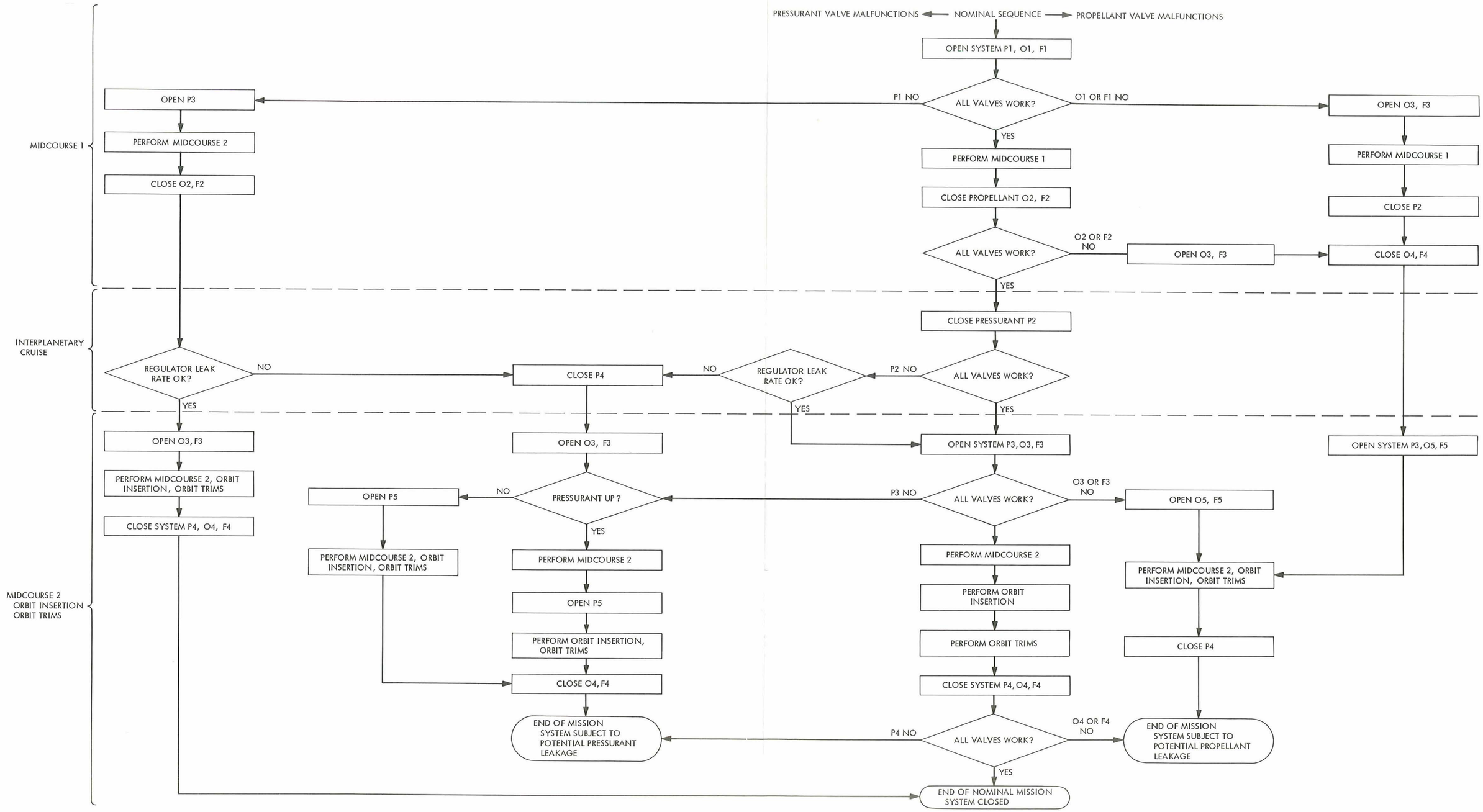

Fig. 34. Pyro valve no-fire operational analysis—single-failure flow chart

II. *Mariner* Venus–Mercury 1973 Project

A. Project Description and Status

1. Description

The *Mariner* Venus–Mercury 1973 Project was authorized in December 1969 to conduct the first dual-planet mission. The primary objective is to conduct exploratory investigations of the planet Mercury's environment, atmosphere, surface, and body characteristics, and to obtain environmental and atmospheric data on the planet Venus (first priority assigned to Mercury investigations). The secondary objectives are to perform interplanetary experiments enroute to Mercury, and to obtain experience with the gravity-assist mission mode.

A single *Mariner* spacecraft is planned for launch by an *Atlas/Centaur* vehicle from Cape Kennedy in October 1973. The Venus encounter, in February 1974, will provide both an opportunity to obtain scientific data at that planet and the necessary energy, by means of gravity-assist, to reach Mercury some 7 wks later. The spacecraft design is expected to resemble that used in the *Mariner* Mars 1969 mission and that being developed for the *Mariner* Mars 1971 mission, with appropriate modifications defined by the Venus–Mercury mission requirements. The scientific experiments, assumed to include television and other planet-oriented elements together with interplanetary fields-and-particles investigations, will be selected by NASA Headquarters during July 1970. The Deep Space Network and other NASA facilities will be committed to support the mission. It is planned that a System-Integration Contractor will be selected in early 1971. The Contractor's effort would encompass the spacecraft detail engineering, system assembly, test and operations, and selected support to other elements of the Project.

2. Status

A briefing of some 45 industrial firms was held on February 24, 1970 to acquaint them with the preliminary Project planning and to solicit their suggestions regarding

the most cost-effective approach to use in implementing the Project. The industry suggestions and an internal system contracting study will form the basis for establishing the detail implementation plans for the Project.

B. Guidance and Control

1. Power Subsystem

a. Introduction. The *Mariner* Venus–Mercury 1973 (MVM '73) spacecraft power subsystem is presently planned to be a modification of the *Mariner* Mars 1971 (MM '71) design. Modifications are required primarily for operation in the vicinity of Mercury, as well as for a revised power profile. The following text describes why these changes are required and presents a preliminary description of the overall power subsystem.

b. Power requirements. A preliminary power profile depicting the subsystem power requirements for four key operational modes near Earth and Mercury is shown in Table 1. Examination of these requirements, which take into account the power conditioning and conversion efficiencies, shows a maximum raw power requirement of 538 W in one of the near-Mercury modes. A preliminary functional block diagram of the MVM '73 power subsystem components is shown in Fig. 1. A tentative science payload is included; however, final selection of the science payload will not be made before July 1970.

c. Solar panel. Because of a significant increase in temperature, associated with an increase in solar intensity at Mercury, two types of solar panel configurations are currently being investigated. The present baseline philosophy is to make use of two MM '71-type panels by incorporating a spacecraft capability to include a one-step solar panel tilt to a predetermined angle of incidence. This reduces the solar panel temperature to an acceptable value. At present, 140 and 128°C temperatures are expected at Venus and Mercury, respectively. The objective of the tilt is to provide solar panel output voltages that are compatible with the MM '71 power subsystem components (37.5–50 Vdc). As a variation to this approach, the concept of a panel with continuously varying angle of incidence is also being investigated. Preliminary analysis of the two-panel one-step tilt configuration shows that available power at near-Earth is approximately 409 W at 50 Vdc, which increases to approximately 475 W at 37.5 Vdc at Venus. Following Venus encounter, the panels are tilted to an angle of 60 deg and the power remains at 475 W, whereas the voltage increases to 50 Vdc. Available power at Mercury increases to 540 W at 37.5 Vdc. As of this reporting period, with power requirements in the preliminary stages, it appears that additional solar panel area is required over that provided by the MM '71 design. A tabulation of total raw power required and available power and output voltage is given in Table 2 for several key operating modes and for the two types of solar panel configuration being investigated.

The second solar panel approach being investigated is to consider four non-tiltable panels. This configuration will require a newly developed technique for limiting the solar radiation actually reaching the cell. Techniques being considered include selective filtering or reflective coatings. Even with these controls, the panel output voltage will drop to approximately 44 Vdc, depending on the actual operating temperature of the panels. Adequate power and voltage within power conditioning operating tolerances (37.5–50 Vdc) is provided in all operational modes. By July 1970, it is expected that the results of the current solar panel advanced development effort will define anticipated performance in sufficient depth, to allow selection and sizing of either the two solar panel tilting system or the four panel non-tilting configuration.

d. Battery. The MM '71 26-cell 20 A-h nickel–cadmium battery is currently planned for use on this mission. Energy demands to be supplied by the battery may range up to approximately 450 W-h. This demand may occur during any of three planned maneuvers, each of which may last up to 80 min. With the addition of the launch mode, sun occultation at Mercury and a possible fourth maneuver, a total of six battery discharge/charge cycles are required.

The MM '71 battery charger may be used for battery charging which occurs immediately after acquiring solar panel power. The charger provides a maximum charging current of 2 A (c/10 rate) and a low-rate charge rate of 0.65 A (c/30 rate). The charger has the capability of accepting an input voltage varying from 25 to 50 Vdc.

e. Power conditioning and distribution. A preliminary functional block diagram of the MVM '73 spacecraft power subsystem is shown in Fig. 1. Solar panels provide raw power through blocking diodes to the dc bus.

The main booster regulator converts solar panel voltage to a regulated 56 Vdc at a tolerance of $\pm 1\%$. An identical standby booster regulator serves as a backup to

Table 1. Preliminary power profile

Item	Key operational modes			
	Earth		Mercury	
	High-rate battery charge (no science)	Low-rate battery charge (Earth science on)	High power transmission, low-rate battery charge (all science on, gyros on)	High power transmission, low-rate battery charge (all science on, gyros off)
Science instruments				
UV spectrometer	0.0	0.0	3.0	3.0
Plasma science	0.0	13.0	13.0	13.0
Film imaging	0.0	60.0	60.0	60.0
Gamma ray spectrometer	0.0	3.0	3.0	3.0
IR radiometer	0.0	0.0	2.5	2.5
DC magnetometer	0.0	4.0	4.0	4.0
Plasma wave	0.0	3.4	3.4	3.4
Charged particle	0.0	4.5	4.5	4.5
Science data subsystem	0.0	25.0	25.0	25.0
Total science output, W	0.0	112.9	118.4	118.4
Engineering subsystems				
Thermal control 1	40.0	0.0	0.0	0.0
Scan electronics	4.3	26.0	26.0	26.0
Data storage	10.0	18.0	18.0	18.0
Flight telemetry	15.2	15.2	15.2	15.2
Flight command	3.0	3.0	3.0	3.0
Radio frequency	24.0	24.0	24.0	24.0
Pyro	1.0	1.0	1.0	1.0
Central computer and sequencer	18.5	21.5	21.5	21.5
Attitude control	27.0	11.0	27.0	11.0
Gyro 1	12.0	0.0	12.0	0.0
Power distribution	10.0	10.0	10.0	10.0
Total engineering output, W	165.0	129.7	157.7	129.7
Total 2.4-kHz main inverter output, W (efficiency)	165.0 (0.904)	242.6 (0.915)	276.1 (0.915)	248.1 (0.915)
Total 2.4-kHz main inverter input, W	182.5	265.14	301.6	271.0
Scan motor, 400 Hz, 1-phase (efficiency)	0.0 (0.797)	11.79 (0.797)	11.79 (0.797)	11.79 (0.797)
Gyro 2, 400 Hz, 3-phase (efficiency)	11.6 (0.775)	0.0 (0.775)	11.6 (0.775)	0.0 (0.775)
Total boost regulator output required, W (efficiency)	194.1 (0.874)	276.93 (0.886)	324.99 (0.886)	282.79 (0.886)
Total boost regulator input, W	222.08	312.56	366.80	319.17
Unregulated dc power required				
Boost regulator	222.08	312.56	366.80	319.17
Battery charger	95.00	35.00	35.00	35.00
Traveling-wave tube	57.00	57.00	93.00	93.00
Boost regulator failure sensor	1.50	1.50	1.50	1.50
Thermal control 2	25.00	25.00	25.00	25.00
Total power, W (diode efficiency)	400.58 (0.97)	431.06 (0.97)	521.3 (0.97)	473.67 (0.97)
Total raw power required, W	413	444	538	489

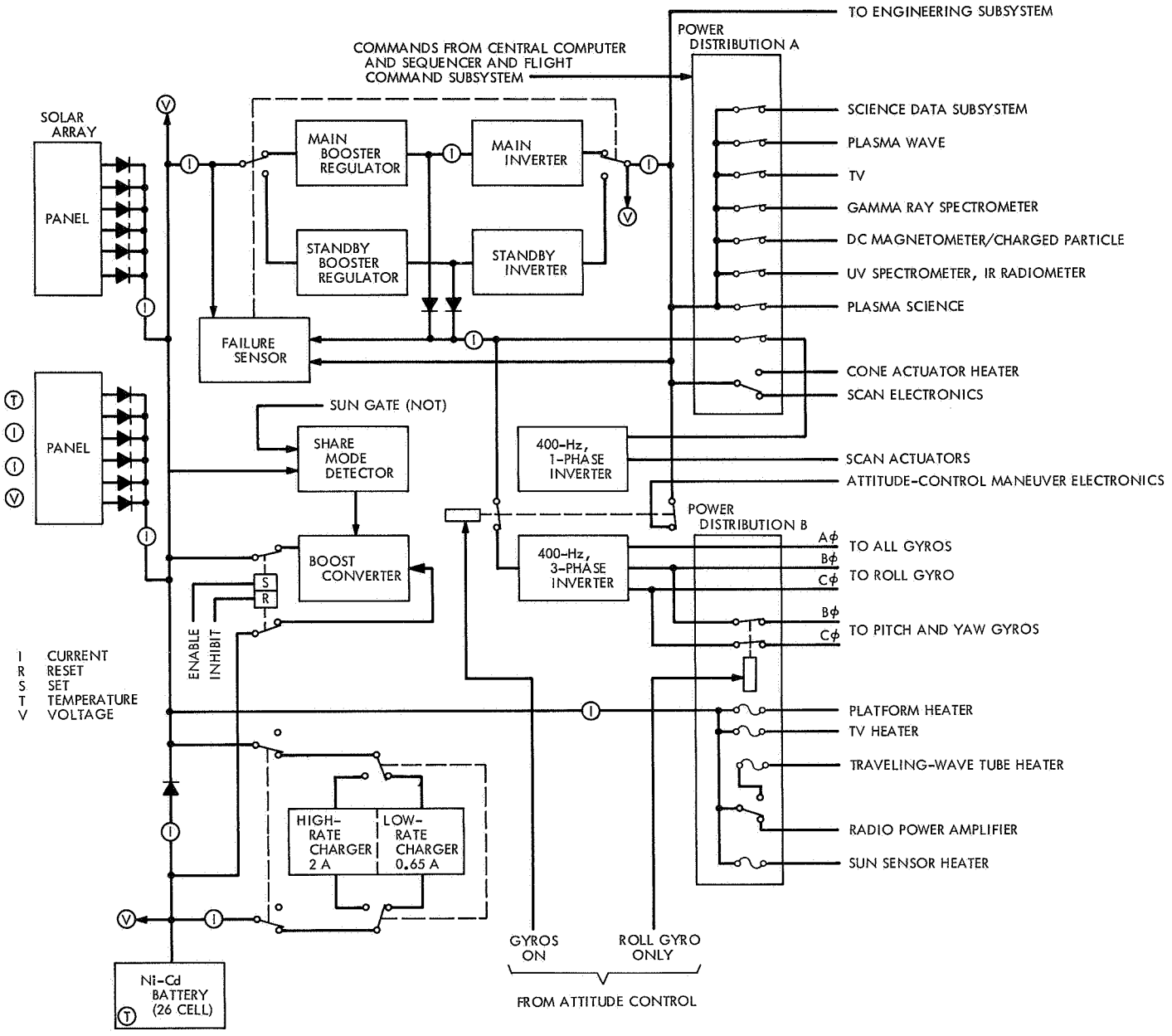

Fig. 1. Power subsystem functional block diagram

Table 2. Comparison of preliminary power required vs power available with operating voltages for both the tilting and non-tilting solar panels

Parameter	Key operating modes						
	Cruise (near Earth)			Venus	Mercury		
	Low-rate battery charge (no science)	High-rate battery charge (no science)	Low-rate battery charge (science on)	High-power transmission, low-rate battery charge (science on)	High-rate transmission (gyros on, science on)		High-rate transmission, low-rate battery charge (gyros off, science on)
					No battery charge	Low-rate battery charge	
Power required, W	303	413	444	485	504	538	489
Available power (tilting panel), W	409 (50 Vdc)	409 (50 Vdc)	409 (50 Vdc)	[a]475 (37.5 Vdc) [b]475 (50 Vdc)	540 (37.5 Vdc)	540 (37.5 Vdc)	540 (37.5 Vdc)
Available power (non-tilting panel), W	496 (50 Vdc)	496 (50 Vdc)	496 (50 Vdc)	1100 (44 Vdc)	655 (37.5 Vdc)		655 (37.5 Vdc)

[a]Contingency not included: before tilt.

[b]Contingency not included: after 60-deg tilt.

the main booster regulator and will provide power in case of failure of the main booster regulator. Switchover is controlled by onboard detection of over-or-under voltage at the output of the main booster regulator. The maximum power output of both the MM '71 main and standby booster regulators is 295 W. However, the preliminary power requirements determined during this reporting period require a redesign for increased power output, as shown in Table 3.

The main inverter output is designed to provide 2.4 kHz ±0.01% single-phase, square-wave power at 50 V (rms) +2 or −3% from a regulated 56 Vdc ±1% input. Timing signals to the central computer and sequencer are provided from the main inverter. In event of failure of the main inverter, the system will switch to a standby inverter with identical output characteristics. The maximum power output of the MM '71 main and standby inverters is 250 W. At the present time, a redesign is being contemplated based on the preliminary requirements shown in Table 4.

The 400-Hz inverter consists of both single-phase and three-phase outputs. The output characteristics of the single-phase portion, including both amplitude and frequency, are 28 V (rms) ±5% square wave and 400 Hz ±0.01% in the normal mode, respectively. Average power output is 15 W at 28 V with a peak loading of 21 W. The 400-Hz three-phase power output characteristics, including both frequency and amplitude, are 400 Hz ±0.01% in the normal mode and 27.2 V (rms) ±5% line-to-line, quasi-square wave, respectively. Average power of the three-phase output is 12 W with a peak of 15 W.

Table 3. Booster regulator 56 Vdc power available vs power required

Item	Earth		Mercury	
	Min	Max	Min	Max[a]
2.4-kHz main inverter	182.5	242.6	271.0	301.6[a]
Scan motor	0.0	11.8	11.8	11.8
Gyro 2	11.6	0.0	0.0	11.6[a]
Total power required, W	194.1	254.4	282.8	325.0[a]
Total power available (MM '71), W	295	295	295	295

[a]All-axis inertial control at encounter: includes all science on; gyro 1 on (12 W); attitude control increase (16 W).

f. Power subsystem weight. A weight breakdown of the current MVM '73 power subsystem and design status is shown in Table 5.

Table 4. Main inverter 2.4-kHz power available vs power required

Item	Earth		Mercury
	Min	Max	
Engineering subsystems	165	129.7	129.7 (157.7)[a]
Science instruments	0	112.9	118.4[b]
Total power required, W	165	242.6	248.1 (276.1)[a]
Total power available (MM '71), W	250	250	250

[a]All-axis inertial control at encounter: includes all science on; gyro 1 on (12 W); attitude control increase (16 W).

[b]Includes 3-W increase for UV spectrometer, and 2.5-W increase for IR radiometer at Mercury only.

Table 5. Power subsystem weight breakdown

Item	Weight, lb	Design status
Solar cells (not including structure, mirrors) EST.	20.0 (est)	New
Battery, including chassis, Ni–Cd	65.0	*Mariner* Mars 1971 (same)
Battery charger	3.5	*Mariner* Mars 1971 (same)
Main inverter, 2.4-kHz (2)	5.90	*Mariner* Mars 1971 (modified)
Boost regulator (2)	11.6	*Mariner* Mars 1971 (modified)
Inverter (400-Hz, 1- and 3-phase)	3.7	*Mariner* Mars 1971 (same)
Power control	2.44	*Mariner* Mars 1971 (modified)
Power source logic	10.75	*Mariner* Mars 1971 (modified)
Power distribution	5.0	*Mariner* Mars 1971 (modified)
Total	127.89	

III. *Viking* Project, Orbiter System and Project Support

A. Project Description and Status

1. Description

The primary objective of the *Viking* Project is to send two vehicles to the planet Mars to perform scientific experiments directed toward enhancing current knowledge about the physical characteristics of the planet, particularly its capability for supporting life and possible evidence of life. The two vehicles, each consisting of an orbiter system and a lander system, are anticipated for launch during 1975. The orbiter system will be developed by JPL, and the lander system will be developed by the Martin-Marietta Corp. Langley Research Center has overall management responsibility for the *Viking* Project.

The orbiter system will transport and inject the lander system at the appropriate point for a selected landing site and will relay telemetered data from the lander to earth. Scientific instruments on the orbiter will be used to measure atmospheric and surface parameters at various times and locations to determine the dynamic characteristics of the planet. The topography of Mars will be mapped during orbital operations, with special emphasis on mapping the proposed landing site prior to deorbit of the lander system and on supporting the lander after it is on the surface of Mars by determining if changes are apparent in the vicinity of the lander. Both visual and infrared coverage will be possible during the presently planned 140 days of orbital operations.

During entry and after landing, the scientific instruments on the lander will measure Mars' atmospheric composition, temperature, pressure, and density. After landing, the topography of the landing site will be mapped, and measurements will be made of the planet's surface composition, temperature, pressure, humidity, and wind speed. Of particular interest in the surface measurements are the type of organic compounds present, if any, and the amount and form of water. A gas chromatograph/mass spectrometer, for measuring both atmospheric and surface composition, is being developed by JPL. The surface soil analyses will be directed at detecting evidence of growth and/or metabolism.

2. Status

During this period, authorization was received from the Langley Research Center to proceed with the plans on the *Viking* 1975 mission. Accordingly, intensive efforts were initiated to prepare cost estimates for the redirected orbiter activities.

Commonality studies are being conducted with the *Mariner* Venus–Mercury 1973 Project Office to determine if such an approach is a cost-effective measure. Specific subsystem areas being investigated include flight data, TV, data storage, S-band radio, and central computer.

Significant progress was made in identifying JPL's responsibilities and overall schedule activities in mission analysis and design. A study was conducted on *Viking* 1975 navigational characteristics to provide a consistent basis for forthcoming hardware system proposals. Effort was also initiated to develop the capability to analyze the navigational accuracy requirements of broken plane trajectories.

B. Space Sciences

1. Development of an Optimal Optical Design for the Mars Atmospheric Water Detection Spectrometer

a. Introduction. A high-resolution spectrometer has been selected for the orbiter science experiment of the *Viking* 1975 mission to determine the amount and distribution of water vapor in the Martian atmosphere. The experiment proposal by Dr. C. B. Farmer, Principal Investigator, outlined the considerations leading to the choice of an instrument operating in the 1.4-μ region with a spectral resolution of no more than 0.5 cm^{-1}.

b. Design constraints. In order to measure the radiant flux from Mars at this spectral resolution, a monochromator with a relative aperture of *f*/5 and a focal length of 1000 mm was needed. The preliminary design proposed a double-cassegrain monochromator permitting the overall package length to be approximately one-half the required focal length. This made it feasible to achieve the size limit that would be reasonable for a spacecraft instrument.

Plans were to measure the intensity in four narrow frequency bands between 7231.18 cm^{-1} and 7234.06 cm^{-1}, the bandwidth to be controlled by an entrance slit 0.25 mm wide by 1.0 mm high and measured by lead sulphide detectors placed at the spectral image plane. A 300-line/mm (fourth-order), or a 1200-line/mm (first-order) grating would be needed to disperse the energy with the appropriate spectral resolution.

c. Preliminary ray-trace design. Based upon the constraints needed for the high-resolution spectrometer, a contract was awarded to Beckman Instruments, Inc., to ray-trace the cassegrain monochromator configuration as well as any other configuration capable of providing all requirements.

As reported in Ref. 1, eight other monochromator configurations were subsequently ray-traced and compared in performance and structural desirability with the cassegrain configuration. These eight systems were all double-pass monochromators; the second pass through the monochromator occurs after the first spectral image is returned by a corner reflector located in the image plane.

The eight configurations that were studied are as follows:

(1) An Ebert system, with a spherical collimating mirror and a corner return mirror.

(2) An Ebert system, with a spherical collimating mirror and a corner return prism.

(3) An Ebert system, with a parabolic collimating mirror and a corner return mirror.

(4) An Ebert system, with a parabolic collimating mirror and a corner return prism.

(5) A Littrow system, with a spherical collimating mirror and a corner return mirror.

(6) A Littrow system, with a spherical collimating mirror and a corner return prism.

(7) A Littrow system, with a parabolic collimating mirror and a corner return mirror.

(8) A Littrow system, with a parabolic collimating mirror and a corner return prism.

From the ray-trace analysis of these eight configurations, only one was of sufficiently high spectral image quality to meet the requirements. This was the Littrow double-pass with parabolic collimating mirror and corner return prism.

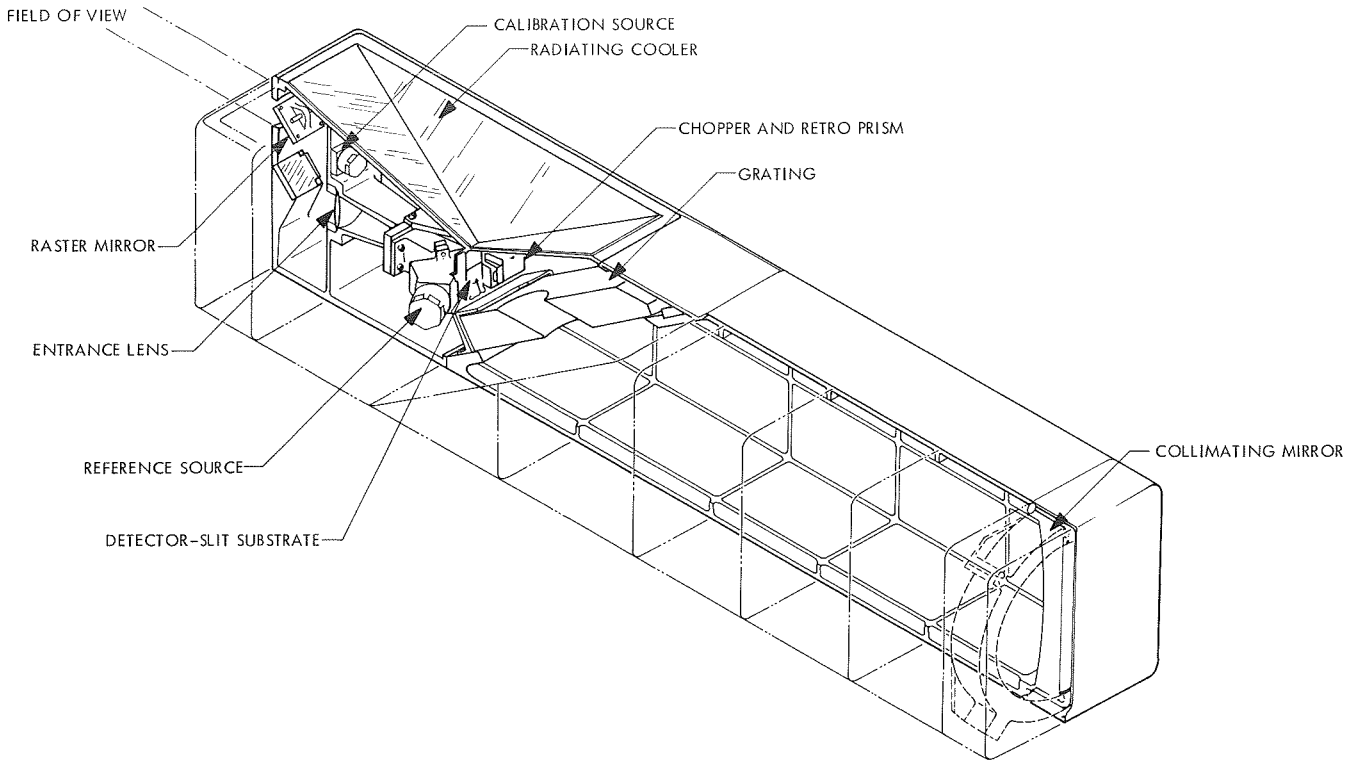

Fig. 1. Conceptual configuration of the Mars atmospheric water detection spectrometer

This configuration was selected for further analysis for the final spectrometer design. The cassegrain configuration, although a little shorter than the double-pass monochromator, would be twice as large in linear dimensions of both the grating and collimating mirror, producing a unit which would be eight times more massive. This then made the Littrow configuration even more attractive for spacecraft use.

d. Final ray-trace design. During the second phase of the contract, a ray-trace analysis was conducted on the double-pass Littrow monochromator. A final report (Ref. 2) presents a critical analysis of the optical system giving the locations of all the optical elements and optimizes both mechanical design considerations and spectral image quality.

For the final design, five new frequencies were specified instead of the four used in the preliminary study (still in the 1.4-μ region). In addition, an investigation of available line emission sources to be used for frequency calibration was undertaken. The investigation showed that a krypton arc produced a strong isolated line about 1.6 mm from the entrance slit on the side opposite from the location of the five specified frequencies.

e. Conclusions. The final report on the ray-trace study provides the necessary data for an optimal optical instrument within the capability of present-day techniques for fabrication. Based upon this ray-trace, a feasibility model was built which incorporated all the critical optical features of a flight instrument. Figure 1 shows the general arrangement of the spectrometer; Fig. 2 is a photograph of the unit.

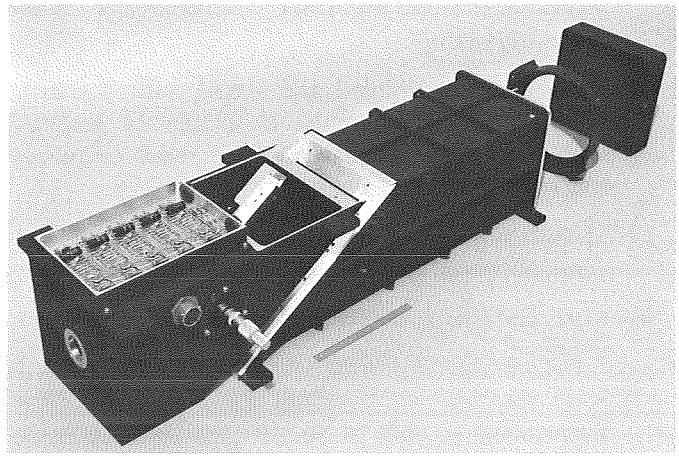

Fig. 2. Mars atmospheric water detection spectrometer

This feasibility model has demonstrated that the design concept is correct and the performance is as predicted and meets the experiment requirements. In addition, the model has pointed the way toward proper fabrication, assembly, alignment, test, and calibration techniques to be used on future instruments.

References

1. Henderson, B. D., Preliminary Report IR-2579-101. Beckman Instruments, Inc., Fullerton, Calif., May 23, 1969.
2. Henderson, B. D., Final Report FR-2579-101. Beckman Instruments, Inc., Fullerton, Calif. (undated).

C. Telecommunications

1. *Viking* Orbiter 1975 Radio Frequency Subsystem

a. Introduction. The *Viking* Orbiter 1975 radio frequency subsystem (RFS) will be basically the same as the *Mariner* Mars 1971 RFS with some relatively minor design changes. A proposed redundant receiver represents the only major change. As with previous *Mariner* radio subsystems, the *Viking* Orbiter 1975 RFS will provide the communications and tracking link between the flight orbiter and the ground-based Deep Space Instrumentation Facility (DSIF). The RFS will provide the following functions:

(1) Receive the S-band radio frequency (RF) signal transmitted from the DSIF.

(2) From the RF signal, demodulate the composite command signal and send it to the orbiter and lander command subsystems for direct commands to the orbiter and lander prior to separation.

(3) From the RF signal, demodulate the ranging signal transmitted from the DSIF and condition it for retransmission.

(4) Transmit a modulated RF signal with a carrier which is phase coherent with either the received carrier or with an internally generated frequency source.

(5) Modulate the transmitted carrier with the composite engineering and science telemetry signals.

(6) Modulate the transmitted carrier with the receiver-detected ranging signal.

(7) Send the received ranging signal to the X-band experiment as well as an RF signal which is coherent with either the received carrier or with an internally generated frequency source.

To accomplish these functions the RFS contains the subassemblies shown in the block diagram of Fig. 3. The S-band antenna subsystem [high-gain antenna (HGA), medium-gain antenna (MGA), and low-gain antenna (LGA)] is not part of the RFS and is shown for information only. The nominal parameters of the RFS are given in Table 1.

b. Receiver and diplexer subassemblies. The receiver and diplexer subassemblies, when normally interconnected, form the narrow band, double conversion, automatic phase and frequency tracking spacecraft RFS receiver. When the receiver is phase-locked to the transmitted uplink signal, it supplies an output frequency to the exciter which is phase and frequency coherent to the received signal. The exciter multiplies the frequency and phase by 120 for transmission at S-band. In this mode, the receiver and exciter form the transponder which coherently translates the frequency and phase of the received signal by a fixed ratio of 240/221. The transponder provides for coherent two-way doppler tracking of the spacecraft which permits an accurate method of determining the spacecraft trajectory. When the receiver is phase-locked to a received signal, which has been

Table 1. Nominal values of significant RFS parameters

Parameter	Value
Receiver input frequency, MHz	2115±5
Receiver tracking threshold, dBmW	−153
Receiver tracking loop noise bandwidth at threshold, Hz	18
Command channel noise bandwidth (single-sided), kHz	2.5
Ranging channel noise bandwidth (single-sided), MHz	1.5
Receiver noise figure, dB	7.5
Dynamic signal level range, dBmW	−70 to threshold
Transmit/receive frequency ratio	240/221
Transmitter output frequency, MHz	2295±5
Transmitter output power, W	
Low-power mode	10
High-power mode	20
Telemetry and ranging channel modulation bandwidth, MHz	1.5
Power required, W	
2.4 kHz 50 V	30
25–50 Vdc TWT HP/LP	92/56
Weight of radio assembly (including case and case harness assembly), lb	63

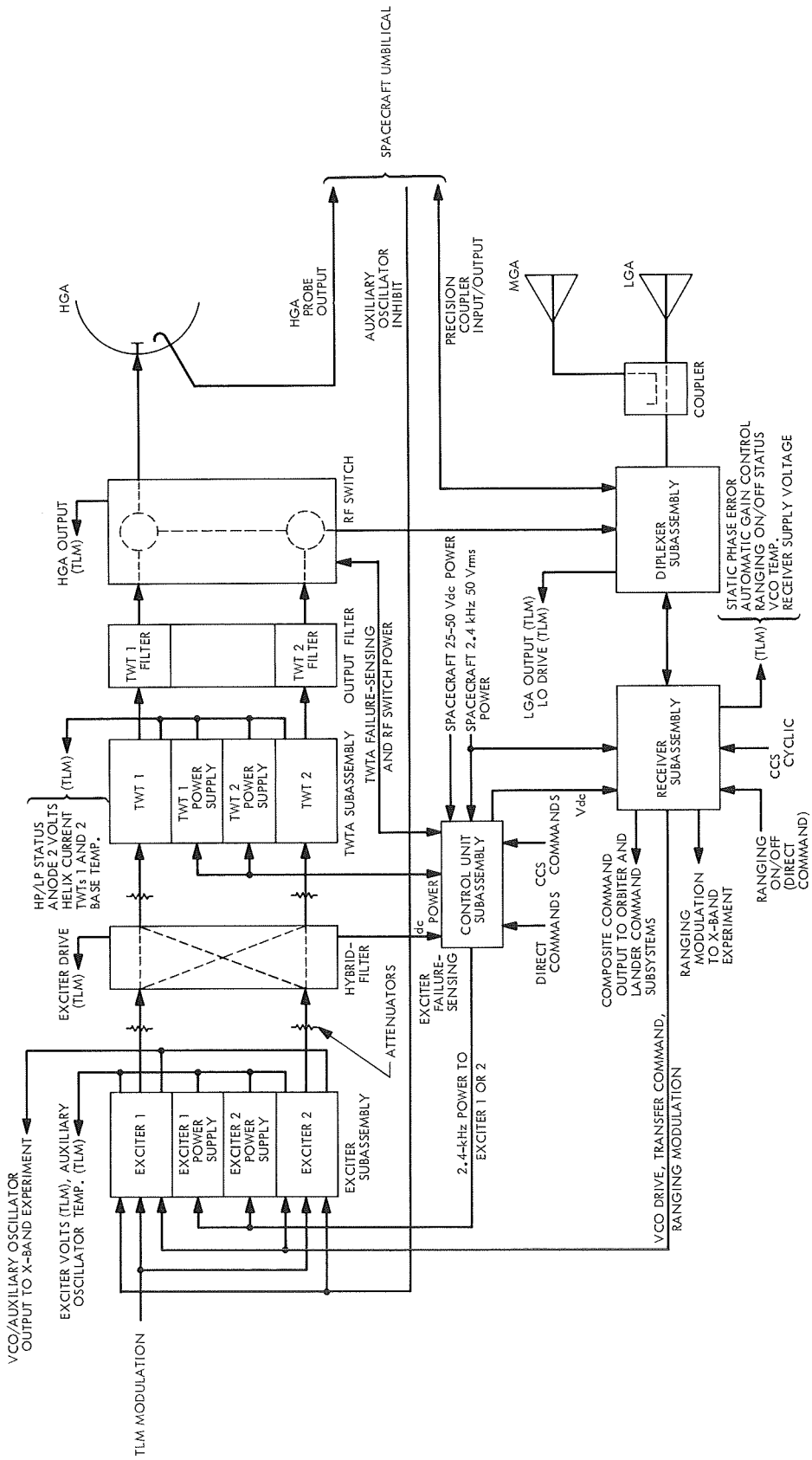

Fig. 3. *Viking* orbiter radio frequency subsystem

phase-modulated with the composite command signal, the receiver demodulates the signal and sends it to the orbiter command subsystem for direct commanding of the orbiter spacecraft. For *Viking* 1975 a second output is provided for the lander command subsystem. This allows commanding of the lander prior to separation via the orbiter S-band link. The receiver also demodulates the ranging code from the uplink signal, amplifies and limits it, and sends it to the exciter for modulation on the downlink carrier. This permits precise measurement of the distance and rate of change of distance to the spacecraft. For *Viking* Orbiter 1975 a separate ranging output will be provided for the X-band experiment (see *Paragraph g*).

The receiver has six analog telemetry (TLM) signals sent to the flight data subsystem. AGC 1 (TLM) and AGC 2 (TLM) indicate the level of the spacecraft received carrier; static phase error (TLM) indicates the operating frequency of the receiver voltage-controlled oscillator (VCO); LO drive (TLM) indicates the drive level of the first local oscillator (LO) into the first mixer. The receiver supply voltage (TLM) is new for *Viking* 1975 and will indicate the relative level of the ±15-Vdc receiver supply. A temperature transducer located on the VCO module provides a telemetry indication of the VCO temperature (TLM) and allows prediction of the temperature variable VCO best lock frequency. (Best lock frequency is the ground transmitter frequency which has the highest probability of obtaining receiver phase lock in the shortest amount of time.)

The receiver has a self-contained power supply which converts the orbiter 2.4-kHz power to the dc voltages required by the receiver. A circuit breaker in the supply protects the 2.4-kHz spacecraft power when an excessive current load is drawn by the receiver. If the receiver draws a current greater than a preset level, the receiver power is turned off. Since the overcurrent could be momentary, a computer command subsystem (CCS) cyclic will reset the circuit breaker only if the excess current load is no longer present. The supply also provides a voltage to the first stages of the receiver video amplifier module. This voltage turns the ranging channel *on* or *off* by a direct command or *off* by a CCS cyclic. The channel status is indicated by a voltage sent to a telemetry status channel to indicate whether the ranging channel is *on* or *off*. The turning *off* of the ranging channel by the CCS cyclic is a safeguard against the feedback observed on the *Mariner* Mars 1964 RFS which created "self-lock" and was observed briefly and noncatastrophically in the *Mariner VI* receiver. "Self-lock" can cause performance degradation or a complete loss of command and two-way tracking capabilities.

c. Exciter subassembly. The exciter subassembly consists of two identical and fully redundant S-band exciters. The output power of each exciter is divided in half by the hybrid-filter and presented to the input of both of the redundant traveling-wave tube amplifiers (TWTAs). Thus, the exciters and TWTAs provide a fully redundant transmitter chain. The exciters are phase-modulated by the composite telemetry signal for transmission of scientific and engineering information from the orbiter. If the receiver ranging channel is *on*, the exciter carrier is also modulated with the ranging signal from the receiver. The exciter output signal is derived from either an internal crystal-controlled oscillator or from the receiver VCO. When the receiver is phase-locked to an uplink carrier, a switching voltage from the receiver inhibits the internal oscillator and allows the VCO to drive the multiplier chain for coherent two-way doppler tracking. When the receiver is out of lock, the receiver switching voltage changes and enables the internal auxiliary oscillator. The *Mariner* Mars 1971 RFS has added a spacecraft umbilical control which inhibits the transfer from VCO to the internal auxiliary oscillator. This is used to measure the free-running (unlocked) VCO frequency on the downlink, which allows the measurement of best lock frequency in test and on the launch pad. For *Viking* Orbiter 1975 a separate output from each of the two exciter auxiliary oscillators is provided for the X-band experiment (see *Paragraph g*).

The exciter power supply converts the spacecraft 2.4-kHz power to the dc power required by the three exciter modules. Two fully redundant supplies are housed in one module; one supply is *off* and one supply provides power to only one exciter. Switching of exciters is accomplished in the control unit, which switches the 2.4-kHz power to either of the supplies. The switching is accomplished in one of three ways: direct command or two failure modes. If the exciter draws excessive 2.4-kHz current, the overcurrent sensor in the control unit automatically switches to the other exciter. Also, a diode in the hybrid-filter samples the exciter S-band output signal and provides an output voltage to the control unit proportional to the RF power level. If the power level drops below a preset level, a CCS cyclic will initiate a switch to the redundant exciter. A second power detector provides the voltages proportional to the exciter output for exciter drive telemetry.

The telemetry relay module is common to both exciters. It provides the functions of conditioning the composite telemetry signal before reaching the phase modulator and of switching between two telemetry functions depending on which exciter is *on*. One of the switched telemetry signals is a monitor of the dc power supply voltage. This voltage is conditioned in each power supply so that the returned telemetry will indicate which exciter is operating. The temperature transducers located on each of the auxiliary oscillator modules are also switched. This temperature measurement allows accurate prediction of the temperature variable downlink auxiliary oscillator frequency.

d. Control unit. The control unit accepts direct commands from the orbiter command subsystem, the computer command subsystem (CCS), and the failure-sensing circuits in the RFS. From these inputs it selects the appropriate RFS operating mode.

The functions of the control unit are:

(1) To switch the transmitter output to the high-gain or low-gain antenna upon receipt of direct or CCS commands.

(2) To sense the TWTA and exciter power output level and, if either is low, to switch to the redundant unit upon receipt of the CCS cyclic command.

(3) To sense overcurrent conditions in the TWTA or exciter power supplies and switch immediately to the redundant unit, and to switch to either element upon receipt of a direct command.

(4) To select high- (HP) or low-power (LP) output from the TWTA upon receipt of direct or CCS commands.

(5) To supply switching logic voltage to the receiver power supply ranging and overcurrent functions.

e. Traveling-wave tube amplifiers. The traveling-wave tube amplifier (TWTA) consists of two Hughes Aircraft Co. Model 242H traveling-wave tubes (similar to the Model 394H used on the *Apollo* program), each with its encapsulated, modular, solid-state power supply. Both TWTAs are mounted in a single case.

The TWTA functions as a power amplifier of the phase-modulated S-band signal from the exciter. It provides two output power levels, nominally 10 or 20 W, by changing the voltages applied to the TWT helix, collector, and first anode. A timer delays application of high voltage to the TWT for 90 to 150 s to allow the heater to warm up.

In each of the two independent dc-to-dc power supplies, the primary 25- to 50-Vdc line voltage is converted to a stable 20 V, which is then converted to voltages suitable for the TWT filament, first and second anodes, helix, and collector. Only one supply is *on* at a time and supplies power to only one TWT. The stable 20 V is also used to control the circulator switches in the transmitter output circuits via the control unit and to provide the voltage for failure-sensing of TWTA output power in the control unit.

A feature added to the *Mariner* Mars 1971 spacecraft will be retained for *Viking* Orbiter 1975. By direct or CCS command, the raw 25- to 50-Vdc power can be turned *on* or *off* to the RFS via the power subsystem. When the power to the TWTs is turned *off*, to conserve spacecraft power or to prevent RF interference with future S-band missions, some of the power is routed to heater resistors to maintain a thermal balance in the RFS and the spacecraft.

The TWTA functions which are telemetered are helix current, second anode voltage, and a high/low-power mode status indicator. The second anode voltage is conditioned to indicate which of the redundant units is operating. The TWTA output level, which is sampled by a diode detector in the RF switch, provides a voltage proportional to the RF level to the control unit. If the power drops below a preset limit, a CCS cyclic will initiate a switch to the redundant TWTA. The TWTA has a provision for failure-switching in the event of an overcurrent as well as a backup set of fuses on the raw dc power line. If a TWTA draws current above a preset level, as sensed in the control unit, the overcurrent sensor automatically switches to the other TWTA. The TWTs can also be switched by a direct command.

f. Microwave components. The microwave components consist of the hybrid-filter, output filter, RF switch, and diplexer. The electrical characteristics are shown in Table 2. The hybrid-filter, RF switch, and diplexer use stripline on polyphenylene oxide construction for the hybrid and all power monitors. Coaxial cavities are used in the other circuits.

Table 2. Electrical characteristics of microwave components

Component	Insertion loss, dB		Rejection level, dB	Reverse isolation, dB	
	Transmit[a]	Receive[b]		Minimum	Ambient (25 ± 5°C)
Hybrid-filter	4.5	>100	>100 (dc to 2117 MHz) >60 (2199.8 and 2391.8 MHz) >100 (2477 to 4000 MHz) >70 (4000 to 10,000 MHz)		
Output filter	<0.3	>60	>30 (2100 and 2125 MHz) >70 (4580 to 10,000 MHz)		
Diplexer					
LGA to receiver	>100	<1.2	>100 (dc to 1988.4 MHz) >70 (1988.4 to 2048.4 MHz) >70 (4580 to 10,000 MHz)		
Transmitter to LGA	<0.3				
Transmitter to receiver		>50			
RF switch					
TWTA 1 to HGA	<0.35			>20	>30
TWTA 2 to HGA	<0.7			>40	>60
TWTA 1 to LGA	<0.7			>40	>60
TWTA 2 to LGA	<0.35			>20	>30

[a]2290.2 to 2301.3 MHz.

[b]2108.7 to 2119.2 MHz.

The hybrid-filter divides the power output from each exciter and furnishes drive power to both TWTs simultaneously through band-pass and low-pass filters. The hybrid-filter also contains two diode monitors for telemetry and failure mode sensing of the exciter RF output level. Attenuators are used in the hybrid-filter input and output circuits to adjust the exciter drive to an optimum value for each TWTA, and to compensate for hybrid-filter unbalance.

The output filter is used in the TWTA output circuit; it has minimum insertion loss at transmitter frequencies, a band-reject filter at receiver frequencies, and a low-pass filter to attenuate transmitter output harmonics.

The RF switch consists of two ferrite RF circulators making a four-port circulator switch. It provides a means of connecting either TWT to the high-gain or the low-gain antenna. A permanent magnet assures that TWTA 1 will be connected to the high-gain antenna with about a 3-dB power loss in case the dc switch coil voltage supply fails. Failure-sensing for the output of each TWT is accomplished at the input to each circulator by diode power monitors, and the high-gain antenna telemetry power monitor is at the high-gain antenna output of the switch.

The diplexer provides a band-reject filter at receiver frequencies between the transmitter output (RF switch) and the receiver input and a band-pass filter (at the receiver frequency) and a low-pass filter between the low-gain antenna and receiver (first mixer) input. The diplexer also has a precision (directional) coupler. This coupler provides the means for measuring transmitter output power to the low-gain antenna. It also provides a calibrated path to the receiver for uplink receiver measurements, and orbiter commanding during ground testing. Access to the precision coupler input/output is provided via the spacecraft umbilical connector.

g. S-X-band experiment interface. One of the changes to the *Mariner* Mars 1971 RFS design for *Viking* Orbiter 1975 is to provide a ranging and VCO/auxiliary oscillator output to the X-band experiment. The X-band experiment will transmit via the S-X-band high-gain antenna a nominal 8415-MHz signal (compared to the 2295-MHz S-band signal). By comparing the doppler and ranging measurements of the X- and S-band signals, information

about the transmission media between the orbiter antenna and the ground antenna will be obtained (e.g., space electron charge densities, Mars and earth ionospheres, earth and Mars neutral atmospheres, and solar atmosphere).

Figure 4 shows a block diagram of the interface between the RFS and the X-band experiment. The system as shown will allow S- and X-band tracking in three modes and will allow either of the redundant auxiliary oscillators to drive the X-band transmitter. The two primary modes are two-way tracking and two-way tracking with ranging. When the RFS is in two-way track, the receiver VCO drives the S- and X-band transmitters. Doppler deviations between the S- and X-band signals can be coherently compared to the signal transmitted to the spacecraft from the DSIF. When the ranging code is being modulated on the uplink during two-way S-band tracking, the receiver demodulates, amplifies, and limits the ranging signal. This ranging signal is then modulated on the S- and X-band carriers. Range deviations between the two signals can then be compared. The third mode is when the RFS is in one-way track. For this case the internal auxiliary oscillator of the RFS drives the S- and X-band transmitters. This provides two signals coherent to the same source for measurement of one-way doppler deviation of the two signals.

The isolation switch, shown between the RFS auxiliary oscillator outputs and the X-band multipliers, has been added to prevent possible VCO leakage from the *off* auxiliary oscillator from modulating the X-band multiplier. Special tests on the VCO isolation of an unpowered auxiliary oscillator may show that this switch is not required.

As presently planned, the X-band experiment is as shown in Fig. 4. The RFS VCO or auxiliary oscillator output frequency is multiplied by four and then phase-modulated by the ranging signal (if present) from the RFS. The times 10 and times 11 multipliers provide an additional multiplication of 110 for a total multiplication of 440. The output of the final multiplier is expected to be about 200 mW at 8415 MHz. The X-band signal only drives the dual-feed S-X-band high-gain antenna.

h. Redundant RFS receivers. Because of mission dependence on command and two-way tracking, as well as increased operating lifetime from *Viking* 1973 to *Viking* 1975, a study of redundant RFS receivers was initiated.

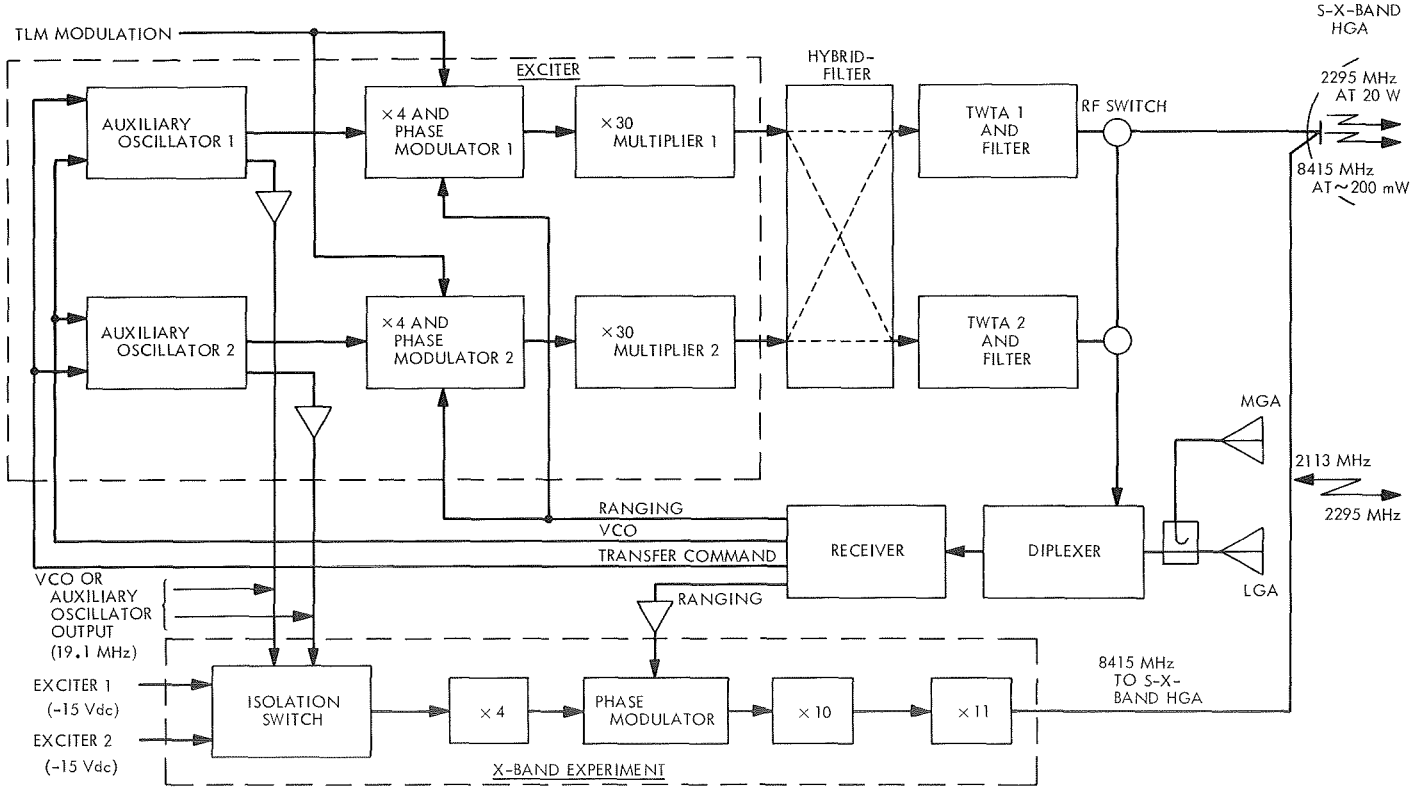

Fig. 4. S-band RFS and X-band experiment interface

This would represent a major design change to the *Viking* Orbiter 1975 RFS. The study on redundant receivers has also instigated a study of the overall redundancy in the telecommunications subsystems. This includes redundant receivers, command detectors, telemetry modulators, and the existing redundant transmitters. Since it is difficult to discuss RFS redundancy without involving command or telemetry, Figs. 5 and 6 include the telemetry modulators and the command detectors. Figure 5 represents the simplest form of redundancy, which might be called "functional" redundancy. In this case one receiver, command detector, telemetry modulator, exciter, and power amplifier make up one "functional" receive/transmit chain. The redundant chain is identical and separate. There is no cross coupling among the redundant elements. If any one element fails, the entire functional backup chain must be selected for full receive/transmit capability. Figure 6 represents a more complex form of redundancy, which could be called "block" redundancy. In this case each "block" or subassembly, such as an exciter or a command detector, can be individually selected to operate. This form of redundancy provides the maximum cross coupling between redundant elements. If any one element fails, just its redundant element need be switched. For example, the present redundant transmitter chain shown in Fig. 3 represents a form of "block" redundancy; either TWTA or either exciter can be selected if one element fails.

A number of tradeoff and reliability studies remains to be considered prior to selection of the final design.

2. *Viking* Orbiter Relay System

a. Introduction. The *Viking* Orbiter Relay System provides receiving and detection capability for communications via a UHF lander–orbiter link. This system operates at various times in the mission with the orbiter acting as a data relay point between the lander and earth. The lander data is pulse-code-modulated–frequency-shift-keyed (PCM–FSK) at one of two available bit rates (4 or 16 kbits/s). The received data is recorded in the orbiter and, in the case of the 4-kbits/s transmission, may also be relayed to earth in real time via the orbiter–earth S-band link. Recorded data is relayed to earth via S-band at a later time.

The Orbiter Relay System encompasses two electronic subsystems and a UHF antenna. These are:

(1) Relay radio subsystem.

(2) Relay telemetry subsystem.

(3) Relay antenna subsystem.

Operation of the Orbiter Relay System is initiated by ground command and/or computer command subsystem (CCS) command.

b. Relay link requirements. The Orbiter Relay System is required to support the relay link during the following mission phases:

(1) Lander–orbiter separation to touchdown.

(2) Touchdown to first setting of the orbiter.

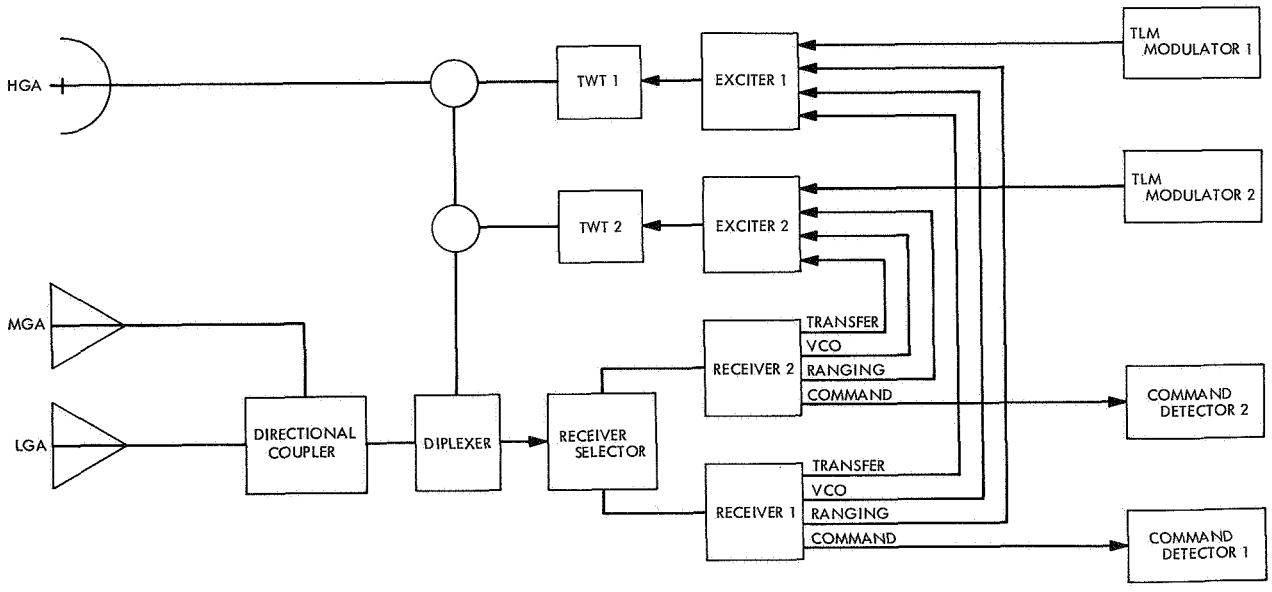

Fig. 5. *Viking* 1975 telecommunications "functional" redundant configuration (minimum cross coupling)

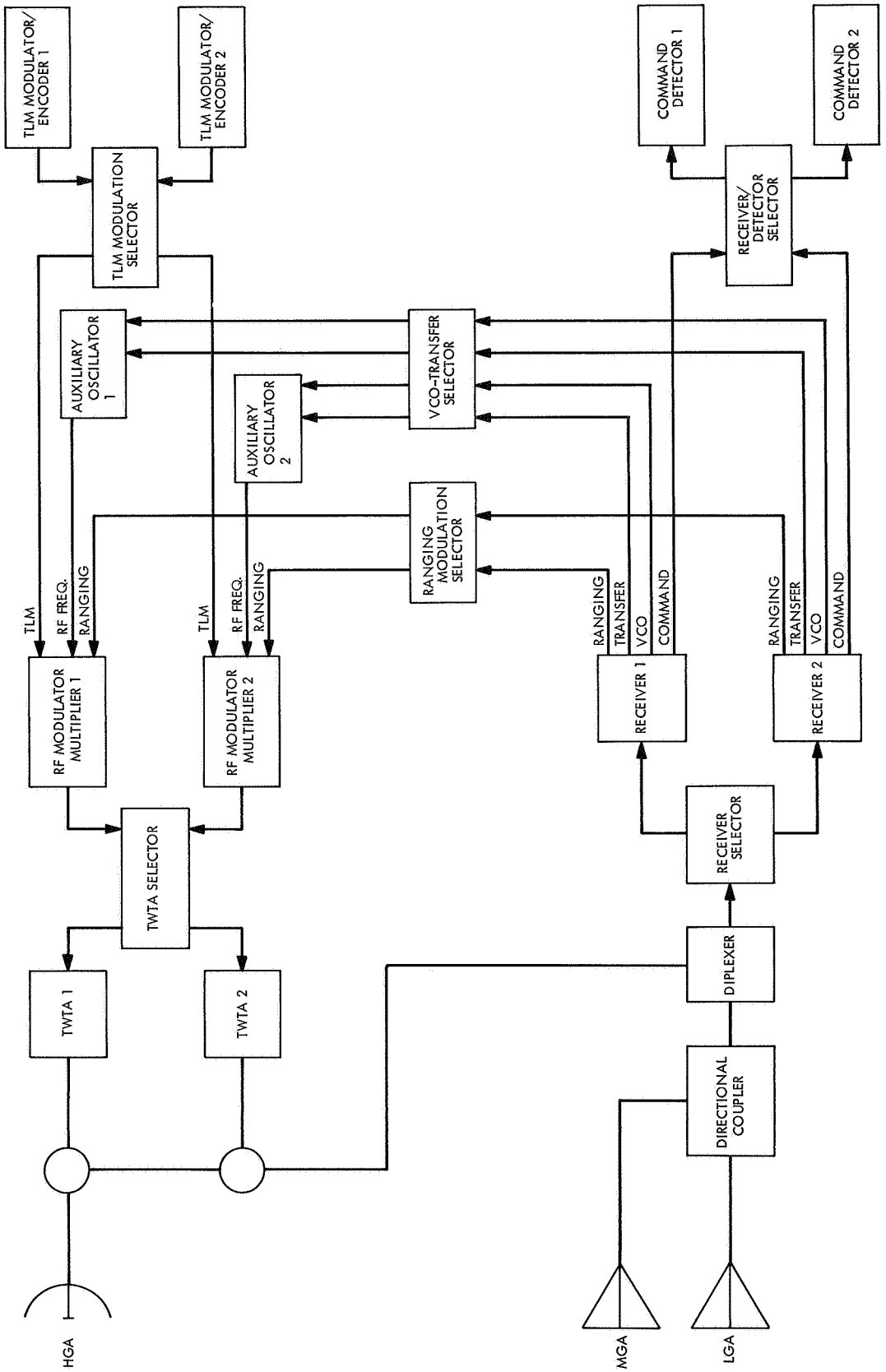

Fig. 6. *Viking* 1975 telecommunications "block" redundant configuration (maximum cross coupling)

(3) Once each pass for the first five days after landing.

(4) At least once every 30 days for the sixth through ninetieth days after landing.

If required by the lander, Phase 3 may be extended up to 90 days after landing.

During Phase 1, the lander transmits data at 4 kbits/s with 10 W of RF power. Transmission is continuous from separation to the end of de-orbit burn, then intermittent until 30 min prior to entry, and then again continuous until touchdown. Data received at the orbiter is recorded in the data storage subsystem (DSS) and also relayed in real time to earth via S-band.

Phase 2 begins at lander touchdown. The lander immediately switches to a 16-kbit/s transmission with 30 W of RF power. Data received at the orbiter is recorded in the DSS until the link drops below threshold as the orbiter sets. At least 10^7 bits of data is required in this phase.

During Phase 3, the relay link is operational once each day as the orbiter passes over the lander near periapsis. Data is sent at 16 kbits/s with 30 W of lander RF power for recording in the orbiter. This phase requires recording of at least 10^7 bits during each pass.

Phase 4 requires the relay link to be operational for at least one pass near periapsis every 30 days. These passes are a product of opportunity as the landing site occasionally comes into view to the orbiter. Normally, the link would be operated in this phase only when the orbiter's elevation angle is above 15 deg and lander–orbiter range is less than 5000 km. These passes will be supported by the lander at 4 kbits/s and 30 W of RF power.

c. Relay link performance estimates. The relay link is designed to support Phases 1 through 4 with a single configuration. Ordinarily the link would be operated with elevation angles of 15 deg or higher and ranges below 5000 km. For a periapsis pass during the first 5 days after landing, the nominal performance is estimated to be as shown in Fig. 7. This curve is based on the parameters of Table 3 for a 16-kbit/s transmission. Curves bounding the nominal for best- and worst-case multipath variations are included on Fig. 7 (a specular post-landed multipath model is assumed with relative permittivity $\epsilon_r = 3.0$). The multipath will cause rhythmic variations in margin within the envelope shown on Fig. 7. These variations are a function of elevation angle and

Table 3. *Viking* 1975 relay link parameters[a]

Parameter	Value
Transmitter power (lander), W	30
Transmitting antenna gain (peak), dB	4.5
Receiving antenna gain (peak), dB	4.5
System noise temperature, °K	618
Threshold ST_b/N_0, dB	12.3
Periapsis altitude, km	1400
PER (true anomaly of landing site), deg	−11.3
Cross-ranging, deg	0
Lander slope, deg	0

[a]High-rate data at 16 kbits/s.

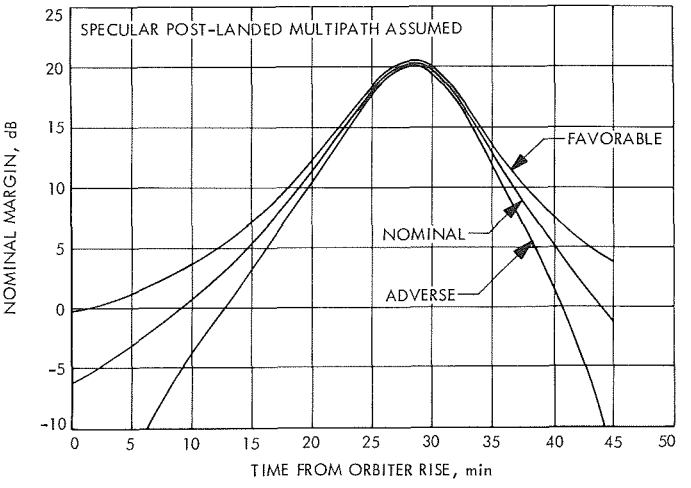

Fig. 7. *Viking* 1975 relay link performance curve showing multipath envelope

antenna height above the surface. Including actual multipath effects for an antenna height of 1 m produces the performance curve of Fig. 8.

The time above horizon and peak performance is critically dependent on the trajectory of the orbiter. Figure 9 shows performance curves for the nominal and bounding periapsis altitudes of 1000, 1400, and 1800 km. The lower the periapsis altitude, the lesser time the orbiter is in view. In order to meet the requirement of 10^7 bits per pass, the link must be above threshold for at least 10.42 min. Hence, the lower altitudes place the most severe limitation on the link from a time standpoint.

d. Beacon considerations. The Orbiter Relay System can be commanded into operation by ground or CCS command. In order to activate the lander equipment, it

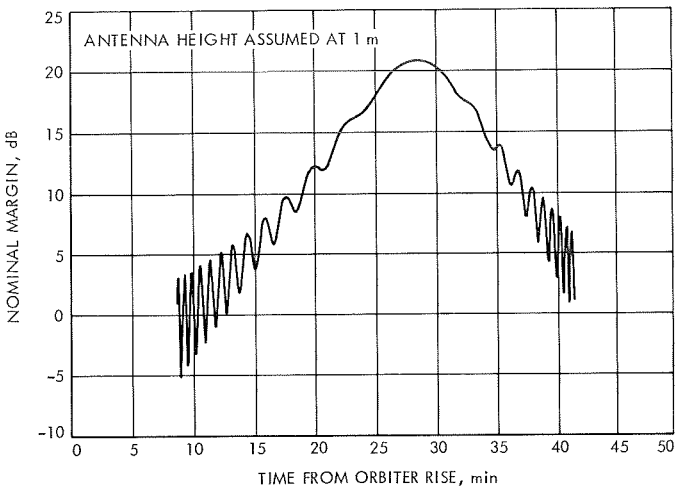

Fig. 8. *Viking* 1975 relay link performance with post-landed multipath

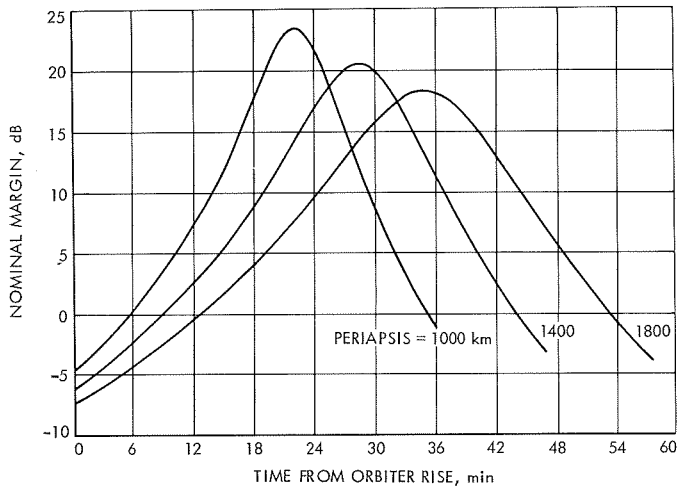

Fig. 9. *Viking* 1975 relay link performance vs time

is proposed to implement a beacon transmitter in the orbiter. This transmitter would be commanded *on* prior to orbiter rise. An address tone would be amplitude modulated on the beacon to select the desired lander. When detected at the lander, UHF transmission would begin with real-time data. After data lock is achieved in the orbiter, the address tone would be removed and an enable tone sent to the lander. The lander would then initiate playback of recorded data.

Another scheme for link control would be use of a beacon transmitter with address tones as above, but no enable tone. A fixed time delay would be programmed into lander operations to allow sufficient time for orbiter data lock. It may even be possible to devise a scheme whereby internally programmed timing would control both the lander and orbiter with no beacon at all. These possibilities are presently under study as both primary and back-up modes of operation.

e. Relay radio subsystem. The Relay Radio Subsystem (RRS) supports relay link communications by providing:

(1) The receiving, detecting, and routing of the frequency-shift-keyed lander data.

(2) The amplitude-modulated beacon signal to initiate post-landed RF transmission by the lander.

(3) Selectable beacon modulation frequencies to allow addressing any lander and to advise the lander of the lock status of the relay telemetry subsystem (RTS) bit synchronizer.

(4) A telemetered measure of received signal strength to facilitate link performance analysis.

Figure 10 depicts the major elements for deriving the RRS transmitting and receiving functions. The transmitter signal, nominally at 405 MHz, is derived by multiplying, modulating, and amplifying the output from the crystal oscillator. The oscillator must be temperature-compensated and may possibly require an oven to achieve the required frequency stability. The transmitter power amplifier must be capable of being turned *on* or *off* by the orbiter computer command subsystem (CCS). The power amplifier *on–off* control allows the transmitter to be operated in a standby mode for warm-up and frequency stabilization purposes. The leakage signal through the *off* power amplifier can also allow the standby mode to be used for pre-separation checkout of the lander relay communications system. The modulator could be capable of supplying any one of five modulating frequencies (tones). Selection of any one of four lander addressing tones could be by CCS command, while the fifth tone would be selected whenever the RRS receives the RTS signal indicating bit synchronizer "in lock."

The receiver frequency is nominally at 385 MHz. It is a single conversion type employing a low-noise preamplifier, mixer, bandpass filtering, and limiting in the intermediate frequency (IF) stages. The IF signal is routed to two demodulators, each of which employ bandpass filters (BPFs) and square-law detectors centered at the mark and space frequencies.

The demodulator filter bandwidths must accommodate: (1) possible frequency drift of the lander transmitter, (2) possible frequency drift of the RRS receiver local oscillator, (3) the maximum possible doppler frequency

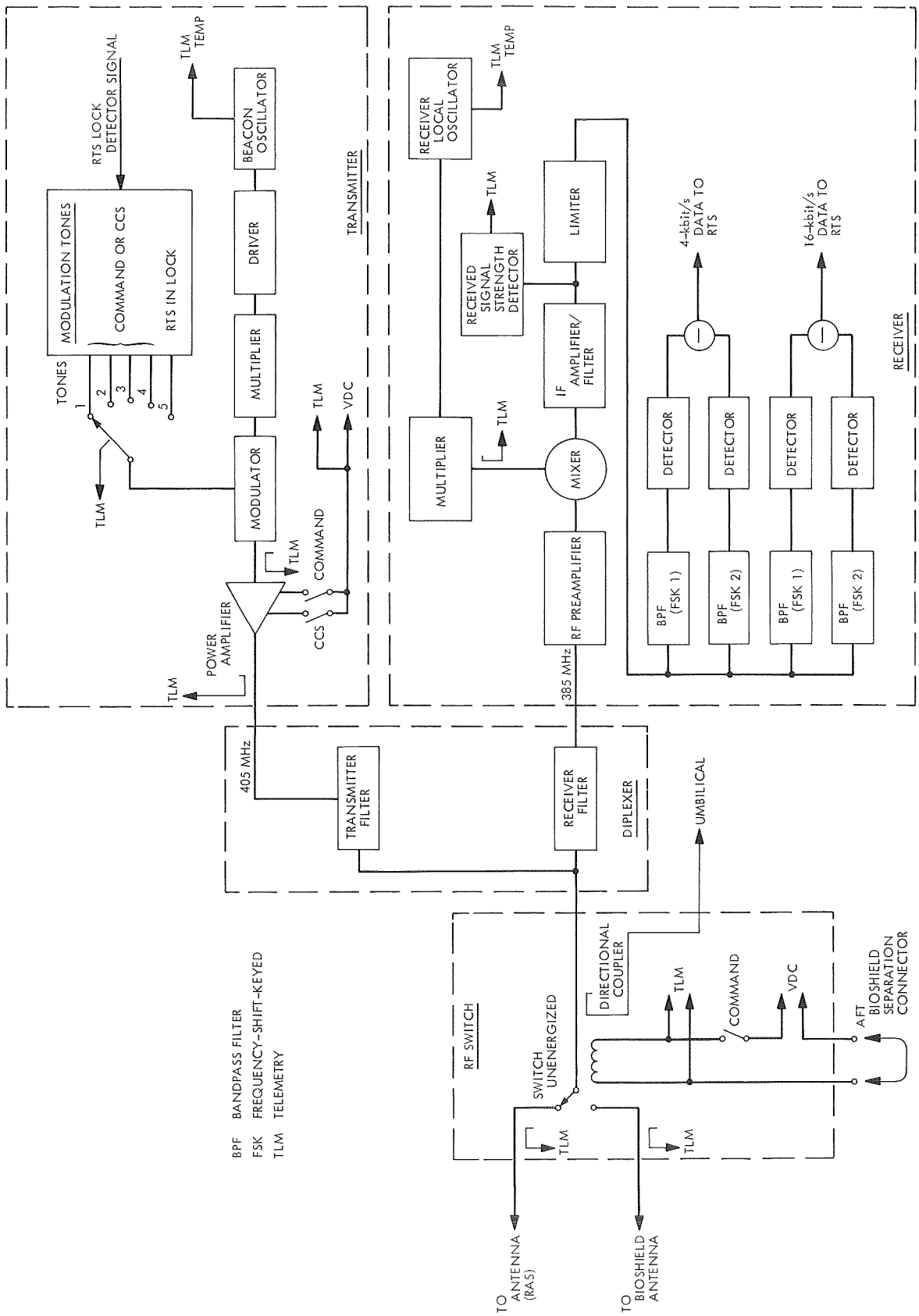

Fig. 10. Relay radio subsystem

shift between the lander and orbiter, and (4) the information bandwidth of the data. Separate demodulators for high-rate (16 kbits/s) and low-rate (4 kbits/s) data retrieval allow each demodulator to employ optimum bandwidths for that specific data rate. The mark and space filter bandwidths for the high-rate demodulator are nominally 110 kHz while the low-rate demodulator employs nominal 55-kHz bandwidths. Because the lander transmits the same mark and space center frequencies regardless of the data rate, little is gained by employing independent high-rate and low-rate IF bandwidths. Hence, the IF bandwidth, nominally 320 kHz, is determined by the same factors that determine the demodulator bandwidth plus the frequency separation between the mark and space frequencies.

The receiver design will incorporate circuitry for measuring the received signal strength at the orbiter. This measurement will be sent to the orbiter flight data subsystem (FDS) to be telemetered to earth. Current plans for implementing this measurement require positive signal-to-noise ratios (SNRs) in the receiver IF stages. At link threshold (a bit error rate of 3×10^{-3}), the SNR in the IF drops below zero dB, making the measurement limited to strong signal values. Performance analyses at weaker signal levels can be made from the RTS signal-to-noise ratio estimate.

The receiver and transmitter are connected to a common transmission network by means of a diplexer. An RF switch located at the diplexer transmit/receive terminal allows the RRS to be connected to the relay antenna or to a pickup probe mounted in the capsule bioshield. Elimination of the RF switch in favor of passive coupling to the relay antenna or to the diplexer transmit/receive line is under investigation. The bioshield probe allows for launch pad and pre-separation checkout of the orbiter and lander relay hardware and for relay link communications during lander separation and orientation prior to the lander de-orbit burn.

During the mission, the RRS will be operated in any one of three possible modes. The RRS will be *off* during the launch and cruise phases of the mission, operated in the *standby* mode during lander checkout, separation, entry, and during orbital phases for which relay communications are not required or feasible, and *on* during periods of required operation. In the standby mode, the RRS operates all elements except the transmitter power amplifier, thereby conserving orbiter prime power, but still providing the necessary data reception during entry. The possibility of turning the RRS *off* during the non-required orbital phases is largely dependent on achieving all necessary RRS operating characteristics with minimum warm-up. The RRS beacon transmitter would be operated during post-landed orbital passes over the lander. This is effected by CCS command to the RRS turning on the transmitter power amplifier.

f. Relay telemetry subsystem. The Relay Telemetry Subsystem (RTS) must perform the following general functions:

(1) Receive from the RRS either of two noisy PCM, split-phase waveforms (4 or 16 kbits/s).

(2) Establish synchronization between the incoming waveform and an internal VCO-driven clock.

(3) Resolve the timing ambiguity due to split-phase coding of the data.

(4) Recover the incoming data in a matched filter and restore it to binary non-return-to-zero (NRZ) form.

(5) Route the recovered PCM data to the flight data subsystem whenever the low-rate relay channel has been selected.

(6) Route the recovered PCM data and sync to the DSS at either of the two data rates.

(7) Indicate by means of a lock detector when sync is established or lost.

(8) Monitor the received SNR by sampling and processing the output of the data detector.

(9) Make up a digital status word for the flight data subsystem to be transmitted over the engineering data channel.

The major functional units of the RTS are a high-rate bit synchronizer, low-rate bit synchronizer, signal-to-noise ratio estimator, lock detectors, and power supply. A functional block diagram of the RTS (excluding the power supply) is shown in Fig. 11.

Bit synchronizer. The high-rate and low-rate bit synchronizers are functionally identical except that one operates at 16 kbits/s and the other operates at 4 kbits/s. The bit synchronizer consists of an input buffer amplifier, symbol tracking loop, bit sync ambiguity resolver, and data-matched filter.

The input to the synchronizer from the RRS is a noisy split-phase PCM waveform. The synchronizer establishes sync between the input and an internal clock, resolves

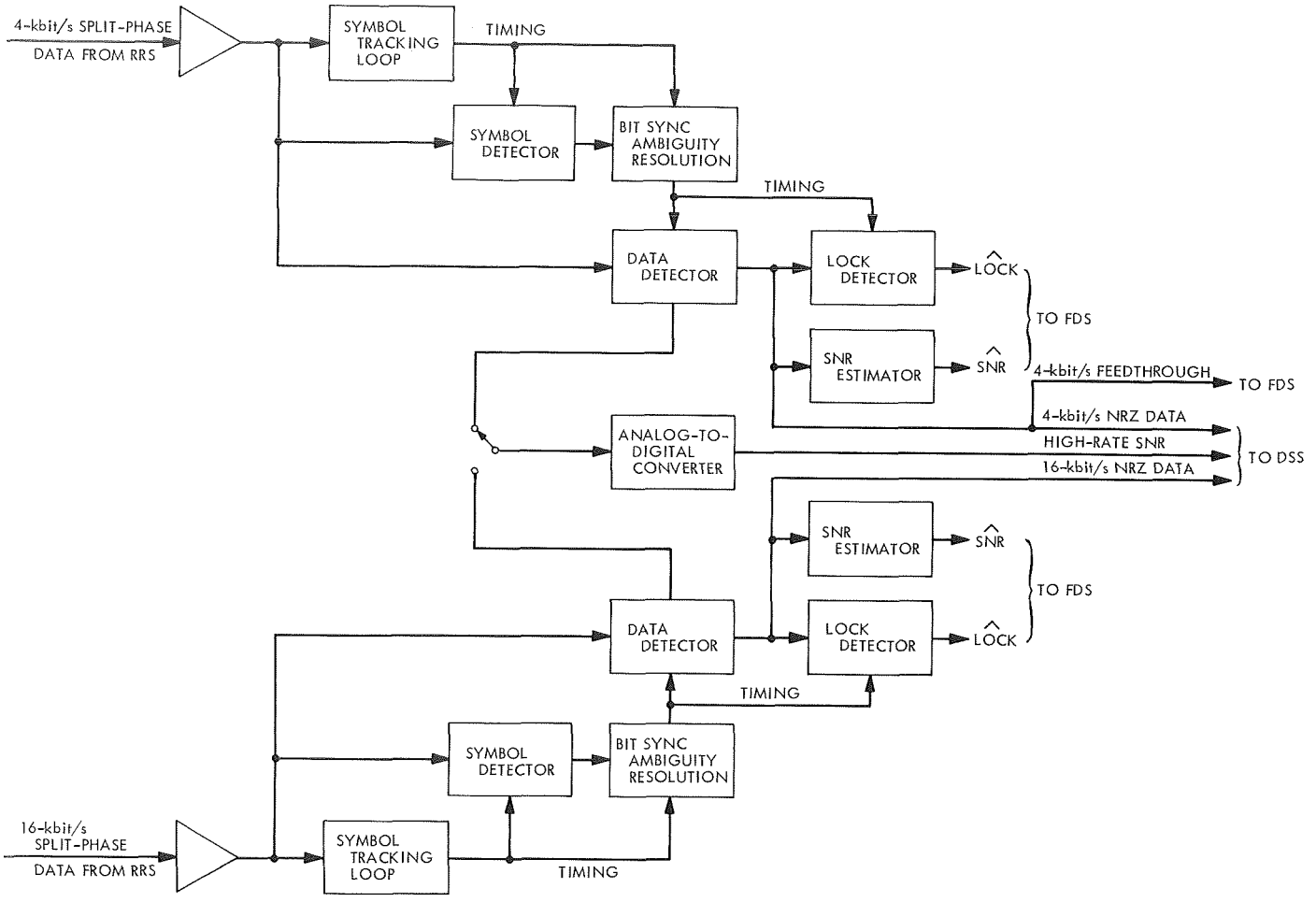

Fig. 11. Relay telemetry subsystem

the timing ambiguity, recovers the incoming data, and converts the incoming data to NRZ.

The symbol tracking loop is an analog approximation to an early–late type data transition tracking loop as shown in detail in Fig. 12. The phase detector for this mechanization consists of two multipliers, two low-pass filters (time constant of 1/3 symbol period), two absolute value circuits, and a subtractor. The subtractor output produces an error signal that controls a voltage-controlled oscillator (VCO). The VCO drives timing logic to produce various timing signals such as the early–late gate multiplying signals (A and B), dump pulse, sample pulse, and bit sync. The loop noise bandwidth ($2\ B_{L_0}$) is selected to be 2% of the bit rate.

Since the sync loop is a symbol transition loop, there will be a phase ambiguity in the bit sync timing signal. Split-phase coding has the property that mid-bit transitions exceed between-bit transitions (except for the all "1" or all "0" case at which time they are equal). The bit period phase ambiguity is readily resolved by using this property. A bit sync phase estimate is chosen to control the direction of transition counts in a 3-bit up–down counter. The bit sync phase estimate is changed only when the counter reaches full scale (or empty). The counter is inhibited from going past either full scale or empty.

Data is recovered by the use of an integrate-and-dump-type matched filter using timing from the bit sync ambiguity resolver. The input data is multiplied by bit sync (in phase with the data) and the multiplier output is integrated for a bit period. The integrator time constant is at least 4 bit periods. The output of the integrator is then fed to a decision circuit to determine whether the bit is a "1" or "0."

Lock detector. Lock detectors are implemented in both the high- and low-rate synchronizers. Their outputs will

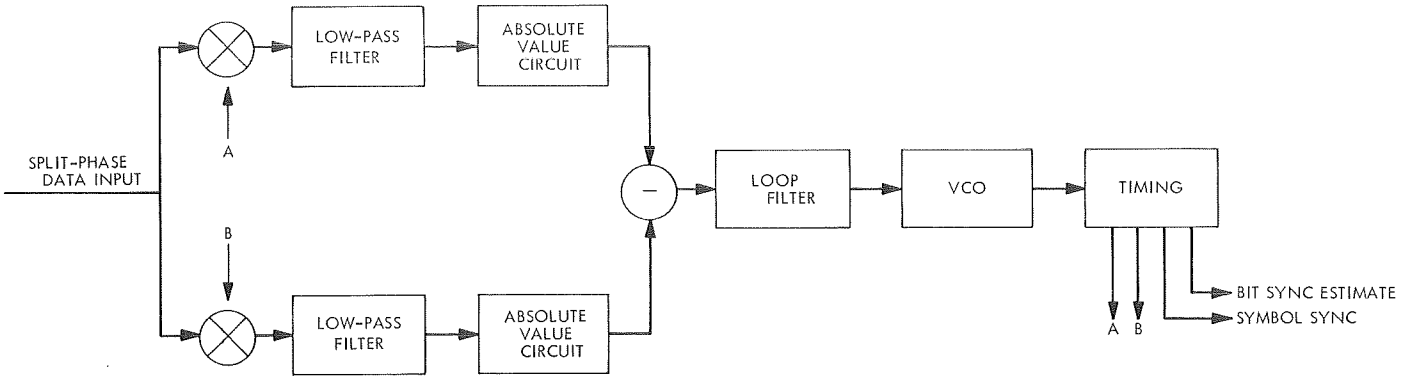

Fig. 12. Relay telemetry subsystem symbol tracking loop

be used for telemetry status information and may be used for selection of a modulation tone on the RRS transmitter. At the present time, the lock detector strategy or requirements have not been fully established. Current implementation plans are to take the absolute value of the output of the data-matched filter, average over several bit periods, and compare with a fixed threshold value. In-lock will be indicated when the fixed threshold value is exceeded.

Signal-to-noise ratio estimation. A means of estimating the relay link SNR will be mechanized as part of the RTS. Present plans call for both a high-resolution measurement to be stored on the DSS and re-transmitted in non-real time, and a lower-resolution real-time measurement telemetered via the flight data subsystem. The high-resolution measurement will consist of digitized samples of the data-matched filter output taken every N bits. Several approaches to processing the real-time SNR estimation onboard are still being considered.

Power supply. The power supply will provide the required dc operating voltages to the RTS from the 2.4-kHz, 50-V rms, square-wave power provided by the orbiter power subsystem. The power subsystem will be capable of turning *on* and *off* the power to the RTS.

Breadboard status. A functional breadboard operating at 400 bits/s is currently being tested and a functional breadboard operating at 4 kbits/s is being constructed. Tests on these breadboards are intended to provide parameter values for interfaces between the RRS and RTS and provide assurance that the implementation scheme satisfies the *Viking* orbiter mission requirements.

g. Relay antenna subsystem. The relay antenna subsystem (RAS) is required to support transmitting and receiving functions of the RRS. Study of the antenna requirements is proceeding using analyses performed for *Voyager*, Capsule System Advanced Development, and other projects. Antenna pointing and pattern development are contingent upon trajectory and mission strategy. Trajectory data for the 1975 missions are expected to be available in the last half of 1970, allowing the antenna design to be updated at that time.

Initial studies suggest use of a single radiator, circularly polarized, fixed antenna. Mechanical clearance problems may require placing the antenna on a boom in order to provide entry coverage as well as post-landed links. Trajectory data for the 1973 missions indicated that a single lobe pattern design was satisfactory for those missions. Peak gain of such an antenna would be about 4.5 dB with a beamwidth of 130 deg.

D. Guidance and Control

1. Proposed *Viking* Attitude-Control Roll-Reacquisition Logic

a. Introduction. An improvement in the functional sequences associated with the roll axis control has been designed for incorporation on the attitude-control system for the *Viking* spacecraft. The proposed sequence eliminates some unnecessary roll search modes. The attitude-control system does not immediately initiate a spacecraft roll search mode upon loss of Canopus, thus affording ground controllers time to override the automatic features of the sequence if circumstances call for it.

b. Viking spacecraft performance after loss of Canopus acquisition. The difference between the performances of the *Viking* and *Mariner* Mars 1971 systems, when Canopus acquisition is lost, is that *Viking* goes through

a timed sequence after loss of Canopus, while *Mariner* Mars 1971 does not. When *Viking* loses Canopus acquisition, while in the cruise mode, the Canopus tracker performs a flyback and sweep operation. If Canopus is not reacquired, the roll gyro turns on and the roll axis is put under inertial control. The system waits in roll inertial until a pulse is received from the spacecraft computer (an hourly pulse). When the pulse arrives, the Canopus tracker performs a flyback and sweep operation. If Canopus is not reacquired, the system waits, still in inertial, until receipt of the second pulse from the computer to flyback and sweep again. Should Canopus acquisition not result from this, the system will switch to the rate mode in roll and begin a roll search, with the roll axis under Canopus tracker control.

Mariner Mars 1971 and *Viking* have a 3-min timer which delays turning *off* the gyros after acquiring Canopus. (The gyros will not turn *off* in the presence of a condition such as straylight.) If Canopus is acquired during one of the pulse-induced flyback and sweep operations, the spacecraft will stay on inertial control in roll until the gyro turns *off*. When the gyro turns *off*, roll control switches to the Canopus tracker. Canopus acquisition has to be held for 3 min and the gyros have to turn *off* for the sequence to be terminated.

When the spacecraft is in orbit about Mars, a straylight condition will periodically occur due to reflected light from the planet. Since this straylight condition invalidates the Canopus tracker output, a signal from the spacecraft computer is sent to the attitude control, setting the roll axis to the inertial mode whenever it occurs. During straylight conditions, when Canopus acquisition is lost, the same sequence as above is activated. Whereas *Mariner* Mars 1971 would stay in inertial until acted upon by ground command, when Canopus is not reacquired, *Viking* eventually will automatically go into roll search.

This sequence can, at any time, be interrupted by ground command and the spacecraft held in inertial indefinitely or an immediate roll search initiated.

During the orbit of Mars by *Viking*, the sun will periodically be occulted. The same sequence of hourly flyback and sweeps and eventual roll search will occur after sun occultation as after straylight. The only difference is that during occultation all three axes are under inertial control. At the conclusion of occultation, the pitch and yaw gyros stay *on* until the roll gyro turns *off*.

The repeated exercise of the flyback and sweep feature in the Canopus tracker ensures that automatic reacquisition without roll search will occur if the initial loss of acquisition is due to reflected light from particles, since particle lifetime is of short duration. The minimum 1-h elapsed time between the loss of Canopus acquisition for any reason and the initiation of roll search provides time for the ground controllers to override the roll search mode should that be judged appropriate.

Figure 13 illustrates the sequence the *Viking* attitude-control system goes through when Canopus acquisition is lost. The termination of the sequence by ground command is not shown.

2. *Viking* Attitude-Control Subsystem Status Register

a. Introduction. The *Viking* spacecraft telemetry subsystem requires that there be a "status register" located in the attitude-control subsystem. This is to replace the "event register" in the *Mariner*-type spacecraft. This article describes the status register and some of the problems associated with the design.

b. Circuit description. Figure 14 is a functional block diagram of the attitude-control status register. The attitude-control logic status is input to the register in parallel. Each bit monitors the condition of a unique logic state in the attitude-control subsystem. At a telemetry bit rate of 33⅓ bits/s, the telemetry system reads the attitude-control status word approximately once every 7 min. At the time that telemetry desires to read the attitude-control status word, the alert pulse line is enabled. This inhibits the inputs from the attitude-control logic and converts the register to shift-right operation. Clock pulses then transfer the status word to telemetry bit by bit.

The preliminary bit assignments for the attitude-control status register are as follows:

Bit 1	Gyros *on* (pitch, yaw, and roll)
Bit 2	Roll gyro *on*
Bit 3	Sun acquired yes/no
Bit 4	Stray light yes/no
Bit 5	Sun occultation yes/no
Bit 6	Star acquired yes/no
Bit 7	Autopilot *on*/gain change yes/no

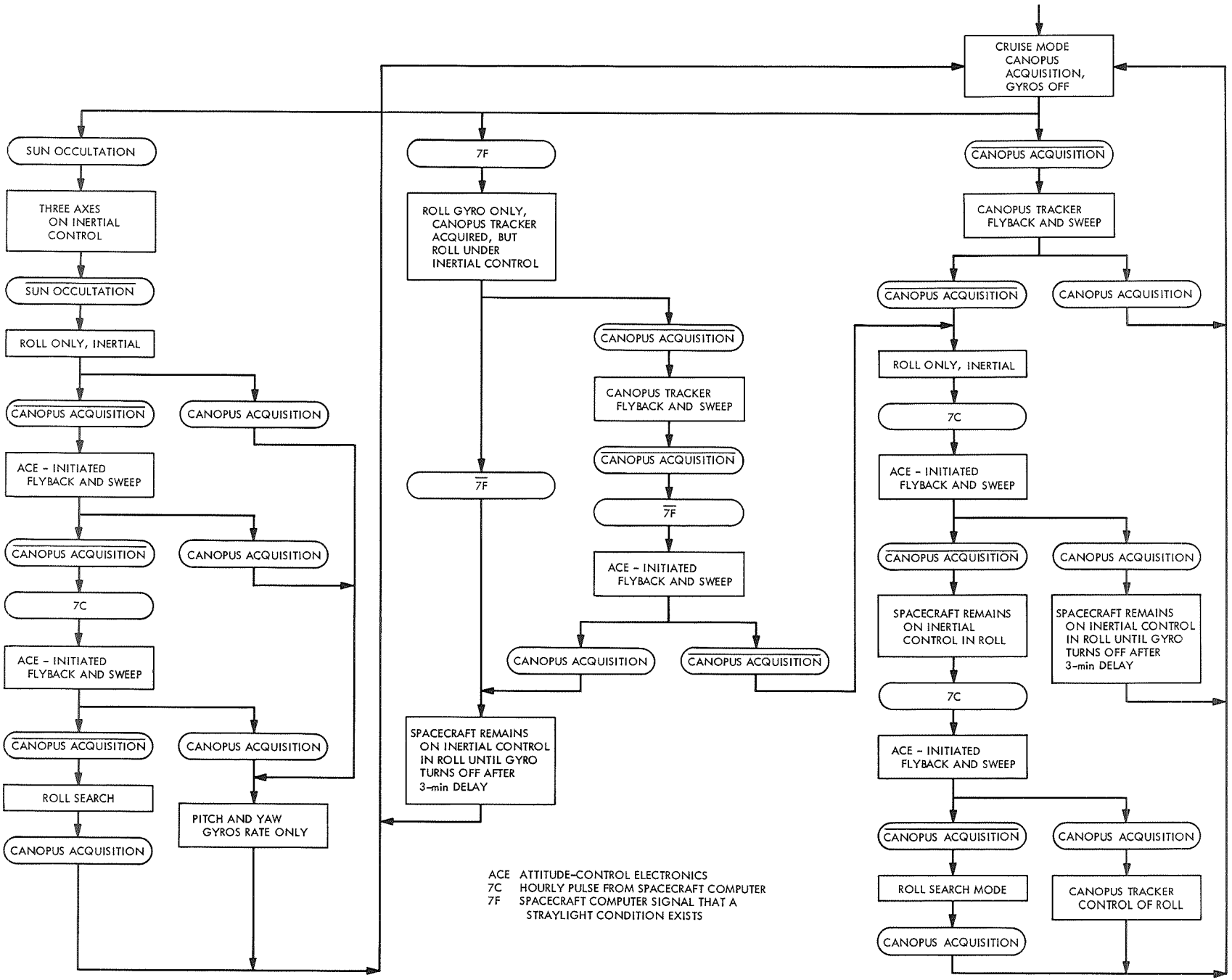

Fig. 13. *Viking* attitude-control sequence for Canopus reacquisition

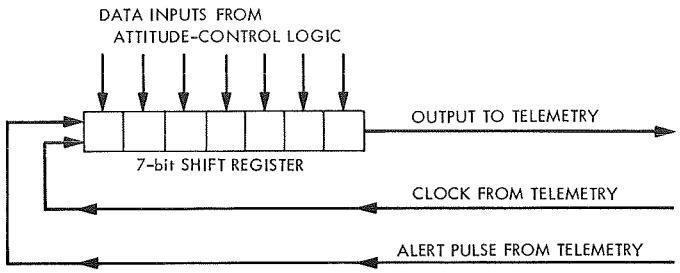

Fig. 14. *Viking* status register functional block diagram

These assignments are not final. It may be preferable to monitor the state of some of the logic switches internal to the attitude-control electronics since some of the functions listed above can be readily determined by telemetry in the high-rate channels.

c. Design considerations. Two designs of the status register are presented in Figs. 15 and 16. Figure 15 shows the design of a status register using Signetics 100-400 diode-transistor-logic (DTL) microcircuits. This family of microcircuits uses a B+ voltage of 4.5 V. Figure 16 shows a status register design using Texas Instruments 54L low-power microcircuits. This family of microcircuits uses a B+ voltage of 5 V. A comparison of alternate design approaches is shown in Table 4.

The table clearly shows the advantages of using low-power microcircuits. It should be noted that Texas Instruments 54L series is used in telemetry; if it is decided to use the Signetics 100 series in attitude control, additional circuits may be required to interface between the telemetry low-power devices and the attitude-control high-power devices.

d. Conclusions. Both status register designs will meet the design requirements of the *Viking* spacecraft. In terms of number of flatpacks and power consumption, the low-power design is clearly superior. However, other considerations, such as the available B+ voltage (4.5 V vs 5 V), may dictate which design is ultimately used.

3. *Viking* Scan Subsystem Mechanization

A modification to the *Mariner* Mars 1971 scan control that results in some hardware economies and in improved operational flexibility is proposed for the *Viking*.

The *Viking* mission imposes new requirements on the scan subsystem that cannot be met without changes to the existing hardware. A platform slew rate of 1 deg/s with a step resolution of 0.25 deg/step is required. The

Table 4. Microcircuit evaluation

Device	B+ voltage, V	Number of flatpacks	Power, W
Signetics 100-400 series	4.5	13	~0.5
Texas Instruments 54 series	5.0	3	~0.5
Texas Instruments 54L series	5.0	3	~0.06

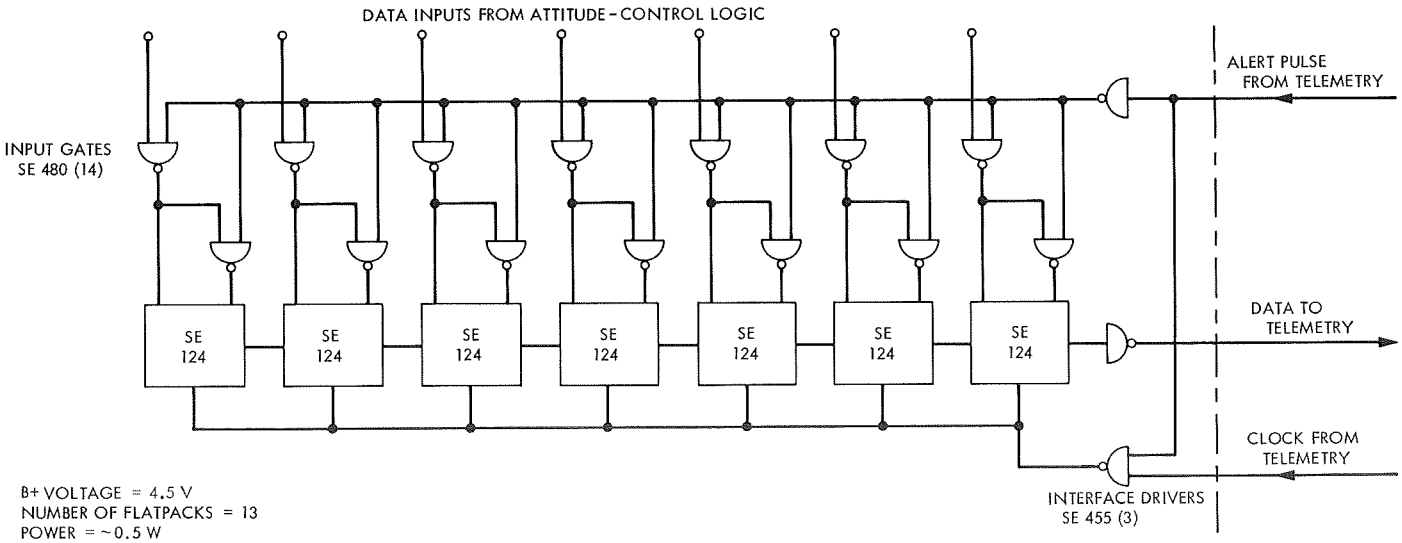

Fig. 15. *Viking* attitude-control status register preliminary design using DTL microcircuits

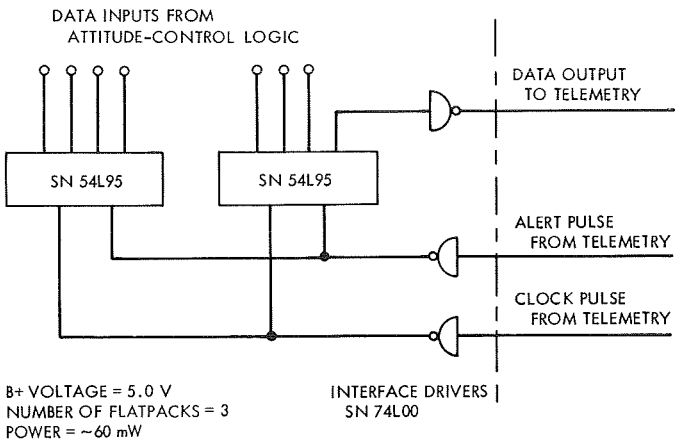

Fig. 16. *Viking* attitude-control status register preliminary design using low-power microcircuits

Mariner Mars 1971 hardware has a 1-deg/s slew rate with a step resolution of 1 deg/step.

Figure 17 is a block diagram of the scan subsystem. The shift register and the two digital-to-analog converters serve as memory devices in lieu of the previously used stepper motor-driven potentiometers. A 20-bit word corresponding to the angular clock and cone positions is shifted serially into the register. The two 10-bit digital-to-analog converters generate two analog voltages corresponding to cone and clock angular positions. Each converter has a dynamic range of 1024 and assuming that a 0.25-deg resolution is implemented, this results in a total range of the platform of 256 deg per axis. A correspondingly higher total range can be obtained at the cost of angular resolution. A two-line interface with the computer command subsystem (CCS) is assumed consisting of an information line and a clock line. This interface is very similar to the *Mariner* Mars 1971 ACE–CCS (attitude-control electronics–computer command subsystem) autopilot pre-aim interface. A coded command backup mode to perform identically to the CCS interface is shown in Fig. 17.

The platform actuator is slaved to the digital-to-analog converter output via a positional servo. The slewing capability of this system is independent of its angular resolution characteristics and depends only upon the actuator and load properties of the subsystem. Assuming these to be similar to the *Mariner* Mars 1971, a nominal slew speed of 1.3 deg/s can be achieved.

This proposed *Viking* mechanization eliminates the need for a pressurized electromechanical module containing stepper motor-driven potentiometers and results in the saving of approximately 20 electronic piece parts over the existing scan subsystem design. The proposed usage of the shift register digital-to-analog combination in contrast to the existing design results in a volatile memory. Because of the difference in missions between the *Viking* and the *Mariner* Mars 1971, the non-volatile memory is no longer a requirement.

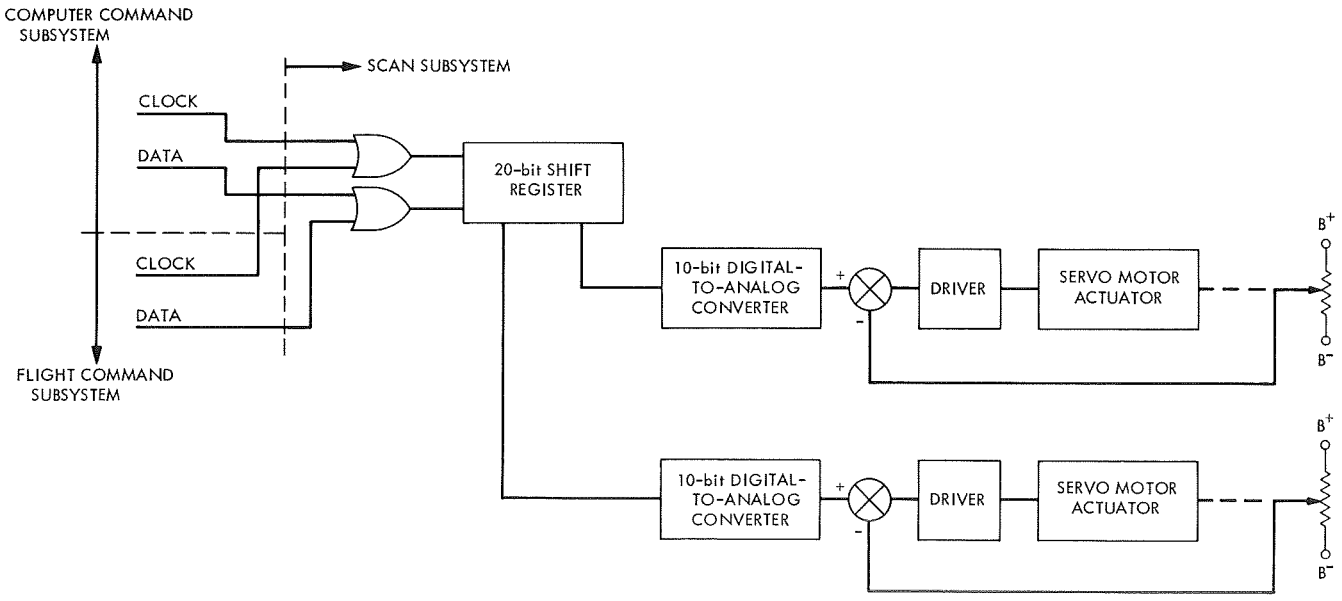

Fig. 17. *Viking* scan subsystem

Subject Index

Subject Index (contd)

NASA — JPL — Coml., L.A., Calif.